AD_____

Award Number: DAMD17-01-2-0047

TITLE: Disaster Relief and Emergency Medical Services Project (DREAMS TM): Science, Triage and Treatment (STAT)

PRINCIPAL INVESTIGATOR: S. Ward Casscells, M.D.

CONTRACTING ORGANIZATION: The University of Texas Health Science Center
Houston, TX 77030-3900

REPORT DATE: October 2004

TYPE OF REPORT: Final

PREPARED FOR: U.S. Army Medical Research and Materiel Command
Fort Detrick, Maryland 21702-5012

DISTRIBUTION STATEMENT: Approved for Public Release;
Distribution Unlimited

REPORT DOCUMENTATION PAGE

Form Approved
OMB No. 074-0188

1. AGENCY USE ONLY (Leave blank)	2. REPORT DATE	3. REPORT TYPE AND DATES COVERED
	October 2004	Final (15 Sep 2001 - 15 Sep 2004)

4. TITLE AND SUBTITLE
Disaster Relief and Emergency Medical Services Project (DREAMS TM): Science, Triage and Treatment (STAT)

5. FUNDING NUMBERS
DAMD17-01-2-0047

6. AUTHOR(S)

S. Ward Casscells, M.D.

7. PERFORMING ORGANIZATION NAME(S) AND ADDRESS(ES)

The University of Texas Health
Science Center
Houston, TX 77030-3900

E-Mail: S.Ward.Casscells@uth.tmc.edu

8. PERFORMING ORGANIZATION REPORT NUMBER

9. SPONSORING / MONITORING AGENCY NAME(S) AND ADDRESS(ES)
U.S. Army Medical Research and Materiel Command
Fort Detrick, Maryland 21702-5012

10. SPONSORING / MONITORING AGENCY REPORT NUMBER

11. SUPPLEMENTARY NOTES

12a. DISTRIBUTION / AVAILABILITY STATEMENT
Approved for Public Release; Distribution Unlimited

12b. DISTRIBUTION CODE

13. ABSTRACT (Maximum 200 Words)

Science, Triage, and Treatment:STAT is the component of DREAMS (Disaster Relief and Emergency Medica Services) that is developing new ways to diagnose and treat tissue injuries and infection. Progress been the pathophysiology and molecular biology of anthrax, human cytochrome P450 defenses, inflammat oxidation, apoptosis, reperfusion injury, organ failure, and nitric oxide. New techniques have been developed to automatically diagnose ischemia and heart, kidney, and respiratory failure. STAT scien have also developed new techniques to diagnose and image tissue inflammation and necrosis using CT, magnetic resonance, thermal imaging, and near-infrared spectroscopy. These have led to numerous publications, patents, products, clinical trials, and awards. In addition to trauma and infection, likely applications include atherosclerosis and cancer. In summary, DREAMS-STAT is making better th expected progress toward its goal of improving the care of battlefield injuries.

14. SUBJECT TERMS
DREAMS

15. NUMBER OF PAGES
119

16. PRICE CODE

17. SECURITY CLASSIFICATION OF REPORT	18. SECURITY CLASSIFICATION OF THIS PAGE	19. SECURITY CLASSIFICATION OF ABSTRACT	20. LIMITATION OF ABSTRACT
Unclassified	Unclassified	Unclassified	Unlimited

Table of Contents

Project I.A.

Administrative Section

Investigators: James T. Willerson, M.D.
S. Ward Casscells, M.D.

For DREAMS:STAT, we have utilized Administrative funds for providing assistance, coordination of the various research programs, statistical analysis assistance, and miscellaneous items required by various investigators in this project.

All salaries are in accordance with the policies and procedures of the University of Texas-Houston Health Science Center. Fringe benefits are calculated at a rate of 21.5%.

Dr. Ward Casscells is the Principal Investigator for DREAMS:STAT and some financial support for his level of effort is budgeted in this section. Dr. James Willerson is an Associate Principal Investigator and financial support for his level of effort is also included in the budget. Scott Harrison is the Administrator for the DREAMS-STAT program. He coordinates research schedules, administrative reports, purchasing activities, and serves to help each investigator solve administrative problems that arise. Funds are also budgeted for statistical assistance for data evaluation in each of the research sections and for office supplies, including paper, pencils, pens, as well as storage items, computer costs, and such for each of the investigators.

Again, DREAMS:Science, Triage, and Treatment (STAT) well exceeded expectations, as there were more fundamental discoveries and practical inventions, mostly in the areas of tissue injury, inflammation, infection, and imaging. Publications, patents, presentations, and awards were numerous and exceeded those of DREAMS:STAT 2001. Several projects originally included in the DREAMS:STAT program have since been terminated and thus, are no longer allocated funds. Drs. Willerson and Casscells concluded that the key goals of the aforementioned project were no longer parallel with the overall objectives set forth by DREAMS-STAT.

Of particular relevance to the critical role of the USAMRMC in bioterrorism, DREAMS PI Dr. Casscells founded DefenseOfHouston, the citizen group that on September 6, 2002 was awarded the Best Practice Award of the US Department of Health and Human Services. Dr Casscells was chosen to serve on several task forces including the Mayor's Advisory Committee to the Medical Strike Team, the Houston Task Force on Terrorism, The University of Texas Homeland Security Committee, the Governor's Council on Health and Bioterrorism, the Pharmacology and Vaccine task force of the Center for Strategic and International Studies in Washington, and the Bush-Cheney Healthcare Advisory Committee.

In 2005, we aim to initiate our newest research endeavor, T5: Texas Training and Technology Against Trauma and Terrorism. This comprehensive project will continue to develop the basic biology and technology needed to improve the care of battlefield injuries. All T5 investigators look forward to a prosperous and exciting year of research in 2005.

The DREAMS-STAT investigators are thoroughly grateful for the financial support provided by the United States Army for carrying out this research. We are sincerely honored to be working with United States Army and look to further advance the knowledge of battlefield medical care with the Army's needs in mind.

Project I.B.

Mechanisms of Cardiomyocyte Injury in Shock

Investigator: L. Maximilian Buja, M.D.

INTRODUCTION

Exposure of mammalian cells to bacterial endotoxin (lipopolysaccharide, LPS), a component of bacterial cell walls, leads to profound and diverse effects. This response contributes to the cardiovascular collapse and death of patients with sepsis (Gates 1994). Since cardiomyocytes are terminally differentiated cells and cannot be replaced by cell division, any loss of these cells can lead to profound cardiovascular sequellae. Previous reports have indicated that exposure of isolated rat hearts or adult cardiac myocytes in culture leads to the initiation of programmed cell death (Comstock, Krown et al. 1998). Our initial goals were to delineate the mechanisms and pathways by which LPS initiates apoptosis in cardiac myocytes. This in turn may identify potential pharmacological interventions capable of protecting sepsis patients from the long term, cardiac damaging consequences of infection.

RESULTS AND DISCUSSION

Our studies were designed to be completed in isolated neonatal rat ventricular myocytes (NRVM's)(Comstock, Krown et al. 1998). This model system had been well characterized and used extensively within the lab for earlier studies. These cells represent significant advantages over alternatives; the cells are easy to isolate and yield essentially pure populations of cells in sufficient quantities to permit biochemical analysis.

In initial experiments NRVM's were treated with LPS at doses previously shown to induce apoptosis in adult rat ventricular myocytes (ARVM's). Markers of apoptosis, including cytochrome c release from the mitochondia, caspase-3 activation and loss of mitochondrial membrane potential, were then assessed. Unlike ARVM's, the NRVM's displayed a resistance to LPS induced apoptosis as assessed by these multiple criteria. Exposure to high

levels of LPS for extended periods of time did not induce apoptosis. Thus the neonatal model demonstrates a "resistance" to LPS-induced apoptosis, which is lost as the heart matures. We have previously demonstrated that NRVM's can be induced to apoptose by other treatments, including exposure to the saturated fatty acid palmitate and hypoxia (Hickson-Bick, Buja et al. 2000; Jung, Weiland et al. 2001). Our continuing studies therefore attempted to understand the nature of this protection with a view to possibly exploiting it's pathways in a clinical setting.

Although LPS was unable induce apoptosis in NRVM's it did elicit production of TNFα by these cells (Figure 1). LPS also induces a rapid (<10min) translocation of the redox sensitive signaling molecule, NFκB from the cytoplasm to the nucleus (Figure 2A). In adult cardiomyocytes this translocation is critical for TNFα production (Wright, Singh et al. 2002). In our cells this translocation is the result of an activation of IκB kinase, which phosphorylates IκBα causing it to dissociate from NFκB in the cytoplasm (Figure 2B) The NFκB is then able to translocate to the nucleus while the IκBα is targeted for degradation by ubiquination. This is not associated with an increase in apoptosis as assessed by caspase-3 activation (Figure 2C). NFκB translocation is often redox sensitive, and we have previously demonstrated that the addition of the Zn/Cu ion chelator diethylthiocarbamate (DDC), which inhibits the transformation of cytosolic superoxide to hydrogen peroxide, induces a significant stimulation in the nuclear binding of NF B (Hickson-Bick, Sparagna et al. 2002). The presence of DDC, while sufficient to increase superoxide production, only promoted a slight increase in caspase-3 activation (Figure 3). N-acetyl cysteine (NAC), a precursor for glutathione formation and previously shown to increase glutathione content of NRVM's (Inserte AJP 2000), was able to block the DDC response. These data suggest that the NRVM's are either not generating significant ROS in response to LPS, or maintain enhanced defenses against ROS-mediated damage.

Activation by phosphorylation via PI-3 kinase of the enzyme Akt (protein kinase B; PKB) is proposed to initiate protective pathways within the heart (Matsui and Rosenzweig 2005). LPS treatment of NRVM's leads to a phosphorylation of cellular Akt (Figure 4A & 4B).

However, the protection against apoptosis induction is not abrogated by the presence of the PI-3 kinase inhibitor wortmannin (Figure 4C). Our results thus indicate that Akt is not playing a role in the protection against toxic shock in these cells. Similarly, phosphorylation of p38 and ERK, mitogen activated protein kinases, are stimulated by LPS, but specific inhibition of these phosphorylation events do not induce apoptosis after LPS treatment (data not shown)

In other cell types an early effect of LPS stimulation is a change in arachidonic acid metabolism, probably due to induced changes in intracellular Ca^{2+} regulation(Aderem and Cohn 1986; Dennis, Ackermann et al. 1995). We examined the inflammatory/anti-inflammatory pathways activated by LPS in NRVM's. Protein levels of cyclooxygenase-2 (COX-2), 5'lipoxygenase and the cytochrome P450 isoform, cyp4F are all increased in the neonatal cardiac myocyte by LPS treatment (Figure 5A, 5B and 5C respectively). Levels of COX-1 remain unchanged. COX-2 activity can lead to the production of downstream inflammatory and anti-inflammatory eicosanoids. We observed that LPS stimulated the production of prostaglandin E2 (PGE2) and the cyclopentenone prostaglandin, 15dPGJ2 (Figure 6). 15dPGJ2 is a natural metabolite derived from PGD_2 (Figure 7) and an endogenous ligand for peroxisome proliferator-activated receptor γ (PPARγ). PPAR's, when heterodimerized with the retinoid X receptor (RXR), act as a transcription factor in many cell types, including the heart. Many proteins involved in lipid metabolism and metabolic energy supply contain response elements for PPAR's. Exogenous 15dPGJ2, when added to NRVM's in culture, attenuated nuclear translocation of NFκB in a dose dependent manner (Figure 8A & 8B), and induced caspase-3 activation (Figure 8C). However the concentrations required are significantly higher than are produced by the cells in culture. These results would indicate that although 15dPGJ2 can induce apoptosis in these cells this requires pharmacological levels, which are not achieved by cardiac myocyte production alone.

LPS also induces mitochondrial changes in the neonatal rat cardiomyocyte. LPS exposure leads to a transient loss of energized mitochondria. We also observed a change in the protein expression of uncoupling proteins, specifically

UCP3 after treatment with LPS. The expression of UCP3 is temporally associated with the loss in the mitochondrial membrane potential (Figure 9). The mode of action of uncoupling proteins is an area of intense study (Garlid, Jaburek et al. 2001). There proposed mechanisms of action include the reversible production of a proton leak causing an uncoupling of ATP production from oxygen consumption, decreasing the mitochondrial membrane potential and thereby reducing the production of reactive oxygen species. In our experiments we were unable to induce apoptosis by increasing cellular ROS, suggesting this is not a protective mechanism in this experimental system. Alternatively, UCP3 may play a role in fatty acid metabolism by acting as an exporter of fatty acid anions from the mitochondrion (Schrauwen and Hesselink 2004). Many investigators have observed a reduction in the oxidation of fatty acids by cardiac myocytes after LPS exposure (Liu and Spitzer 1977; Memon, Feingold et al. 1998; Memon, Fuller et al. 1998; Memon, Bass et al. 1999). This is associated with an accumulation of myocyte triglycerides, i.e. supply of fatty acids exceeds oxidative capacity. Potentially dangerous long chain fatty acids anions may accumulate in the mitochondria under these conditions. Uncoupling proteins can transport fatty acid, and a proposed physiological protective role of these proteins is to protect mitochondria from "lipotoxicity" (Unger and Zhou 2001; Russell, Finck et al. 2005).

Statistical Analysis. Differences between experimental and control groups were analyzed using a ANOVA. Where appropriate, results are shown as the mean of the measurement ± the standard error.

Key Research Accomplishments

- We have identified a phenotype in NRVM's, not found in adult hearts that protects these cells from damage by LPS leading to apoptosis.
- LPS induces the production of TNFα by NRVM's.
- LPS treatment of NRVM's initiates a rapid translocation of NFκB into the nucleus. This translocation is the result of an increased degradation of IκBα.

- Reactive oxygen species do not play a role in the protection of these cells.
- Activation of Akt, Erk and P38 are not sufficient to induce protection from apoptosis.
- LPS changes the metabolism of arachadonic acid in these cells by stimulating the activity of pro and anti-inflammatory pathways. Some of the products of these pathways can induce apoptosis in these cells. However, the doses required to induce apoptosis would indicate that this may a pharmacological rather than a physiological effect.
- LPS rapidly effects mitochondrial metabolism within NRVM's. Induction of uncoupling proteins may play a protective role. This avenue of research is being actively pursued within the lab.

Reportable Outcomes

1)CYCLOPENTENONE MEDIATE APOPTOSIS BY LPS IN NEONATAL CARDIOMYOCYTES.

Chad Jones, Jeanie B. McMillin and L. Max Buja. World Congress of the International Society for Heart Research, Winnipeg Canada, p.114 (2001).

2)TNF-ALPHA DOES NOT MEDIATE ENDOTOXIN-INDUCED APOPTOSIS IN NEONATAL RAT CARDIOMYOCYTES.

Chad E. Jones, L.Max Buja and Jeanie B. McMillin. Exp. Biol. LB257 (2002).

3)LPS TREATMENT OF RAT CARDIOMYOCYTES ALTERS MITOCHONDRIAL MEMBRANE POTENTIAL AND INCREASES UNCOUPLING PROTEIN EXPRESSION.

Diane Hickson-Bick, Chad Jones, L. Max Buja. Journal of Molecular and Cellular Cardiology **37**:188 (2004).

4)THE RESPONSE OF THE NEONATAL CARDIAC MYOCYTE TO ENDOTOXIN EXPOSURE.

Diane Hickson-Bick, Chad Jones, L. Max Buja. Journal of Molecular and Cellular Cardiology **37**:266 (2004).

5) MITOCHONDRIAL ALTERATIONS IN NEONATAL CARDIAC MYOCYTES AS A RESPONSE TO ENDOTOXIN EXPOSURE.

Diane Hickson-Bick PhD, Chad Jones, L. Maximilian Buja MD. Submitted FASEB 2005.

Conclusions

The mechanism of injury and apoptosis is the major theme of this work and is directly related to all projects contained in this investigation.

The initial purpose of this project was to determine the basic science behind endotoxin-mediated induced cell death in cardiac myocytes. We extended these investigations to examining the inflammatory response to LPS and its resolution via anti-inflammatory mediators in neonatal cardiac myocytes. Our research has uncovered an innate protective phenotype of the newborn heart against endotoxin-induced cell death. Our observations in neonatal heart suggest that the heart is able to mount an effective defense against endotoxin-induced cell death. The pathway by which this occurs is a characteristic of the developing heart and, we postulate, could be primed in the adult cardiac myocyte by de novo expression of protective genes. Reactivation of these pathways in the adult heart may thus prevent the cardiac deleterious effects of LPS. We are pursing these goals by extending our studies into adult rat cardiomyocytes and whole hearts.

The longterm goal of this research is to exploit the knowledge obtained in model systems into translational situations aimed at prolonging cardiac viability under clinical conditions. The dissection of initial events upon exposure to bacterial toxins will enable a thoughtful plan of action for a rapid medical response to provide emergency ministrations to affected populations at the time of exposure, in the absence of prior sufficient warning.

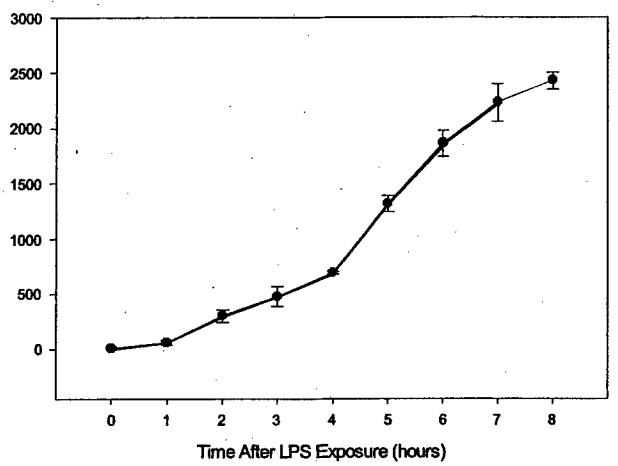

Figure 1: TNFα production by NRVM's after LPS exposure. Cell were exposed to 1μg/ml LPS for 1 hour. TNFα levels were measured in the media by ELIZA. All values represent the mean of at least 3 independent measurements. Error bars represent standard error.

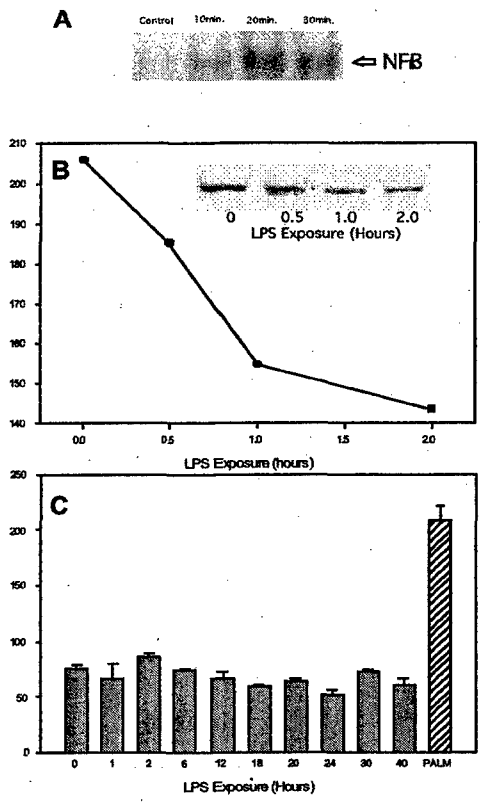

Figure 2. NFκB translocation, IκB degradation and caspase-3 activation of NRVM's exposed to LPS (1μg/ml). Nuclear translocation of NFκB (A) was determined by electromobility shift assay of nuclear extracts isolated from treated cells. IκBα degradation (B) was followed by Western analysis using specific antibodies; inset shows a representative gel. Caspase-3 activity (C) was determined using procedures already described by this lab; the palmitate measurement is positive control for apoptosis in these cells are previously described by this lab (Sparagna and Hickson-Bick 1999; Hickson-Bick, Buja et al. 2000; Sparagna, Hickson-Bick et al. 2000).

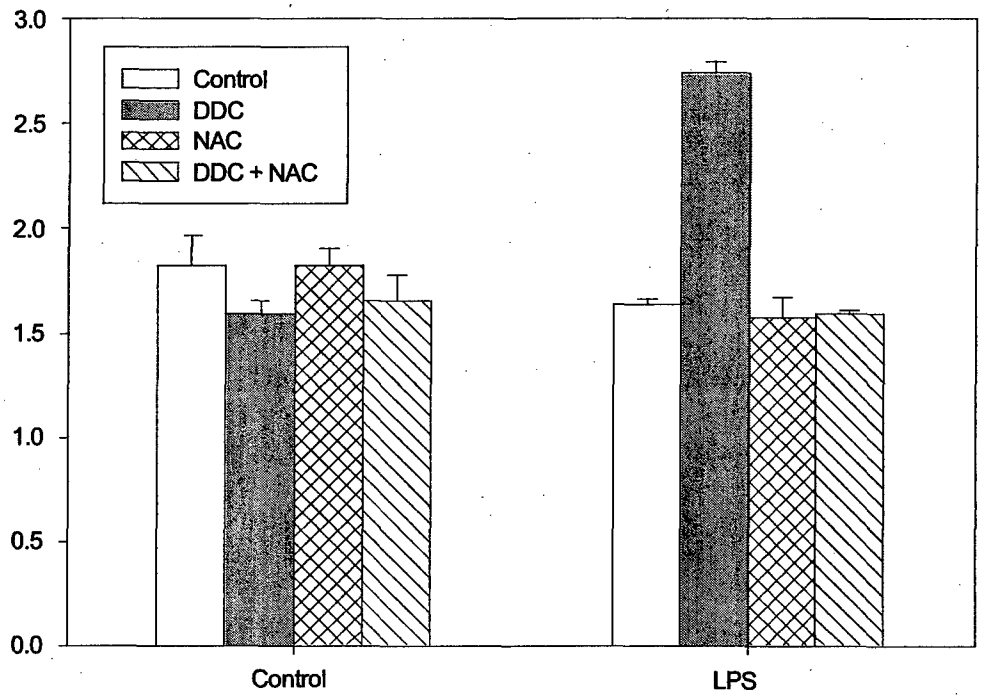

Figure 3: Increased ROS production can lead to apoptosis in NRVM's. Cells were incubated in the presence or absence of LPS (1μg/ml). DDC (75μM), a superoxide dismutase inhibitor and NAC (75μM) were added alone or incombination.

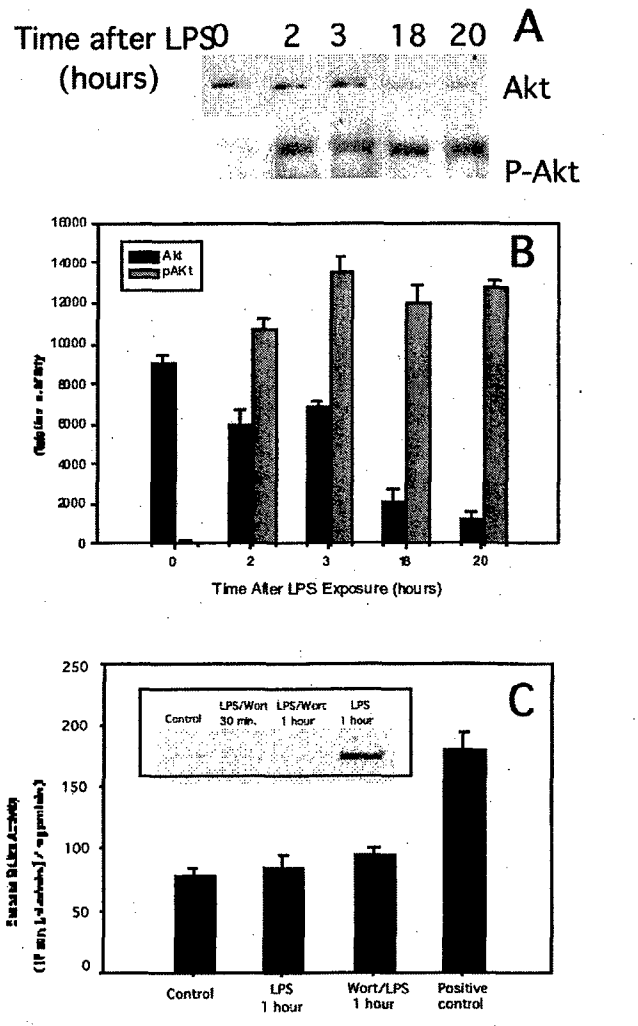

Figure 4. LPS stimulate phosphorylation of Akt. Akt and phosphorylated Akt (pAkt) in NRVM's after LPS treatment (1µg/ml) were determined by Western blot (A). Multiple blots were integrated and the combined results graphically represented (B). Addition of wortmannin, a specific inhibitor of the upstream kinase, did not induce apoptosis (C) although phosphorylation of Akt was blocked (inset)

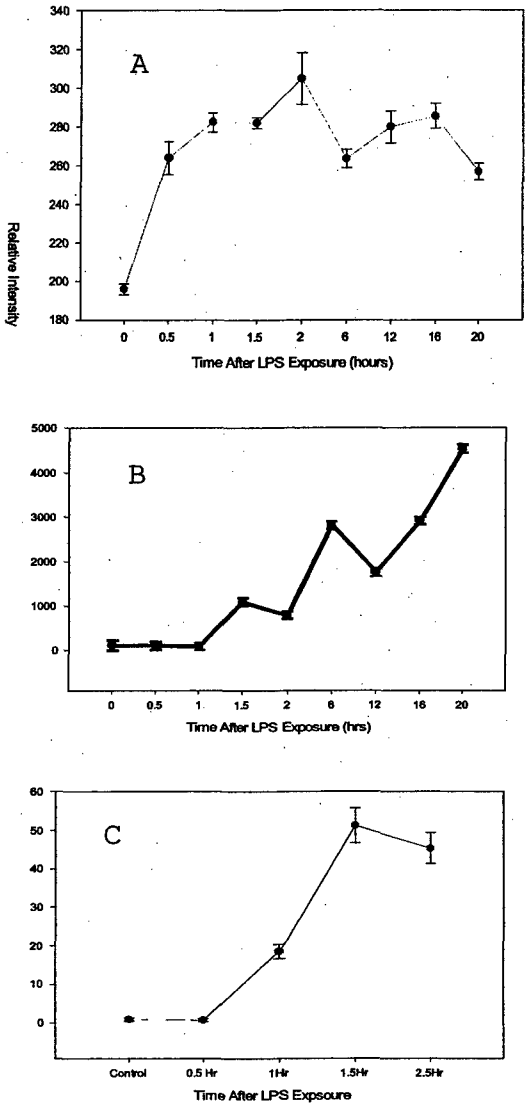

Figure 5. Changes in enzymes of arachidonic acid metabolism after LPS exposure. Intracellular COX-2 expression (A), nuclear associated (active) 5'LOX (B) and the cytochrome P450 isoform, Cyp4F (C)

Protein levels were measured by Western blot analysis and the integrated signal from multiple (≥3) gels combined. Results represent the means ± SE.

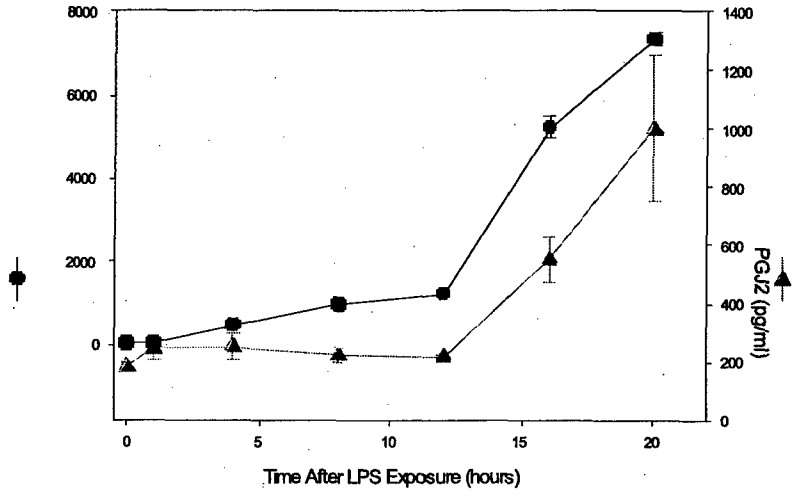

Figure 6. NRVM synthesis of PGE2 and PGJ2 after LPS exposure.

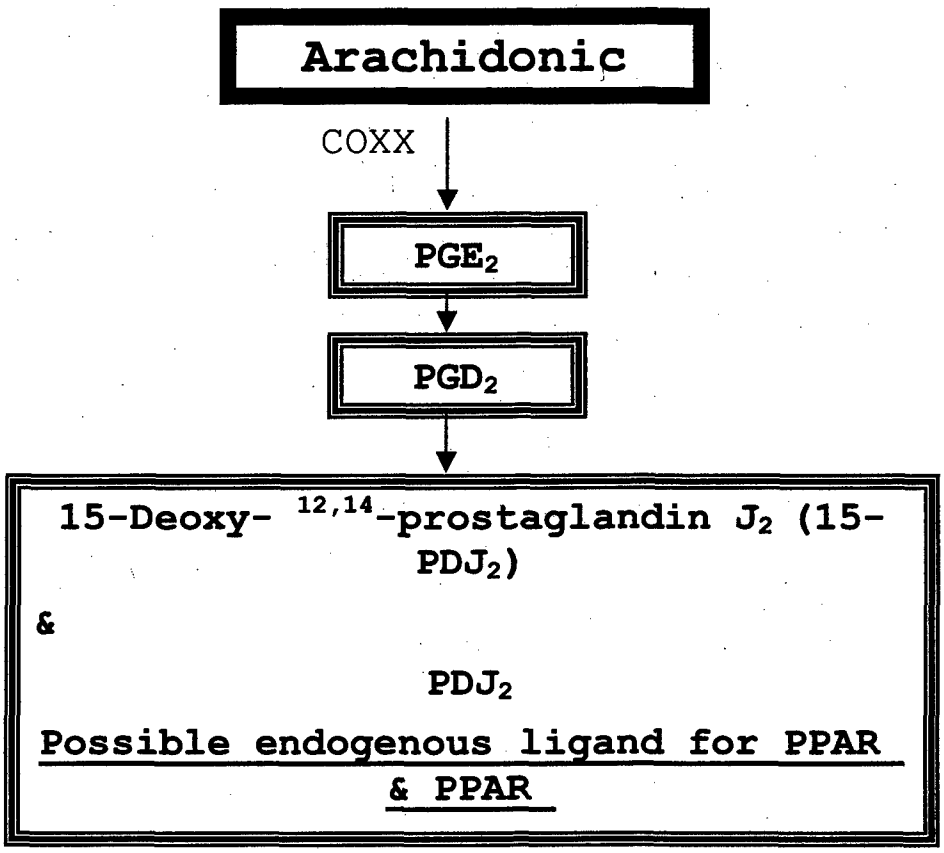

Figure7. Synthetic routes for the production of 15dPGJ2.

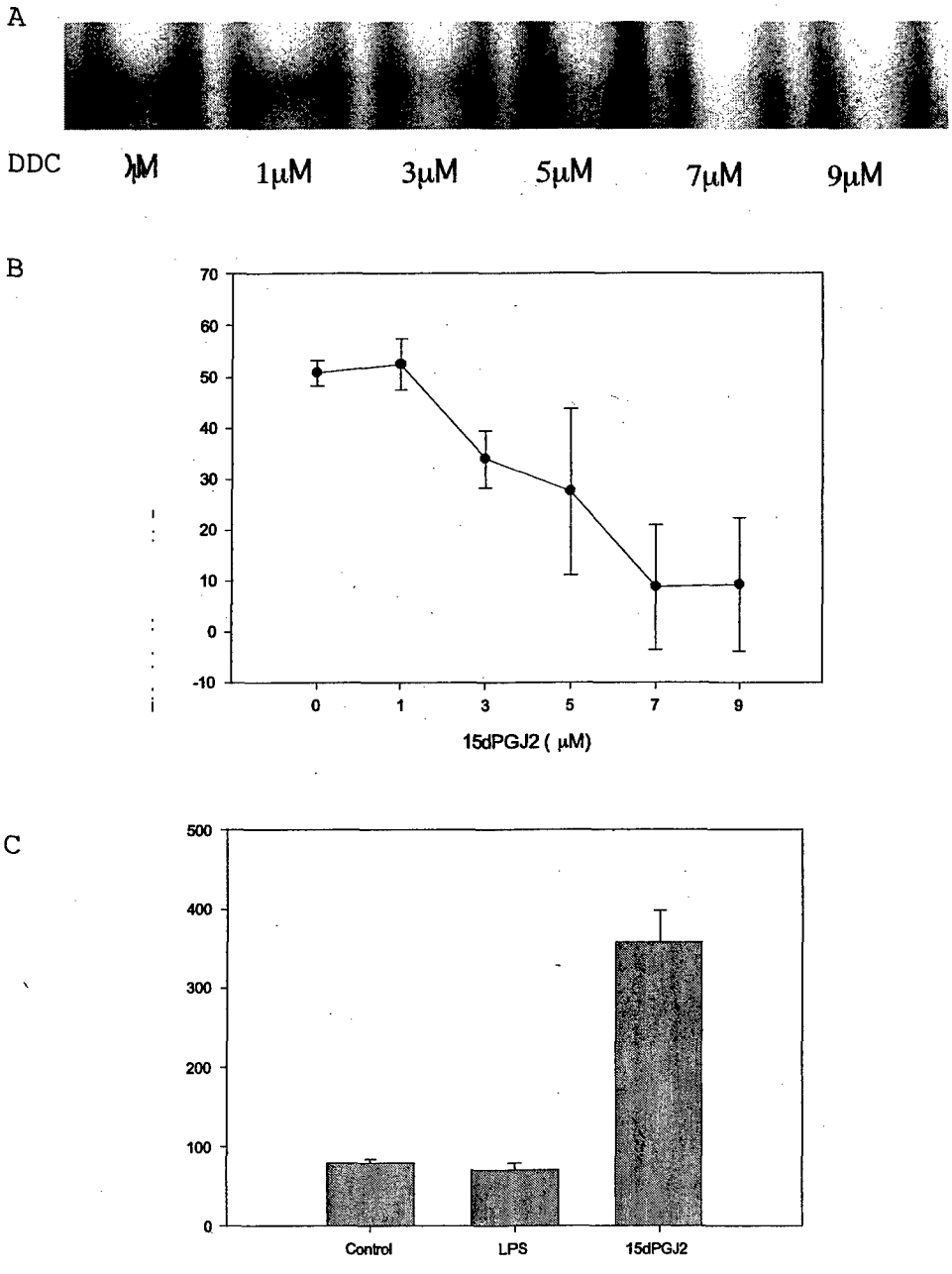

Figure 8. Effect of exogenous 15dPGJ2 on NFκB translocation in NRVM's. 15dPGJ2 blocks nuclear translocation of NFκB in a dose dependent manner, this was determined by EMSA (A). Multiple gels were integrated and the data combined (B). Addition of 15dPGJ2(7μM) sufficient to block NFκB translocation induces caspase 3 (C).

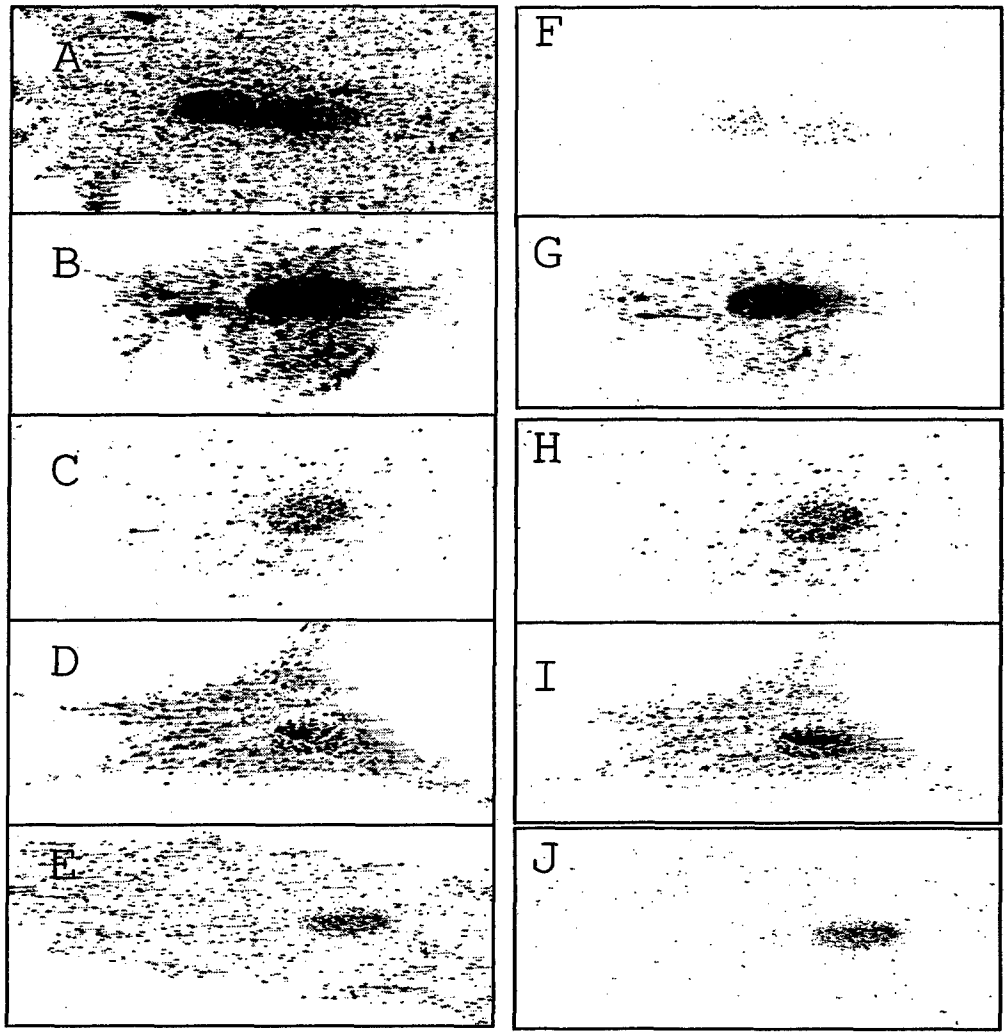

Figure 9. Inverse correlation between energized mitochondria and UCP-3 expression in NRVM's using deconvolution microscopy. Energised mitochondria were visualized using the membrane potential dye TMRE, as previously described by this lab(Sparagna, Hickson-Bick et al. 2000). UCP-3 was detected using an antibody and an appropriate fluorescent secondary antibody. Control cells (A & F) were not exposed to LPS. Subsequent images represent cells exposed to LPS for increasing periods of time; 1 hour (B & G), 2 hours (C & H), 4 hours (D & I) and 20 hours (E & J). Panels A through E include signals for

both TMRE and UCP-3 protein. In panels F through J only the signal for UCP-3 is reported.

References

Aderem, A. A. and Z. A. Cohn (1986). "Bacterial lipopolysaccharides modify signal transduction in the arachidonic acid cascade in macrophages." Ciba Found Symp **118**: 196-210.

Comstock, K. L., K. A. Krown, et al. (1998). "LPS-induced TNF-alpha release from and apoptosis in rat cardiomyocytes: obligatory role for CD14 in mediating the LPS response." J Mol Cell Cardiol **30**(12): 2761-75.

Dennis, E. A., E. J. Ackermann, et al. (1995). "Multiple forms of phospholipase A2 in macrophages capable of arachidonic acid release for eicosanoid biosynthesis." Adv Prostaglandin Thromboxane Leukot Res **23**: 75-80.

Garlid, K. D., M. Jaburek, et al. (2001). "Mechanism of uncoupling protein action." Biochem Soc Trans **29**(Pt 6): 803-6.

Gates, D. M. (1994). "Cardiac dysfunction in septic shock and multiple organ dysfunction syndrome." Crit Care Nurs Q **16**(4): 39-48.

Hickson-Bick, D. L., M. L. Buja, et al. (2000). "Palmitate-mediated alterations in the fatty acid metabolism of rat neonatal cardiac myocytes." J Mol Cell Cardiol **32**(3): 511-9.

Hickson-Bick, D. L., G. C. Sparagna, et al. (2002). "Palmitate-induced apoptosis in neonatal cardiomyocytes is not dependent on the generation of ROS." Am J Physiol Heart Circ Physiol **282**(2): H656-64.

Jung, F., U. Weiland, et al. (2001). "Chronic hypoxia induces apoptosis in cardiac myocytes: a possible role for Bcl-2-like proteins." Biochem Biophys Res Commun **286**(2): 419-25.

Liu, M. S. and J. J. Spitzer (1977). "In vitro effects of E. coli endotoxin on fatty acid and lactate oxidation in canine myocardium." Circ Shock **4**(2): 181-90.

Matsui, T. and A. Rosenzweig (2005). "Convergent signal transduction pathways controlling cardiomyocyte survival and function: the role of PI 3-kinase and Akt." J Mol Cell Cardiol **38**(1): 63-71.

Memon, R. A., N. M. Bass, et al. (1999). "Down-regulation of liver and heart specific fatty acid binding proteins by endotoxin and cytokines in vivo." Biochim Biophys Acta **1440**(1): 118-26.

Memon, R. A., K. R. Feingold, et al. (1998). "Regulation of fatty acid transport protein and fatty acid translocase mRNA levels by endotoxin and cytokines." Am J Physiol **274**(2 Pt 1): E210-7.

Memon, R. A., J. Fuller, et al. (1998). "In vivo regulation of acyl-CoA synthetase mRNA and activity by endotoxin and cytokines." Am J Physiol **275**(1 Pt 1): E64-72.

Russell, L. K., B. N. Finck, et al. (2005). "Mouse models of mitochondrial dysfunction and heart failure." J Mol Cell Cardiol **38**(1): 81-91.

Schrauwen, P. and M. K. Hesselink (2004). "The role of uncoupling protein 3 in fatty acid metabolism: protection against lipotoxicity?" Proc Nutr Soc **63**(2): 287-92.

Sparagna, G. C. and D. L. Hickson-Bick (1999). "Cardiac fatty acid metabolism and the induction of apoptosis." Am J Med Sci **318**(1): 15-21.

Sparagna, G. C., D. L. Hickson-Bick, et al. (2000). "A metabolic role for mitochondria in palmitate-induced cardiac myocyte apoptosis." Am J Physiol Heart Circ Physiol **279**(5): H2124-32.

Unger, R. H. and Y. T. Zhou (2001). "Lipotoxicity of beta-cells in obesity and in other causes of fatty acid spillover." Diabetes **50 Suppl 1**: S118-21.

Wright, G., I. S. Singh, et al. (2002). "Endotoxin stress-response in cardiomyocytes: NF-kappaB activation and tumor necrosis factor-alpha expression." Am J Physiol Heart Circ Physiol **282**(3): H872-9.

Project I.C.1.

Molecular Regulation of Apoptosis in Wound Healing

Investigator: Yong-Jian Geng, M.D., Ph.D.

1. Scientific background

Tissue response to injury caused by biochemical and biophysical factors in war and civilian life is a very complicated biological process. One of the most prominent pathological alterations occurring in tissue-injury and wound healing is the death of tissue cells. Cells may die through a death pathway, called necrosis, which caused primarily by extracellular insults, or through an intrinsic activation or inactivation of genes involved in a death process, referred to as apoptosis, a Greek word meaning "falling off of leaves and flowers from trees and plants". As a form of genetically programmed cell death, apoptosis plays an important role in elimination of damaged, aging and unwanted cells. The apoptotic death process occurs when expression of death-regulating genes is altered by intracellular and extracellular death signals. Several groups of proteins have been recently identified including the caspase family, the tumor necrosis factor receptor/Fas system, the anti-oncogene p53, and the Bcl2/Bax protein family. In contrast to necrosis, a form of non-programmed, accident cell death, apoptosis does not cause inflammatory response and exerts little damage to the tissue.

The healing phase of the tissue response to injury is equally complicated as the damage phase. Tissues undergoing wound healing exhibit great degrees of alterations in both cell type and number, involving a series of rapid increases in specific cell populations that repair the wounded tissues. Some of the tissue-repairing cells, in particular inflammatory cells and excess numbers of vascular cells, will be removed from the tissue with wound healing. Any group of the cells that stays in the tissue too short or too long ends up being an irritation and delays the ultimate outcome. Indeed, tissue repair requires rapid increases in specific cell populations to perform a specific task such as

inflammation, new blood vessel formation, and matrix protein synthesis. Upon completion of those tasks, the cells must leave the wound to allow for regeneration of the tissue. Eventually, the healing wound will become acellular and avascular. The potential mechanism that governs these events is apoptosis. Deregulation of apoptosis has been shown to disturb the wound healing process. Progression in understanding of the mechanisms controlling apoptosis and tissue repair may help develop new therapeutic strategies for healing the wound more effectively and quickly.

2. Hypothesis and specific aims

We hypothesize that apoptosis represents an important mechanism for regulation of cellular components in the wound healing process involved in vascular disease such as atherosclerosis. We plan to use genetically manipulated, atherosclerosis-prone animal models to examine apoptosis-regulating gene expression. Several gene products or proteins such as Fas, scavenger receptor and stress proteins may function alone or synergistically in regulation of lipid metabolism and apoptosis during wound healing. In this project, we will employ an in vitro cell culture system and molecular biology approaches to achieve the following aims:

Specific Aim 1: Characterize whether heat shock proteins regulate apoptosis by influencing expression of Fas and scavenger receptors in macrophages and vascular cells.

Specific Aim 2: Seek for and identify novel stress proteins, such as apolipoprotein-J, for their role in regulation of apoptosis of macrophages and vascular cells induced by oxidized lipoproteins and oxysterols.

3. Results

Fas-mediated vascular cell death in atherosclerosis.

We investigated whether the death-signaling receptor Fas is expressed in the aorta of apolipoprotein-E mice that develop hypercholesterolemia and atherosclerosis, highly similar to human atherosclerotic disease. Using microarray technology, we analyzed hundreds of different types of

genes including those regulating apoptosis in vascular cells stimulated with pro-apoptotic factors. Immunohistochemistry with anti-Fas antibodies was conducted on frozen sections. We observed that exposed to hypercholesterolemia, the aorta of apoE-null but not the wild type normal aorta developed atherosclerotic plaques that contained numerous Fas positive cells. Morphological and immunostaining revealed that those Fas positive cells had markers for macrophages and smooth muscle cells, suggesting that they came from the two cell lineages. TUNEL staining further confirmed the presence of apoptotic cells in the lesions which colocalized with Fas positive cells. Fluorescent microscopy of the sections stained with the fluorochrome DAPI displayed nuclear fragmentation and chromatin condensation, features of apoptotic nuclei.

Oxidative cholesterol-induced apoptosis of macrophages and smooth muscle cells.

Treatment with the oxidative derivatives of cholesterol induced apoptosis of vascular cells and macrophages in a dose-dependent manner. Analysis of DNA fragmentation by agarose gel electrophoresis shows marked increased internucleosomal fragments in the cultures. Western blot also showed release of cytochrome-C from the treated but not the untreated controls. Caspase staining and immunoblotting further showed the presence of activated caspases in the lesions. Both macrophages and smooth muscle cells contained apoptotic markers and the apoptotic cells localized in the lesional tissue but not normal arterial tissue.

Cholesterol cystalization and apoptosis of macrophages.

In the first year of this proposal, we focused on apoptosis of macrophages, a major type of inflammatory cells in wound healing. We observed that the products of lipoprotein oxidation trigger apoptosis of macrophages (1). We also found that expression of the class-A scavenger receptor, one of the receptors for oxidized low density lipoproteins, confers resistance of macrophages to apoptotic stimulation of oxidized lipoproteins and cholesteryl oxides. Human THP-1 cells express both Fas and caspase-3 but no major change in their expression were detected when apoptosis was induced by oxysterol and sodium fluoride. Analysis of mRNA and proteins indicates expression of heat shock proteins in arterial tissue

injured with atherosclerosis (2). However, some isoforms of the heat shock proteins appeared at lower levels compared to others, suggesting differences in expression of stress proteins in the tissue healing process. Thus, expression of lipid-binding and stress proteins may participate in regulation of apoptosis in wound healing.

4. Military significance and public purpose

Repairing or healing a wounded tissue is a process with significant influence on the lives of wounded solders from the battlefield as well as civilians during the war and peacetime. In particular, continuing previous work, this study has provided evidence that atherogenic substances may have impact on vascular cell death by apoptosis. Several potential molecular mechanisms responsible for apoptosis in wound have been exploited including stress-responding proteins. Experimental information from this study may help design new methods to promoting wound healing. Accomplishment of this goal is anticipated to shed new insight into the etiology and diagnosis of wound healing disorders, which threaten lives of both solders and civilians.

5. Technical Objectives and Methods

This study employed a variety of techniques in biochemistry and cellular and molecular biology to determine the molecules involved in regulation of apoptosis including the state-of-the art real time quantitative PCR, in situ DNA end-labeling, pulse field DNA electrophoresis and cDNA microarrays. By immunocytochemistry and immunoblotting, both anti- and pro-apoptotic proteins will be determined in inflammatory cells and vascular cells such as macrophages, endothelial cells, and smooth muscle cells. In addition, extracellular matrix proteins were examined for their integrity and biological function in regulation of apoptosis as well as proliferation. Recombination techniques were used for producing proteins from wounded tissues, and tested for their effects on apoptosis and proliferation.

6. Personnel

Yong-Jian Geng, MD, PhD, Associate Professor of Medicine and Director, Research Center for Cardiovascular Biology

and Atherosclerosis, responsible for experiment designation and performance, data collection and evaluation, and for supervising research fellows and technicians, and coordinating with other projects.

Kilsoo Kil, PhD, research fellow, responsible for laboratory management and for analysis of expression of apoptosis-regulating genes.

Mitra Rajabi, MD, research fellow, graduated in Telran University, took charge of the studies on stress response and expression of iNOS in vascular cells.

7. Human study

No human subject studies will be performed in this project.

8 Animal study

No in vivo studies are performed on animals in this projects.

9. Bibliography

Peer-reviewed full-size publications

1. **Geng YJ**. Molecular signal transduction in vascular cell apoptosis. Cell Res. 2001;11:253-64.
2. **Geng YJ**. Biologic effect and molecular regulation of vascular apoptosis in atherosclerosis. Curr Atheroscler Rep. 2001;3:234-42.
3. Phillips JE, **Geng YJ**, Mason RP. 7-Ketocholesterol forms crystalline domains in model membranes and murine aortic smooth muscle cells. Atherosclerosis. 2001;159:125-135.
4. Hardt SE, **Geng YJ**, Montagne O, Asai K, Hong C, Yang GP, Bishop SP, Kim SJ, Vatner DE, Seidman CE, Seidman JG, Homcy CJ, Vatner SF. Accelerated cardiomyopathy in mice with overexpression of cardiac G(s)alpha and a missense mutation in the alpha-myosin heavy chain. Circulation. 2002;105:614-620.
5. Wang J, **Geng YJ**, Guo B, Klima T, Lal BN, Willerson JT, Casscells W. Near-infrared spectroscopic characterization of human advanced atherosclerotic

plaques. Journal of the American College of Cardiology. 2002;39:1305-1313.

6. De Nigris F, Lerman A, Ignarro LJ, Williams-Ignarro S, Sica V, Baker AH, Lerman LO, **Geng YJ**, Napoli C. Oxidation-sensitive mechanisms, vascular apoptosis and atherosclerosis. Trends in Molecular Medicine. 2003;9:351-359.
7. **Geng YJ**. Molecular mechanisms for cardiovascular stem cell apoptosis and growth in the hearts with atherosclerotic coronary disease and ischemic heart failure. In: Apoptosis: From Signaling Pathways to Therapeutic Tools; 2003:687-697.
8. **Geng YJ**, Phillips JE, Mason RP, Casscells SW. Cholesterol crystallization and macrophage apoptosis: implication for atherosclerotic plaque instability and rupture. Biochemical Pharmacology. 2003;66:1485-1492.
9. Perin EC, Dohmann HFR, Borojevic R, Silva SA, Sousa ALS, Mesquita CT, Rossi MID, Carvalho AC, Dutra HS, Dohmann HJF, Silva GV, Belem L, Vivacqua R, Rangel FOD, Esporcatte R, **Geng YJ**, Vaughn WK, Assad JAR, Mesquita ET, Willerson JT. Transendocardial, autologous bone marrow cell transplantation for severe, chronic ischemic heart failure. Circulation. 2003;107:2294-2302.
10. Perin EC, **Geng YJ**, Willerson JT. Adult stem cell therapy in perspective. Circulation. 2003;107:935-938.
11. Guidry TV, Olsen M, Kil KS, Hunter RL, **Geng YJ**, Actor JK. Failure of CD1D(-/-) mice to elicit hypersensitive granulomas to mycobacterial cord factor trehalose 6,6 '-dimycolate. Journal of Interferon and Cytokine Research. 2004;24:362-371.
12. Li S, Lin J, Lenehan E, Liu J, Long C, Liu J, **Geng YJ**. Myocardial protection of warm cardioplegic induction on the isolated perfused rat heart model. J Extra Corpor Technol. 2004;36(1):58-65.
13. Silva GV, Litovsky S, Assad JAR, Sousa ALS, Martin BR, Vela D, Coulter SC, Ling J, Ober J, Vaughn WK, Branco RVC, Oliveira ED, He R, **Geng YJ**, Willerson JT, Perin EC. Mesenchymal Stem Cells Differentiate into an Endothelial Phenotype, Enhance Vascular Density, and Improve Heart Function in a Canine Chronic Ischemia Model. Circulation. 2004;In press.

Cited Abstracts

1. Chang J, Willerson JT, Knowlton AA, **Geng YJ**, He D, Lal BN, Tewatia T, Casscells W. Differential expression of heat shock proteins in human atherosclerotic plaques. Faseb Journal. 2000;14:A453-A453.
2. **Geng YJ**, Kil KS, Casscells SW, Willerson JT. cDNA array analysis of gene expression in the aortas of apolipoprotein-E deficient mice with atherosclerosis. Circulation. 2000;102:43-43.
3. Mason RP, **Geng YJ**, Phillips JE. 7-ketocholesterol, but not 25-hydroxycholesterol, forms immiscible domains in model membranes and murine aortic smooth muscle cells. Biophysical Journal. 2000;78:184A-184A.
4. McAneny CS, Bogdanov M, Xu XQ, Dowhan W, Willerson JT, **Geng YJ**. Apolipoprotein-J expression and binding to plaque-derived lipids in apolipoprotein-E deficient mice: Characterization by Eastern-Western blotting. Circulation. 2000;102:315-315.
5. Lal BN, Casscells SW, Willerson JT, **Geng YJ**. Short term thermal treatment enhances apoptosis, reduces cytokine expression in atherosclerotic plaques, and inactivates NF-kappa B in cultured macrophages. Circulation. 2001;104:294-294.
6. Litovsky S, **Geng YJ**, Naghavi M, Casscells W, Willerson JT, Buja LM. What are the ultrastructural correlates of apoptosis in the atherosclerotic plaque? Modern Pathology. 2001;14:45A-45A.
7. **Geng YJ**, Han XL, Carville AAL, Simon MA, Shannon RP. Cardiac expression of TNF alpha is associated with upregulation of the fas receptor on cardiac myocytes and increased myocyte apoptosis in non human primates with AIDS cardiomyopathy. Circulation. 2001;104:294-294.
8. Tewatia T, Wu CJ, Xu XG, Kil KS, Willerson JT, Casscells SW, **Geng YJ**. Selective induction of apoptosis in the atherosclerotic aortas of apolipoprotein-E deficient mice by short-term thermal therapy. Journal of the American College of Cardiology. 2001;37:256A-256A.
9. Ahmed S, **Geng YJ**, Zhang K, Arnett F, Tan F. Systemic sclerosis sera induces apoptosis and expression of fibrillin-1 in human dermal endothelial cells. Arthritis and Rheumatism. 2002;46:S601-S601.
10. Kim SJ, Kim YK, Takagi G, Huang CH, **Geng YJ**, Vatner SF. Enhanced iNOS function in myocytes one day after brief ischemic episode. American Journal of

Physiology-Heart and Circulatory Physiology. 2002;282:H423-H428.

11. Li S, Lin J, **Geng YJ.** Assessment of embryonic stem cell emigration into the ischemic myocardium by use of a Langendorff perfusion model. Circulation. 2002;106:13-13.

12. Ahmed SS, Arnett FC, **Geng YJ**, Jin L, Reveille JD, Mayes MD, Tan FK. The immunoglobulin fraction of scleroderma sera activates pathways of inflammation, fibrosis and apoptosis in adult human dermal endothelial cells. Arthritis and Rheumatism. 2003;48:3619-3619.

13. Kil KS, **Geng YJ.** Regulation of cell survival and apoptosis by the nulear protein, PW29, highly expressed in atherosclerotic lesions. Faseb Journal. 2003;17:A799-A800.

14. Madonna R, Di Napoli P, Grilli A, Massaro M, Felaco M, **Geng YJ**, De Caterina R. Statins attenuate the expression of inducible nitric oxide synthase in cardiac myoblasts - possible link to direct myocardial protection during ischaemia-reperfusion. European Heart Journal. 2003;24:662-662.

15. Madonna R, **Geng YJ**, Di Napoli P, Grilli A, Felaco M, De Caterina R. Inhibition of 3-hydroxy-3-methylglutaryl coenzyme-A reductase attenuates expression of inducible nitric oxide synthase in cardiac mybblasts. Faseb Journal. 2003;17:A264-A264.

16. Morishima S, Wasler MJ, Rosales C, **Geng YJ.** Possible roles of Kv 1.5 potassium channel in the development of mouse cardiomyocytes from embryonic stem cells. Faseb Journal. 2003;17:A684-A684.

17. Perin EC, Dohmann HF, Borojevic R, Sousa ALS, Dohmann H, Carvalho AC, **Geng YJ**, Silva GV, Rangel F, Silva SA, Esporcatte R, Willerson JT. Improvement in symptoms and exercise capacity at eight weeks in a controlled study of autologous bone marrow cell transplant in humans with severe ischemic heart failure. Journal of the American College of Cardiology. 2003;41:44A-44A.

18. Perin EC, Dohmann HF, Borojevic R, Dohmann HJ, Carvalho AC, **Geng YJ**, Sousa ALS, Silva GV, Rangel F, Silva SA, Rossi I, Esporcatte R, Willerson JT. Improvement in global and segmental left ventricular contractility following autologous bone marrow cell transplantation in humans with severe ischemic heart failure. Journal of the American College of Cardiology. 2003;41:219A-219A.

19. Perin EC, **Geng YJ**, Sousa ALS, Silva GV, Coulter S, Jing L, Ober J, Martin BJ, Willerson JT. Intramyocardial delivery of bone marrow-derived mesenchymal stem cells improves myocardial contractility in a chronic ischemic model. Journal of the American College of Cardiology. 2003;41:296A-296A.
20. Rajabi M, Lin J, Casscells SW, Willerson JT, **Geng YJ**. Heat shock regulation of inducible nitric oxide (NO) synthase in aortic smooth muscle cells. Faseb Journal. 2003;17:A660-A660.
21. Rosales C, Morishima S, Lin J, Wassler MJ, **Geng YJ**. Regulation of stem cell survival and differentiation into cardiac myocytes by leukemia inhibiting factor and dimethyl sulfoxide (DMSO). Faseb Journal. 2003;17:A683-A683.
22. Tang DM, Rajabi M, Lin J, **Geng YJ**. High fat diet induces CDI expression in transgenic mice overexpressing apolipoprotein-J. Faseb Journal. 2003;17:A266-A266.
23. Wassler MJ, Morishima S, **Geng YJ**, Shur BD. cDNA cloning and characterization of GtBP1, a NICE-like protein expressed during embryonic cell development. Faseb Journal. 2003;17:A684-A684.
24. **Geng YJ**, Tang DM. Vascular smooth muscle cell express CD1d in response to lipids and present CD1-restricted lipid antigens to T cells. Atherosclerosis Supplements. 2003;4:318-318.
25. Achour HC, Boccalandro F, Buja ML, **Geng YJ**, Amirian J, Felli P, Smalling RW. Effects of mechanical left ventricular unloading on endothelin-1 release and apoptosis. Journal of the American College of Cardiology. 2004;43:263A-264A.
26. Alford AC, Rajabi M, Taffet GE, **Geng YJ**. Apoptosis and stiffness of the arteries of mice prone to atherosclerosis. Journal of the American Geriatrics Society. 2004;52:S8-S8.
27. Li S, Lin J, Lenehan E, Rajabi M, Madonna R, Rosales C, Willerson JT, **Geng YJ**. Cardiac responses to intracoronary-delivered stem cells in apolipoprotein-null mice: Assessment by Langendorff perfusion. Journal of the American College of Cardiology. 2004;43:155A-156A.
28. Lin J, Li S, Lenehan E, Rajabi M, Madonna R, Rosales C, Willerson JT, **Geng YJ**. Ischemic precondition improves performance of the hearts with coronary delivery of embryonic stem cells: Assessment by a

Langendorff perfusion model. Journal of the American College of Cardiology. 2004;43:178A-178A.

29. Madonna R, Li S, Lin J, Rajabi M, Wassler M, **Geng YJ.** Isolation and characterization of undifferentiated endothelial cell progenitors from murine adipose tissue. Faseb Journal. 2004;18:A182-A182.
30. Madonna R, Di Napoli P, Massaro M, Grilli A, Felaco M, **Geng YJ,** De Caterina R. Inhibition of 3-hydroxy-3-methylglutaryl coenzyme a reductase attenuates expression of inducible nitric oxide synthase in cardiac myocytes: A possible link with direct myocardial protection during ischemia-reperfusion. Journal of the American College of Cardiology. 2004;43:27A-28A.
31. Morishima S, Wassler MJ, Rosales C, Cheng MF, Cheng J, **Geng YJ.** Potassium channels contribute to the formation of embryonic bodies from murine embryonic stem cells. Faseb Journal. 2004;18:A1286-A1286.
32. Perin EC, Dohmann HF, Borejevic R, Assad JA, Silva GV, Silva SA, Sousa AL, Vaughn WK, Rossi I, Carvalho AC, **Geng YJ,** Dohrmann HJ, Willerson JT. Transendocardial injection of autologous bone marrow mononuclear cells may enhance myocardial viability around cell injection site. Journal of the American College of Cardiology. 2004;43:186A-187A.
33. Rajabi M, **Geng YJ.** Gelsolin contributes to heat shock-induced reduction in expression of inducible nitric oxide synthase (iNOS) by smooth muscle cells. Faseb Journal. 2004;18:A13-A14.
34. Tang D, **Geng YJ.** Expression of the cluster of differentiation (CD)-1d molecule and lipid antigen presentation in vascular smooth muscle cells. Faseb Journal. 2004;18:A433-A433.

Project I.C.2.
Infrared Spectroscopic Diagnosis of Vulnerable Atherosclerotic Plaque

Investigator: S. Ward Casscells, M.D.

Abstract

Detection of vulnerable plaques as the underlying cause of myocardial infarction is at the center of attention in cardiology. We have previously shown that infiltration of inflammatory cells in atherosclerotic plaques renders these plaques relatively hot and acidic, with substantial plaque temperature and pH variation. The objective of this investigation was to determine whether near-infrared diffuse reflectance spectroscopy (NIRS) could be used to non-destructively measure the tissue pH in atherosclerotic plaques. NIRS and tissue pH electrode measurements were taken on freshly excised carotid plaques maintained under physiological conditions. The coefficient of determination between NIRS and the pH microelectrode measurement was 0.75 using 17 different areas. The estimated accuracy of the NIRS measurement was 0.09 pH units. These results demonstrate the feasibility of using NIRS tissue pH in freshly excised atherosclerotic plaques in light of marked pH heterogeneity and warrants future in-vivo investigations on pH measurement of atherosclerotic plaques.

Introduction

The large body of atherosclerosis research to date describes the vulnerable plaque retrospectively as the culprit lesion prone to rupture or erosion causing acute and/or fatal cardiac events [1]. Structural classification of the relative sizes of the fibrous cap and lipid cores have been used to characterize plaques after surgical intervention and histology, or with several promising new minimally or non-invasive techniques such as intravascular ultrasound [2, 3], MRI [4, 5] and optical coherence tomography [6]. Major and minor criteria for the diagnosis of vulnerable plaque have recently been reviewed [7]. Although it is widely accepted that plaque rupture or erosion depends more on the plaque composition than on the degree of stenosis, new modalities that target the

detection of inflammation, thin cap/large lipid pools, endothelial denudation, and/or plaque fissuring, in addition to standard angiographic stenosis detection, need to be developed in order for the major criteria to be realized and quantified in a high-risk 'vulnerable patient' population.

Functional classification based on physiological and inflammatory processes was initially proposed as an adjunct to structural information by Naghavi et al. [8] Macrophages and inflammatory cells, found preferentially in vulnerable plaque, might contribute to plaque rupture through the release of proteases [9]. Thermal sensors have been employed to study the relation between functional and structural heterogeneity, and may be a useful functional measure of vulnerability [10, 11]. Temperature change correlated with the cell density and proximity of cells to the fibrous cap [10]. Lower pH in lipid-rich plaques and considerable pH heterogeneity has been also demonstrated in human atherosclerotic lesions, and Watanabe cholesterol-fed rabbits [12].

Near-infrared spectroscopy (NIRS) is one of many techniques available for non-destructive analysis of tissues. The determination of tissue pH using NIRS has been reported in the muscle during ischemia [13] and in the intestines during hemorrhagic shock [14]. It is relatively inexpensive compared to other modalities such as NMR, ultrasound, and nuclear (X-ray) radiography. Spectroscopic methods have been proposed by several researchers to characterize the relatively static, structural or chemical properties of atherosclerotic plaques in ex-vivo tissue [15, 16, 17]. In order to investigate a functional classification technique based on metabolism, this study focused on determining the feasibility of using NIRS to measure tissue pH in a oxygenated media bath preparation that maintained the plaque in as close to in-vivo status as possible.

Methods

Tissue Preparation

Fresh carotid plaque tissue was collected from 5 patients at the University of Massachusetts Memorial Medical Center's Vascular Surgery operations at the University Campus over a period of 3 months under approval by the Institutional Review Board for human studies (Docket 10041). The plaque was immediately placed in a tissue

culture medium (minimum essential medium (MEM); Invitrogen, Md., USA) that had a pH of 7.4, and contained 5.6 m*M* glucose, 26.2 m*M* sodium bicarbonate, and non-essential amino acids supplement. The plaque was maintained at 37°C in a heated porcelain bath and bubbled continuously with a 75% O2/20% N2/5% CO2 gas mixture. The media bath was equilibrated with the gas mixture for a half hour prior to tissue addition. The entire tissue bath apparatus was enclosed in a humidified 37°C incubator. The MEM was chosen because it was the only available prepared sterile liquid media with high glucose concentration that did not contain phenol red, a pH-sensitive, colored dye that is used to indicate gross pH changes in the liquid media. Phenol red would interfere with the spectral data collection in the visible (500-700 nm) regions and therefore was avoided. This procedure was used for each plaque from the 5 patients and all spectral, tissue pH, and temperature measurements while the plaque was immersed in the oxygenated media.

Instrumentation

Spectra from 667 to 2,436 nm (15,000-4,097 cm-1) were collected using a Nicolet Nexus 670 Fourier transform near-infrared spectrometer (75 W tungsten-halogen lamp/quartz beam splitter) employing a room temperature InGaAs detector and a fiber optic probe module connected to a fiber optic sensor (described below). The acquisition time was ~42 s for each spectrum; 128 interferogram scans were collected and averaged at a spectral resolution of 32 cm-1 (~2.5 nm). A reference spectrum was collected using a 50% reflectance standard (Labsphere, N.H., USA) prior to each tissue spectrum. The software automatically calculates the absorbance spectrum for each tissue measurement. Additional spectral data from 400 to 1,100 nm were taken with the same fiber optic sensor using a Control Development (South Bend, Ind., USA) 512 element photodiode array (PDA) spectrometer with a room-temperature silicon detector, and converted to absorbance using a dark current-corrected, reference spectrum. The spectral resolution of the PDA spectrometer was 0.5 nm. The light source used was a separate unmodulated, ~7.5 W tungsten-halogen lamp (Ocean Optics, Fla., USA). The integration time was set to 3.6 s, and sample averaging to 15, resulting in an acquisition time of 54 s on the PDA spectrometer. The visible tissue spectrum from the PDA spectrometer was offset to the peak value at 970 nm for the same tissue spectrum collected on the FT-NIR

spectrometer, and the data were spliced together to form a full-range spectrum (400-2,400 nm).

The fiber-optic, diffuse reflectance sensor used in this study had a forward-viewing design with an optical window. The 1-mm-thick quartz optical window was mounted on the face of the sensor. A center bundle of seven fibers was separated from an outer ring of twelve fibers by 0.005 cm, which provided a minimum optical depth penetration of 450 μm thickness in aortic tissue for wavelengths of 500-2,250 nm.

Micro-pH electrodes in a sharp, beveled 21-gauge needle (~750 μm diameter, MI-407; Microelectrodes Inc., N.H,, USA) were used to make the reference tissue pH measurements. The reference junction electrode was placed in the media bath and both electrodes are connected to a Thermo Orion 720A pH meter. The electrodes were calibrated prior to each experiment using five NIST-traceable buffers (Fisher Scientific, 4.00, 6.00, 7.00, 7.40, and 10.00 at 25°C). The pH meter readout was automatically temperature-corrected to the in-vitro media temperature. The tissue pH measurements were recorded after spectral acquisition from the same plaque location used for spectral assessment. Tissue temperature measurements were also made in the same location using a T-type needle thermistor probe (Omega Engineering, Conn., USA). After each tissue pH measurement, the electrodes were rinsed in warm Tergazyme solution and distilled water, then checked for drift in a 4.00 buffer at 37°C. This was done to avoid protein buildup and electrode drift from location to location. The total time allotted for performing accurate measurements (including the 30-min tissue equilibration) was no more than 4 h, to ensure plaques were physiological (data not shown). An average of 4 points were collected from each of the 5 plaques. A total of 20 points were collected.

Data Analysis and Multivariate Calibration

The quantitative determination of NIRS tissue pH was performed using multivariate calibration or chemometric techniques. Partial least squares data analysis (PLS) [18, 19] and leave one sample out cross-validation were performed. Briefly, the spectral data are compressed and a linear regression is made against the known reference tissue pH values (or other desired analyte) and a mathematical model is created. Statistical methods, based on an F-ratio test, are used to remove points that are

extreme outliers from the rest of the data set [19]. The optimal number of vectors to which the spectral data are compressed is determined by the cross-validation procedure such that the error in the NIRS predicted values is minimized. These vectors can be qualitatively reviewed after calibration to determine if the model is appropriate for the system studied [18]. An appropriate model will contain vectors that represent the chemical species responsible for the analyte being measured. The ability of the NIRS model to predict trends in pH is assessed by calculating the coefficient of determination (R2), and the accuracy of the pH measurement is assessed by calculating the cross-validated standard error of prediction [19]. All calculations were performed using Grams32/PLSIQ software (Galactic Industries, N.H., USA).

Results

The reference pH values measured with the microelectrodes and the tissue temperatures were analyzed prior to developing PLS models. No correlation was observed in the points used for the PLS tissue pH model. The correlation (R2) between tissue pH and tissue temperature data was 0.002.

The spectra from 5 plaques (a total of 17 distinct data points from 5 patients) are shown in figure 1. Three pH values were removed from the 20 collected based on statistical outlier detection (F ratio >3). The most accurate PLS models were developed using three distinct spectral regions, rather than the entire spectral range. The spectral regions are marked in figure 1 (region 1: 400-615 nm, region 2: 924-1,889 nm, and region 3: 2,043-2,341 nm). The correlation of the NIRS pH values to the reference values is shown in figure 2. The coefficient of determination was 0.75 and estimated accuracy was 0.09 pH units. The range of the reference tissue pH was 6.99-7.55. The optimal number of vectors in the model was 3. This calibration model has acceptable results using 17 points.

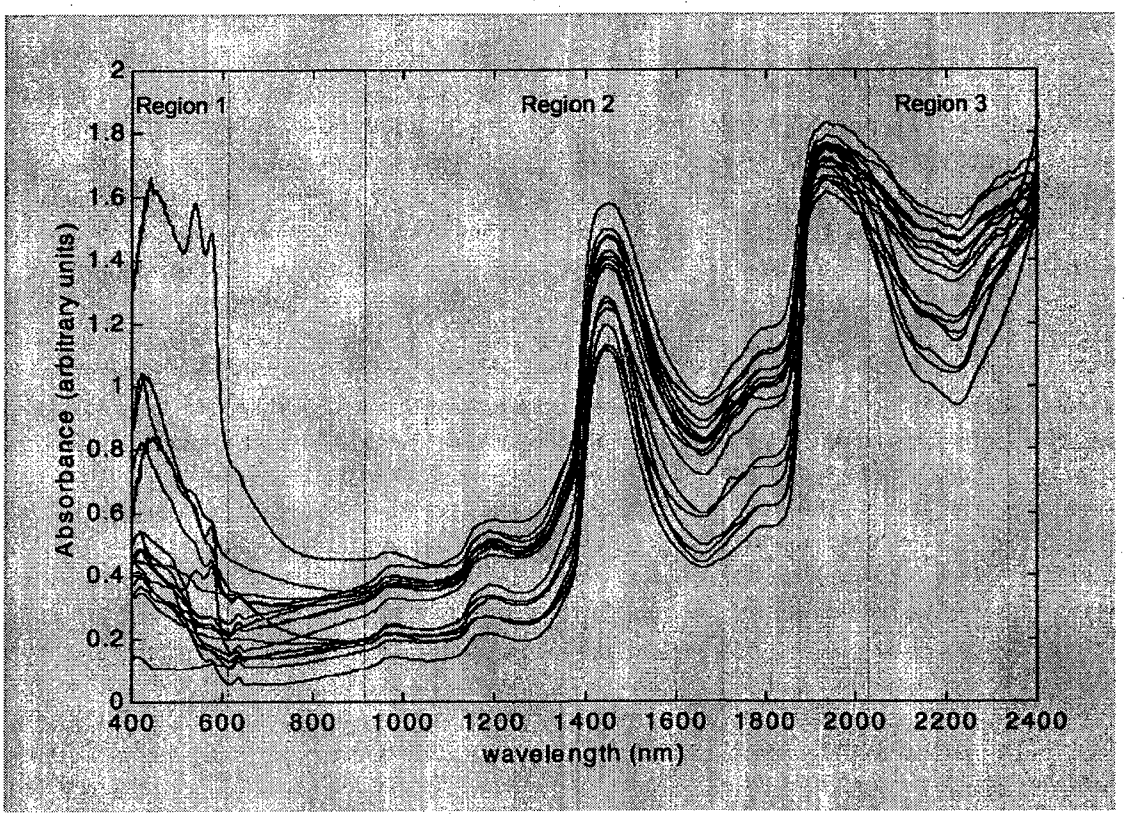

Fig. 1. Seventeen spectra from 5 human carotid plaques measured in-vitro oxygenated tissue culture at 37°C. The three spectral regions used solely for the PLS models are marked. Region 1: 400-615 nm, region 2: 924-1,889 nm, and region 3: 2,043- 2,341 nm.

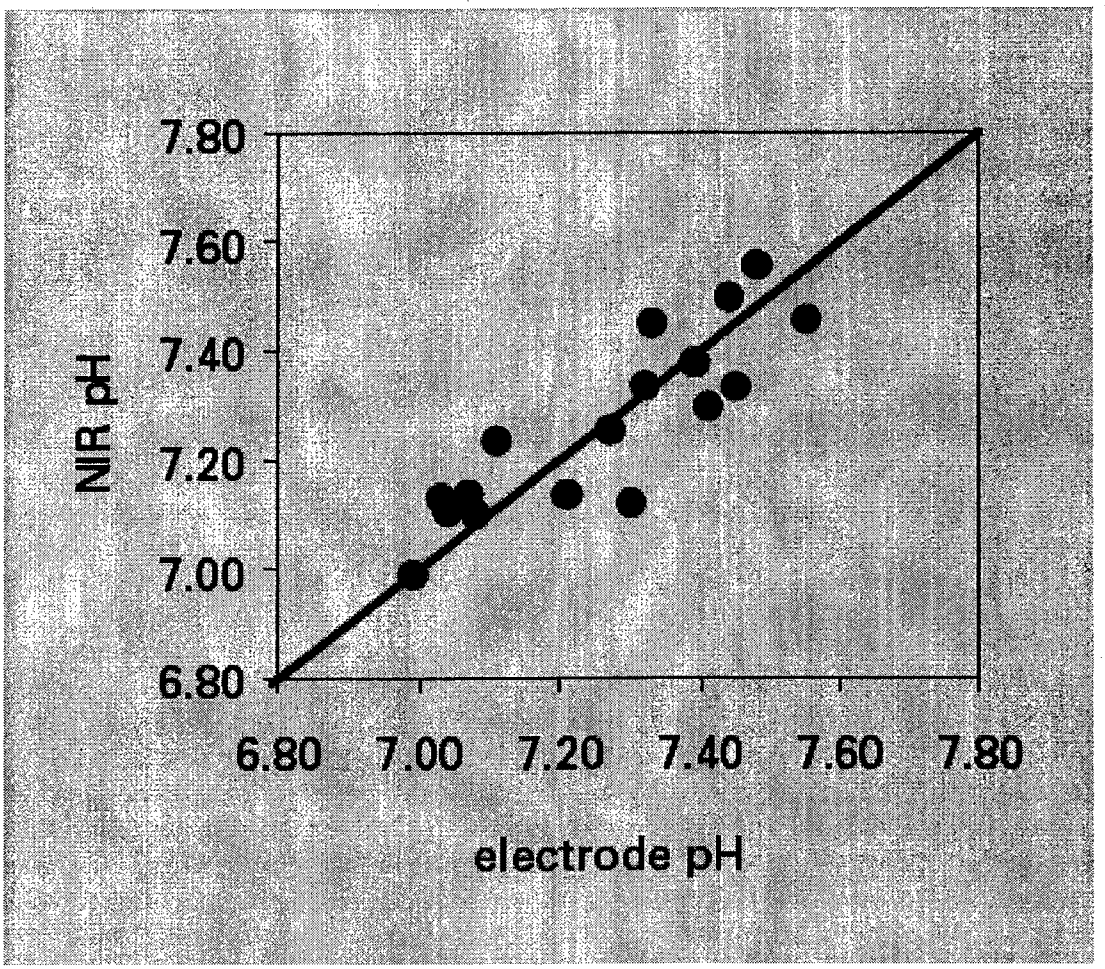

Fig. 2. Correlation between the tissue pH measured with microelectrodes in 5 human carotid-plaque in-vitro tissue culture media and the NIRS pH determination. Solid line is unity line. Coefficient of determination, R2 = 0.75. Estimated accuracy of NIRS pH was 0.09 pH units.

The chemical peaks for the spectra (fig. 1) are assigned and listed in table 1. Between 500 and 600 nm, the spectral features are varied. Not all the spectra exhibit hemoglobin bands, and in some spectra, the signal is

fairly flat and featureless. There is an anomaly observed at 633 nm in all spectra. This was investigated and found to be unrelated to the tissue characteristics, and the spectral data from 615 to 920 nm were not used in the model. The topmost spectrum was taken from an area of plaque that contained a large amount of blood. Below ~515 nm of this spectrum, strong hemoglobin absorption occurs (~10 times or an order of magnitude higher than the amount at 575 nm). The observed muted signal is a result of the spectrometer's decreased efficiency below 515 nm. Region 2 is dominated by the water peak at ~1,450 nm. Various proteins and lipids absorb in both region 2 and 3.

Peak wavelength, nm	Chemical species	References
417	OxyHb	23
540	OxyHb, OxyMb	23, 24
574	OxyHb	23
633	optical anomaly	removed before models built
970	water	25
1,196	water	26
1,449	water	27
1,650	OxyHb	20
1,730 (weak, broad)	cholesterol, lipids, alkyl CH groups, proteins	27, 28
1,780 (weak, broad)	cholesterol, lipids, alkyl CH groups, proteins	27, 28
1,943	water (lipids)	26 (28)
2,168 (weak)	non-specific proteins	27
2,318 (weak, broad, shoulder)	C-H combinations from lipids	17, 28

Hb = Hemoglobin; Mb = myoglobin.

Table 1. Peak assignments for spectra shown in figure 1

The percent variance captured is summarized in table 2. For each additional vector used, the more variance is explained in both the spectral (X) and reference pH (Y) data. The percent variance captured by each vector is calculated by taking the difference between the sum of squares (variance) of the reconstructed spectra using *n* vectors and the variance of the reconstructed spectra

using *n - 1* vectors, over the total variance of the original spectra. This is calculated in a similar fashion for the pH values. The total, or cumulative, % variance describes how much improvement that the successive vector has in capturing the total variability in the original spectra (X) or measured pH values (Y) in an additive fashion. More vectors would capture more variability, and eventually describe the original system. However, too many vectors can also lead to overfit of the model, and lead to erroneous prediction of NIR pH values if not monitored. Incremental variability could be due to spectral noise and not real variability of the tissue pH. Table 2 shows that using three vectors to reconstruct and model the data, 98% of the original spectral variance (X) is captured. The corresponding ability of the three vectors used in the model to predict NIR pH values shows that 84.3% of the original tissue pH variance (Y) is captured.

Factor No.	Spectral variance (X)		Reference tissue pH variance (Y)	
	% variance captured	total %	% variance captured	total %
1	48.9	48.9	57.8	57.8
2	45.1	94	7.3	65.1
3	4.0	98	19.2	84.3

Table 2. Percent variance captured by PLS tissue pH model shown in figure 2. Variance of original data captured by reconstructed spectra (X) and pH values (Y) from each successive vector in a linear additive fashion

Figure 3 depicts the three model vectors used and their contribution to the tissue pH calibration in each wavelength region used. Figure 3a shows the three vectors in spectral region 1 (400-615 nm). The second vector (dashed) clearly shows the oxyhemoglobin doublet at 540 and 574 nm. The first vector (solid line) shows the doublet albeit with a lesser magnitude. Figure 3b shows

the three model vectors in spectral region 2 (924-1,889 nm). The water band at ~1,450 nm is a strong contributor and is apparent in all three vectors in this region. A small oxyhemoglobin band at 1,650 nm is also apparent in all three vectors. Figure 3c shows the three vectors in spectral region 3. Many non-specific proteins and lipids absorb in this region. Using the region 3, model vectors did not significantly improve or degrade the overall model in terms of correlation and accuracy of the NIRS pH values.

Discussion

The quantitative model results showed that tissue pH determination in atherosclerotic plaque is feasible. Qualitatively, this model has vectors that resemble hemoglobin and water absorption. The cumulative percent variation captured by the three vectors, in each wavelength region contributing to the model, showed positive correlation peaks at the wavelengths where oxyhemoglobin absorb in both the visible (fig. 3a, vectors 2 and 3) and near-infrared (fig. 3b, vector 1). Alam et al. [20] demonstrated in lysed blood experiments that the 1,650-nm peak is a pH-inducible shift in the absorption spectrum of the histidine residue of the hemoglobin molecule, further corroborating the validity of the tissue pH model in atherosclerotic plaques. The other dominant feature contributing to the NIRS pH model is water at 1,450 nm (fig. 3, center plot, vector 3). This may be related to hydrogen-bonding effects from pH-induced changes in water. Most of the spectral variation is captured by the third factor (98%); however, only 84% of the variation in the reference tissue pH was explained. This unmodeled variability could account for the limited accuracy of the model. Additional vectors could be used; however, this both increases model complexity and unwanted noise correlation. An optimal model using a three-vector model is acceptable for the 17 points used for the tissue pH determination and does not indicate over- or underfit of the data [21].

The reference pH values were consistent with the pH values observed in prior plaque studies [8, 12]. The electrodes have a reported measurement error of 0.03 pH units. However, the volume of tissue measured optically may be too large compared to the approximate volume measured by the electrode measurement. This difference in volume may affect the calibration accuracy and prediction.

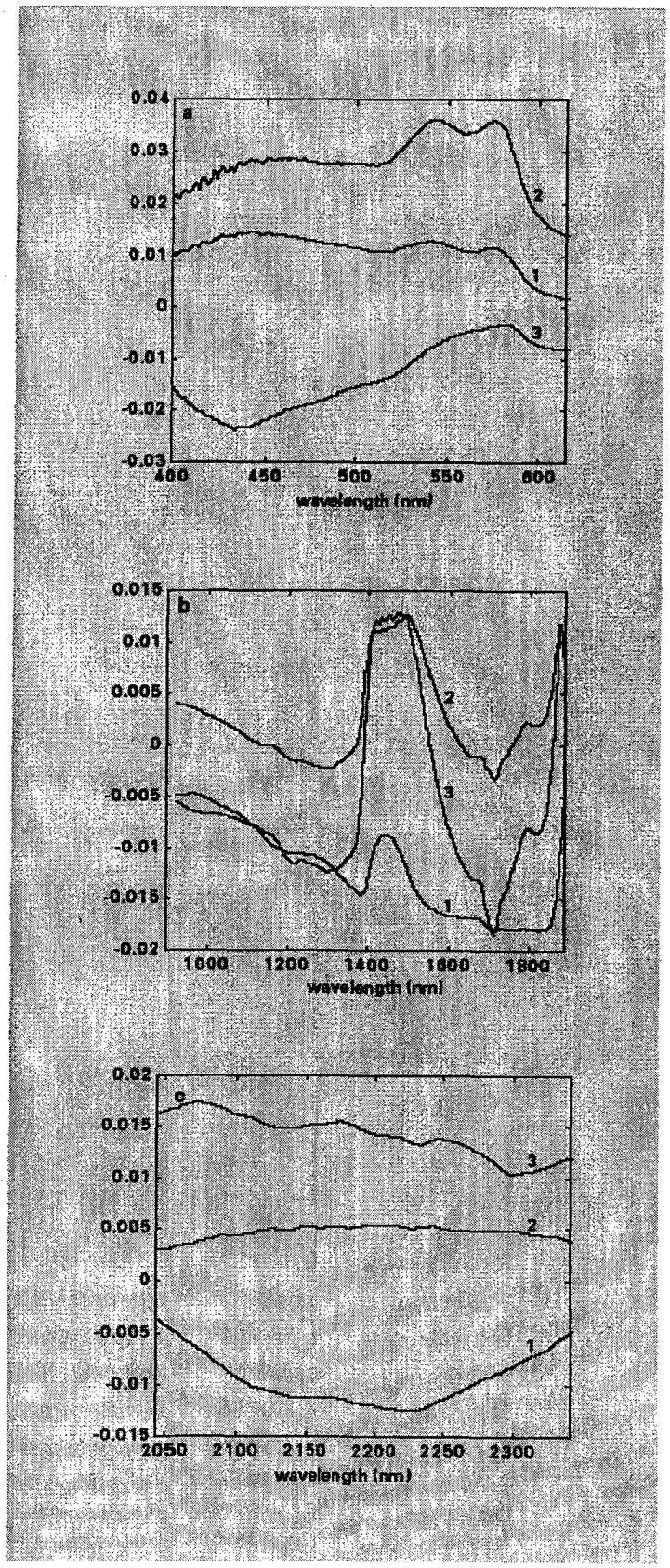

Fig. 3. Tissue pH vectors in each wavelength region of the model: **a** region 1, 400-615 nm, **b** region 2, 924-1,889 nm, **c** region 3, 2,043-2,341 nm. Hemoglobin bands at ~540 and 575, and also at 1,650 nm, are apparent in vector 2 and vector 1 in **a** and **b**, respectively. The water band at ~1,450 nm is also a strong contributor to the model (**b**), all three vectors. Vector numbers as marked.

In a previous work describing optical tissue pH calibration and real tissue pH heterogeneity in vivo in the myocardium [22], similar challenges of matching the optical volume and reference measurement volume were outlined. However, when ischemic changes occur in the intact myocardium, the direction of pH change is homogeneous and may be more optically predictable compared to the atherosclerotic plaque. Improvement of the optical depth resolution that was required in the myocardium was in the order of 3-5 mm. The spatial distribution of tissue pH in the atherosclerotic plaque is more heterogeneous, in the order of microns. In addition, due to the histological variability of necrotic and living tissue in the order of microns, the direction of pH change due to ischemic, hypoxic, or anaerobic conditions in the in-vitro situation may not be as optically predictable. The averaging effect of the optical probe volume in this research may be a large contribution to the limited accuracy of the optical calibration.

Correlation analysis demonstrated that the measured tissue temperature was uncorrelated to the tissue pH reference measurements in this data set. This is an important finding because (1) otherwise, the partial least-squares method employed here could inadvertently model some other variable if it is related to the desired calibration variable of tissue pH, and (2) it leaves open the possibility for independent but complementary information by measuring both pH and temperature. The first consequence indicates the NIRS pH determination is not directly related to temperature, therefore changes in temperature can be ruled out when assessing the validity of the calibration model for this data set. The fact that PLS models could be created with real temperature variation is another indicator that the NIRS pH-determined values in this in-vitro setting is robust with respect to temperature changes that can affect near-infrared measurements. The second consequence suggests that both temperature and pH could be measured by NIRS to selectively characterize the plaque, for example, temperature as a measure of inflammation and macrophage activity, and independently, pH as a measure of ischemia, whether or not it is correlated to macrophage activity. Relatively large changes in temperature could be determined easily by NIRS using the water bands (table 1). However, the temperature changes in atherosclerotic plaques in vivo that have been reported are in the range

of 0.15-1.5°C [11]. It remains to be seen whether NIRS temperature calibration can achieve the same sensitivity as thermistor-based catheter prototypes (0.01°C or better), or a 'far' infrared optical catheter [29]; nevertheless, NIRS tissue pH determination could be integrated without loss of accuracy based on this finding.

Both Casscells et al. [10] and Stefanadis et al. [11] have demonstrated thermal heterogeneity associated with inflammation in atherosclerotic plaques. In this study, no attempt was made to correlate measured tissue temperature with inflammation. It was observed that the tissue temperatures were different in different locations of the plaque and were stable throughout the experiment because of the in-vitro temperature control. Stefanadis et al. [11] described in-vivo human coronary artery studies that showed significant thermal heterogeneity with a novel thermistor-based catheter in stable and unstable angina, and acute myocardial infarction. It should be possible then to determine vulnerability based on metabolic processes of inflammatory cells in the atherosclerotic plaque, whether temperature- or pH-based.

The study shown here demonstrates feasibility of the NIRS measurement of tissue pH in atherosclerotic plaque in vitro. Significant challenges still exist to bring this technique in vivo, such as minimization of the fiber optic sensor size, achieving optimal signal-to-noise ratios, and improving the PLS models with more in-vitro data. Minimally invasive measurements of metabolic derangements such as tissue pH, in combination with one of the localization or structural techniques, could be superior to cholesterol concentration determinations alone. NIRS tissue pH measurement could indicate macrophage activity and acidic plaque, as well as the influence of hypoxic cells on their way to necrosis or apoptosis. A catheter-based fiber- optic, near-infrared spectroscopy system is ultimately envisioned to determine the pH of atherosclerotic plaques. The use of a tissue pH value as a determinant of vulnerability is yet to be evaluated, but by having a non-destructive NIRS tissue pH measurement, it could be potentially valuable for deciding between different interventional therapies to treat the vulnerable plaque.

References

1. Virmani R, Kolodgie FD, Burke AP, Farb A, Schwartz SM: Lessons from sudden coronary death: A comprehensive morphological classification scheme for atherosclerotic lesions. Arterioscler Thromb Vasc Biol 2000;20:1262-1275.

2. Nissen S, Yock P: Intravascular ultrasound: Novel pathophysiological insights and current clinical applications. Circulation 2001;103:604-616.

3. Takano M, Mizuno K, Okamatsu K, Yokoyama S, Ohba T, Sakai S: Mechanical and structural characteristics of vulnerable plaques: Analysis by coronary angioscopy and intravascular ultrasound. J Am Coll Cardiol 2001;38:99-104.

4. Flacke S, Fischer S, Scott M, Fuhrhop R, Allen J, McLean M, Winter P, Sicard G, Gaffney P, Wickline S, Lanza G: Novel MRI contrast agent for molecular imaging of fibrin: Implications for detecting vulnerable plaques. Circulation 2001;104:1280-1285.

5. Fayad Z, Fuster V: Clinical imaging of the high-risk or vulnerable atherosclerotic plaque. Circ Res 2001;89:305-316.

6. Patwari P, Weissman N, Boppart S, Jesser C, Stamper D, Fujimoto J, Brezinski M: Assessment of coronary plaque with optical coherence tomography and high-frequency ultrasound. Am J Cardiol 2000;85:641-644.

7. Naghavi M, Libby P, Falk E, Casscells SW, Litovsky S, Rumberger J, Badimon JJ, Stefanadis C, Moreno P, Pasterkamp G, et al: From vulnerable plaque to vulnerable patient: A call for new definitions and risk assessment strategies. I. Circulation 2003;108:1664-1672.

8. Naghavi M, John R, Nakatani S, Siadaty S, Grasu R, Kurian KC, van Winkle B, Soller BR, Litovsky S, Madjid M, Willerson JT, Casscells W: pH heterogeneity of human and rabbit atherosclerotic plaques: A new insight into detection of vulnerable plaque. Atherosclerosis 2002;164:27-35.

9. Sukhova GK, Shi GP, Simon DI, Chapman HA, Libby P: Expression of the elastolytic cathepsins S and K in human atheroma and regulation of their production in smooth

muscle cells. J Clin Invest 1998;102:576-583.

10. Casscells W, Hathorn B, David M, Krabach T, Vaughn WK, McAllister HA, Bearman G, Willerson JT: Thermal detection of cellular infiltrates in living atherosclerotic plaques: Possible implications for plaque rupture and thrombosis. Lancet 1996;347:1447-1449.

11. Stefanadis C, Diamantopoulos L, Vlachopoulos C, Tsiamis E, Dernellis J, Toutouzas K, Stefanadi E, Toutouzas P: Thermal heterogeneity within human atherosclerotic coronary arteries detected in vivo: A new method of detection by application of a special thermography catheter. Circulation 1999;99:1965-1971.

12. Grasu R, Kurian KC, van Winkle B, Snuggs MB, Siadaty S, John R, Naghavi M, Willerson JT, Casscells W: pH heterogeneity of human and rabbit atherosclerotic plaques. Circulation 1999;100:542-542.

13. Zhang S, Soller BR, Micheels R: Partial least-squares modeling of near infrared reflectance data for noninvasive in-vivo determination of deep tissue pH. Applied Spectroscopy 1998;52:400-406.

14. Puyana JC, Soller BR, Zhang S, Heard SO: Continuous measurement of gut pH with near infrared spectroscopy during hemorrhagic shock. J Trauma 1999;46:9-15.

15. Cassis LA, Lodder RA: Near-IR imaging of atheromas in living tissue. Anal Chem 1993;65:1247-1256.

16. Moreno PR, Lodder RA, Purushothaman KR, Charash WE, O'Connor WN, Muller JE: Detection of lipid pool, thin fibrous cap, and inflammatory cells in human aortic atherosclerotic plaques by near-infrared spectroscopy. Circulation 2002;105:923-927.

17. Wang J, Geng YJ, Guo B, Klima T, Lal BN, Willerson JT, Casscells W: Near-infrared spectroscopic characterization of human advanced atherosclerotic plaques. J Am Coll Cardiol 2002;39:1305-1313.

18. Martens H, Naes T: Multivariate Calibration. New York, Wiley, 1989.

19. Haaland DM, Thomas EV: Partial least-squares methods

for spectral analyses. 1. Relation to other quantitative calibration methods and the extraction of qualitative information. Anal Chem 1988;60:1193-1202.

20. Alam KM, Franke JE, Niemczyk TM, Maynard JD, Rohrscheib MR, Robinson MR, Eaton RP: Characterization of pH variation in lysed blood by near-infrared spectroscopy. Applied Spectroscopy 1998;52:393-399.

21. American Society for Testing and Materials: Standard Practices for Infrared, Multivariate, Quantitative Analysis. Annual Book of ASTM Standards, 3.06(E 1655), 1995, pp 1-24.

22. Zhang S, Soller BR: In-vivo determination of myocardial pH during regional ischemia using near-infrared spectroscopy. SPIE Proc 1998;3257:110-117.

23. Di Iorio E: Hemoglobins; in Antonimi E, Rossi-Bernardi L, Chiancone E (eds): Methods in Enzymology. New York, Academic Press, 1981, vol 76, p 57.

24. Rothgeb TM, Gurd FRN: Biomebranes; in Fleischer S, Packer L (eds): Methods in Enzymology. New York, Academic Press, 1978, vol 52, p 473.

25. Palmer KF, Williams D: Optical properties of water in the near infrared. J Opt Soc Am 1974;64:1107-1110.

26. Hale GM, Querry MR: Optical constants of water in the 200 nm to 200 μm wavelength region. Applied Optics 1973;12:555-563.

27. Martin K: In vivo measurements of water in skin by near-infrared reflectance. Applied Spectroscopy 1998;52:1001-1007.

28. Jaross W, Neumeister V, Lattke P, Schuh D: Determination of cholesterol in atherosclerotic plaques using near infrared diffuse reflectance spectroscopy. Atherosclerosis 1999;147:327-337.

29. Naghavi M, Melling P, Gul K, Madjid M, Willerson JT, Casscells W, Asif M: First prototype of a 4-French 180 degree side-viewing infrared fiber optic catheter for thermal imaging of atherosclerotic plaque. J Am Coll Cardiol 2001;37:3A.

Project I.C.4

Nitric Oxide in Organ Failure

Investigator: Bruce C. Kone, M.D., FACP, FCP

Introduction. Ischemia/reperfusion (I/R) injury to the kidney and gut are common and serious complications in hospitalized patients and trauma victims. There are no proven therapies to prevent or arrest this disorder. Thus, improving the capacity of the kidney and gut to tolerate I/R injury would have important clinical implications. The pathophysiology of I/R injury to these organs is complex and, despite decades of research, still poorly understood. Multiple mediators and pathways have been implicated, including overproduction of nitric oxide (NO). Changes in gene transcription are central to these perturbations.

Given the complexity of the pathways, and the likely interactions between different pathways, a global approach to the assessment of transcriptional responses in renal and gut I/R injury will be most informative. Ideally, potential therapies for I/R injury would be easily administered, have a high therapeutic index, target early, branching cascades leading to injury or repair, be effective at times remote from the initial ischemia, and be cost-effective.

Epithelial injury and repair are central consequences of ischemia and reperfusion of the gut. Intestinal mucosal wounds are repaired in part by epithelial restitution. However, the signaling mechanisms regulating restitution remain poorly understood, and few therapies to enhance restitution have been described. Previously we demonstrated that alpha-melanocyte-stimulating hormone (alpha-MSH) protected against postischemic gut injury in the rat. In addition, ischemic preconditioning (IPC) has been shown to protect organs like the heart following ischemia/reperfusion injury.

Since inducible nitric oxide synthase (iNOS) is the major enzyme responsible for high output NO production during sepsis and inflammation, specific knowledge of transcriptional and post-transcriptional mechanisms

affecting its synthesis is central to the rational design of therapies controlling NO production.

Body. We tested the effects and mechanisms of alpha-MSH on wound restitution of rat small intestine (IEC-6) cells subjected to H2O2 stress with or without scrape wounding. H2O2 treatment resulted in tyrosine phosphorylation of Syk kinase and its downstream target IkappaBalpha, with subsequent NF-kappaB activation. Alpha-MSH and the Syk kinase inhibitor piceatannol blocked these processes. In scrape-wounded cells, H2O2 inhibited wound restitution, and this was partially restored by cotreatment with alpha-MSH or piceatannol. In contrast, overexpression of NF-kappaB p65 or Syk kinase, but not a dominant-negative mutant of Syk kinase, aggravated H2O2 inhibition of wound restitution, and inhibitors of c-Src tyrosine kinase or phosphatidylinositol-3 kinase were without effect. The results indicated an important role for Syk tyrosine kinase and the NF-kappaB pathway in the response to oxidant stress and the impairment of epithelial restitution in IEC-6 cells. The data also disclosed that the beneficial effects of alpha-MSH on gut ischemia/reperfusion injury may relate to its acceleration of epithelial restitution. A manuscript reporting these results was published in Shock.

We also hypothesized that IPC would afford protection from intestinal I/R injury and improve function. Male Sprague Dawley rats were randomized to the following groups: (1) Sham laparotomy, (2) mesenteric ischemia for 30 min and (3) IPC/mesenteric ischemia (three cycles of mesenteric ischemia for 4 min and reperfusion for 10 min followed immediately by mesenteric ischemia for 30 min) and (4) late IPC/ mesenteric ischemia (IPC as above, wait 24 hrs then mesenteric ischemia for 30 min followed by 6 hrs reperfusion). A duodenal catheter was placed to evaluate intestinal transit using FITC-dextran. At 6 hrs, transit was determined by the progression of the FITC-dextran and expressed as the mean geometric center. Ileum was harvested for assessment of mucosal injury (Chiu score by blinded observer) and myeloperoxidase activity. Tissue water was determined using the wet to dry weight ratio to assess gut edema. IPC significantly improved transit, lessened mucosal injury and decreased myeloperoxidase levels in the intestine compared to mesenteric ischemia

alone. We concluded that IPC affords protection from mucosal injury and intestinal dysfunction following I/R. A manuscript reporting these results is in press in Shock.

During the previous funding cycle, we identified a novel mechanism for termination of NO production in cytokine-stimulated mesangial cells in which signal transducers and activators of transcription 3 (STAT3), via direct interactions with NF-kappaB, serves as a dominant-negative inhibitor of NF-kappaB activity to suppress cytokine induction of iNOS transcription. STAT3 is a modular protein with several structurally and functionally defined domains. To define the specific domains of STAT3 that interact with NF-kappaB p65, we synthesized ^{35}S-labeled proteins corresponding to each STAT3 domain and tested their ability to bind specifically a GST-NF-kappaB p65 fusion protein in the GST pull-down assay. The coiled-coil (CCD) and DNA-binding (DBD) domains were specifically retained by GST-NF-kappaB p65, whereas the N-terminal, linker, SH2, and transcriptional activation domains did not interact with NF-kappaB p65. Deletion of the region L^{358} through I^{368} of the STAT3 DBD greatly reduced binding, indicating that this region is necessary for GST- NF-kappaB p65 binding. Alanine substitution mutations at four highly conserved residues --- L^{358}, N^{359}, K^{363}, and V^{366} --- in this region virtually abolished NF-kappaB p65 binding. In contrast to the trans-repression of iNOS promoter activity afforded by wild type STAT3, overexpression of full-length STAT3 harboring these mutations failed to trans-repress an iNOS promoter-reporter construct in mesangial cells. Taken together, our data reveal a novel role for the DBD and CCD domain in the physical and functional coupling to NF-kappaB p65 that appears to be important for regulating iNOS and likely other NF-kappaB p65-responsive genes in mesangial cells. A manuscript reporting these results was published in the American Journal of Physiology.

In further analyzing the controls for iNOS induction and suppression, we investigated epigenetic control of iNOS gene transcription. The methylation of transcriptional control regions in the genome plays a fundamental role in the regulation of gene expression. In susceptible genes containing 5′ CpG islands, cytosine methylation can cause transcriptional repression by promoting the condensation

of chromatin. Treatment of mesangial cells with DNA methylation inhibitors augmented Induction of endogenous NO production and iNOS promoter activity in response to cytokines. We demonstrated that methylation of the murine iNOS promoter was sufficient to silence its expression in cells that can express the endogenous iNOS gene, piNOS-luc was methylated in vitro by SSSI, an enzyme the methylates every CpG dinucleotide, and transiently transfected into mesangial cells. The expression level of methylated iNOS-luc was 100-fold lower that that of its unmethylated counterpart. Treatment with 5-AZA restored the activity of the iNOS promoter and further simulated it after cytokine treatment. To address more specifically the effects of methylation status on iNOS promoter induction, knockdown of DNA methyltransferase-3a by siRNA resulted in a robust increase in iNOS promoter activity and nitrite production. Bisulfite treatment and sequencing analysis of the iNOS promoter showed that almost all potential methylation sites within the iNOS promoter were methylated including a key GAS element. CpG methylation within the GAS element interfered with STAT3 DNA binding. These results provide evidence for a unique molecular mechanism involved in transcriptional regulation of iNOS gene expression. A manuscript reporting these results was published in the Journal of Biological Chemistry.

Little is known about transcriptional regulation of the human iNOS gene in vivo under basal conditions or in sepsis. Accordingly, we developed transgenic mice carrying an insertional human iNOS promoter-reporter gene construct. In these mice, the proximal 8.3 kb of the human iNOS 5'-flanking region controls expression of the reporter gene of enhanced green fluorescent protein (EGFP). Patterns of human iNOS promoter/EGFP transgene expression in tissues were examined by fluorescence microscopy and immunoblotting. Endogenous murine iNOS was basally undetectable in kidney, intestine, spleen, heart, lung, liver, stomach, or brain. In contrast, EGFP from the transgene was basally expressed in kidney, brain, and spleen, but not the other tissues of the transgenic mice. Bacterial lipopolysaccharide induced endogenous iNOS expression in kidney, intestine, spleen, lung, liver, stomach, and heart, but not brain. In contrast, human iNOS promoter/EGFP transgene expression was induced above basal levels only in intestine, spleen, brain, stomach, and lung. Within kidney, human iNOS promoter/EGFP fluorescence was detected most prominently in proximal tubules of the

outer cortex and collecting ducts and colocalized with endogenous mouse iNOS. Within the collecting duct, both endogenous iNOS and the human iNOS promoter/EGFP transgene were expressed in cells lacking aquaporin-2 immunoreactivity, consistent with expression in intercalated cells. Although it remains possible that essential regulatory elements reside in remote locations of the gene, our data concerning this 8.3-kb region provide the first in vivo evidence suggesting differential transcriptional control of the human iNOS gene in these organs and marked differences in transcriptional regulatory regions between the murine and human genes.

Key Research Accomplishments

- Demonstration of an important role for Syk tyrosine kinase and the NF-kappaB pathway in the response to oxidant stress and the impairment of epithelial restitution in IEC-6 cells.
- Demonstration that the beneficial effects of alpha-MSH on gut ischemia/reperfusion injury may relate to its acceleration of epithelial restitution.
- Demonstration that ischemic preconditioning helps to preserve function and histology of the postischemic rat ileum.
- Demonstration of the binding domains of STAT3 with NF-kappaB responsible for inhibition of iNOS transcriptional activation.
- Demonstration of an important effect of DNA methylation in the transcriptional silencing of the iNOS gene.
- Generation and characterization of a transgenic mouse harboring a human iNOS promoter-GFP transgene and its response to endotoxemia.

Reportable Outcomes

Articles:

Yu, Z., and Kone, B.C. The STAT3 DNA-binding domain mediates interaction with NF-kappaB p65 and iNOS *trans*repression in mesangial cells. J. Am. Soc.

Nephrol. 15:585-591, 2004.

Zou, L., Sato, N., and Kone, B.C. alpha-Melanocyte stimulating hormone protects against H_2O_2-induced inhibition of wound restitution in IEC-6 cells via a Syk kinase- and NF-kappaB-dependent mechanism. Shock, 22:453-459, 2004.

Yu, Z., Xia, X., and Kone, B.C. Expression profiles of an inducible nitric oxide synthase promoter-reporter in transgenic mice during endotoxemia. Am. J. Physiol Renal Physiol. 288:F214-F220, 2005.

Moore-Olufemi, S., Zou, L., Kozar, R., Moore, F., and Kone, B.C., Ischemic preconditioning protects against gut dysfunction and mucosal injury after ischemia/reperfusion injury. Shock, in press.

Conclusions

Multiple organ failure is a common, often catastrophic outcome of combat-induced trauma. An improved understanding of the molecular basis for the initiation and amplification of cell and organ injury will ultimately inform the rational design of therapeutic agents to prevent, delay, or reverse post-resuscitation multiple organ failure. In the aggregate, our studies provide new insights into the early molecular events underlying both intestinal ischemia-reperfusion injury and multiple organ failure, new insights into the regulation of epithelial restitution and repair, and novel therapeutic strategies to limit I/R injury and multiple organ failure.

Project I.C.6.

Is Hypothermia an Indicator of Imminent Death in Congestive Heart Failure and Helpful in Triage

Investigator: S. Ward Casscells, M.D.

Introduction

Congestive heart failure (CHF) is the most frequent cause of hospitalization for persons 65 years of age or older and its prevalence is increasing. [1] Despite new therapies and improving outcome, CHF-related mortality increased 135% from 1979 to 1998. [1] Prognostic factors constitute the major consideration in patient selection for therapies such as transplantation, left ventricular assist devices, and investigational drugs. [2] Bedside prognostic factors specifically improve titration of medications. However, there is no agreement about which variables predict an imminent fatal outcome, and few studies have focused on short-term prognosis. [3-6] Even multivariate studies have generally included a partial list of variables and have yielded predictors with only modest sensitivity and specificity. [4,7]

In one of our recent patients with severe CHF, body temperature decreased from 97.0 to 91.7 °F two hours before death, despite a normal heart rate, blood pressure, and mental status. We subsequently made a similar observation in 2 more patients. We therefore undertook a pilot case-control study of 180 CHF-related deaths occurring from 1996 to 1998 and found that, once temperature confounders were excluded, more than half of the remaining 46 deaths were preceded by hypothermia; and there were significant differences between hospitalized patients who died of CHF and those who survived with respect to temperature at the time of hospital admission, average temperature during hospitalization, temperature during the last 12 hours before death or hospital discharge, and last recorded temperature. [8] We designed the current wider, retrospective, cohort study to validate and compare the significance of temperature as a novel predictor of death by itself and in combination with various other bedside variables.

Methods

The study was approved by the Committee for the Protection of Human Subjects of the University of Texas Health Science Center at Houston, Texas. We reviewed 423 admissions between January

and December 1998 to Memorial Hermann Hospital that had a principal discharge diagnosis code of CHF [*International Classification of Diseases, 9th Revision, Clinical Modification (ICD-9 CM)*] and selected 291 patients for this retrospective study. We excluded 97 admissions because they were readmission(s) of the same patient; in these cases, the last readmission was the one included in the study. Another 35 admissions were excluded because temperature variations in those patients might have resulted from temperature confounders such as sepsis, acute stroke, thyroid disease, hepatic failure, ethanol intoxication, or environmental factors.

Patients' deaths were classified as caused by progressive pump failure by treating physicians and by the research team if their deaths were due to progressive cardiac decompensation (symptoms, signs and objective evidence of decompensation of the left or right ventricle such as falling blood pressure and/or progressive pulmonary congestion by symptoms, exam, chest x-ray and pulse oximetry). Patients who died were specifically excluded if they were stable before the sudden episode of ventricular tachycardia, ventricular fibrillation, asystole or myocardial infarction that led to their deaths.
The number of days from admission to discharge or death was entered into Cox regression models as the main dependent variable. Admission temperature was the main independent variable in the analysis and was kept in the analysis regardless of measurement location (oral, rectal, tympanic or axillary). Three body temperature categories were defined *a priori:* admission temperature (T_{adm}) >96.5° F as reference group, and T_{adm} = 95.6° to 96.5° F and Tadm ≤95.5 F as hypothermia groups.

We assessed several other CHF risk factors for confounding the association of hypothermia and survival: age (>=80 years, 70-79, 60-69, and <=59), gender, history of hypertension, history of diabetes mellitus, history of coronary artery disease, cardiomyopathy, New York Heart Association [NYHA] functional class (III, or IV compared to the reference group of I and II), medications, tachycardia (>100 beats/sec.), low systolic blood pressure (<100 mmHg), arrhythmias on admission (atrial fibrillation, premature ventricular tachycardia, ventricular tachycardia, and supraventricular tachycardia); high serum creatinine (Cr > 1.5 mg/dL), hyponatremia (Na^+ < 138 mEq/L), hypokalemia (K^+ < 3.5 mEq/L), hypomagnesemia (Mg^{++} < 1.3 mg/dL), and leukocytosis (count >10,000/mm^3). Several other indicators, including echocardiography-confirmed valvular diseases and left-ventricluar ejection fraction, were dropped because more

than a third of patients lacked data for that variable.

Crude and adjusted hazard ratios and their corresponding confidence intervals were calculated using the SAS software package version 8.0. The study of confounders included univariate analyses of the association between potential confounders and both outcome (Cox regression) and hypothermia on admission (logistic regression). For this, an alpha of 0.25 was chosen to prevent exclusion of important confounders due to small sample size. Next we determined whether adjusting for the confounder would change the hazard ratio by more than 10% at 0.05 alpha level. A factor was not considered a confounder if that factor was not associated with both outcome and exposure, or did not change hazard ratio by at least 10%. A multivariable analysis with the intention of adjusting for those variables that were found confounders was done to calculate adjusted hazard ratios. Finally, a multivariable model for time to death for the whole population was developed with the intention of determining whether hypothermia on admission would stay a significant predictor when other prognostics factors of mortality are included in the model. For this, those prognostic factors that were associated with time to death in a univariate fashion at 0.25 level were used to build a preliminary multivariable model, next dropping those that did not contribute to the model, to reach the final model.

Results

Patient Characteristics

The 291 patients included 137 men and 154 women aged 73±13 years (range, 27 to 97 years). There were 223 patients with T_{adm}>96.5° F, 51 patients with T_{adm} = 95.6° to 96.5° F and 17 patients with Tadm ≤95.5 F. Table 1 shows their baseline characteristics at hospital admission. Patient demographics, including age and gender distributions were similar in 3 baseline temperature groups. Only 165 (57%) of patients underwent an echocardiography, and therefore baseline valvular disease and left ventricular ejection fraction were dropped from further analysis; however, available information from those patients is given in Table 1.

Table 1.

Baseline Characteristics of Study Patients in Temperature Subgroups

Characteristic	Baseline Value*			
	All	**T >96.5**	**T: 95.6-96.5**	**T ≤95.5**
	N= 291	**N= 223**	**N= 51**	**N= 17**
Temperature at admission (°F)	97.3 ± 1.1	97.8 ± 0.8	96.2 ± 0.2	95.0 ± 0.5
Age (y)	67.4 ± 13.4	67.2 ± 14.0	67.9 ± 11.0	73.8 ± 9.6
=> 80	61 (29.9)	49 (21.6)	8 (15.6)	4 (25.5)
70 - 79	69 (23.7)	47 (21.8)	15 (29.4)	7 (41.1)
60 - 69	79 (27.1)	59 (26.4)	15 (29.4)	5 (29.4)
<= 59	82 (28.1)	68 (30.4)	13 (25.4)	1 (5.8)
Sex:				
Male	137 (47.1)	99 (44.3)	29 (56.8)	9 (52.9)
Female	154 (52.9)	124 (55.6)	22 (43.14)	8 (47.1)
History of hypertension	215 (73.8)	171 (76.6)	31 (60.7)	13 (76.5)
Diabetes mellitus	128 (43.9)	100 (44.8)	22 (43.1)	6 (35.3)
Cardiomyopathy	77 (26.4)	59 (26.4)	14 (27.4)	4 (23.5)
NYHA class:				
I/ II	86 (29.5)	71 (31.8)	12 (23.5)	3 (17.6)
III	144 (49.5)	112 (50.2)	24 (47.0)	8 (47.0)
IV	61 (21.0)	40 (17.9)	15 (29.4)	6 (35.2)

Coronary artery disease	159 (55.2)	127 (57.7)	25 (49.0)	7 (41.1)
Tachycardia at admission (> 100 beats/min)	85 (29.4)	68 (30.6)	14 (27.4)	3 (18.7)
Low SBP at admission (< 100 mmHg)	17 (5.8)	12 (5.3)	2 (3.9)	3 (17.6)
Valvular diseases: †	95 (57.5) (N= 165)	75 (59.0) (N= 127)	12 (46.1) (N= 26)	8 (66.6) (N= 12)
Mitral regurgitation	83 (50.3)	64 (50.3)	11 (42.3)	8 (47.0)
Tricuspid regurgitation	52 (31.5)	40 (31.5)	7 (26.9)	5 (41.6)
Aortic insufficiency	31 (18.7)	23 (18.1)	4 (15.3)	4 (33.3)
Aortic stenosis	14 (8.4)	9 (7.0)	3 (11.5)	2 (16.6)
Mitral stenosis	4 (2.4)	3 (2.3)	1 (3.8)	0 (0)
LVEF (percent) at admission †	34.7 ± 16.5	35.4 ± 16.3	36.1 ± 17.6	24.8 ± 14.5
Arrhythmias:	101 (34.8)	72 (32.4)	20 (39.2)	9 (52.2)
Atrial fibrillation	63 (21.7)	46 (20.7)	13 (25.4)	4 (23.5)
Premature ventricular complex	14 (4.8)	11 (4.9)	2 (3.9)	1 (5.8)
Ventricular tachycardia	17 (5.8)	13 (5.8)	2 (3.9)	2 (11.7)
Supraventricular tachycardia	4 (1.3)	2 (0.9)	1 (1.9)	1 (5.8)
Other	3 (1)	0 (0)	2 (3.9)	1 (5.8)
High serum creatinine (>1.5 mg/dL)	93 (32.7)	61 (28.1)	22 (44.0)	10 (58.8)

Low serum Na^+ (<138 mEq/L)	160 (56.3)	117 (53.9)	29 (58.0)	14 (82.3)
Low serum K^+ (<3.5 mEq/L)	22 (7.7)	19 (8.7)	2 (4.0)	1 (5.8)
Low serum Mg^{++} (<1.3 mg/dL)	7 (2.9)	6 (3.2)	1 (2.5)	0 (0)
Leukocytosis (count $>10^4/mm^3$)	53 (19.3)	40 (18.9)	7 (15.2)	6 (35.2)
Medications:				
Diuretics	213 (73.2)	164 (73.5)	37 (72.5)	12 (70.5)
ACE inhibitors	182 (62.5)	145 (65.0)	27 (52.9)	10 (58.8)
Isosorbide	79 (27.1)	64 (28.7)	13 (25.4)	2 (11.7)
Anticoagulants	167 (57.3)	131 (58.7)	29 (56.8)	7 (41.1)
Calcium channel blockers	46 (15.8)	33 (14.8)	12 (23.5)	1 (5.8)
Amiodarone	28 (9.6)	22 (9.8)	3 (5.8)	3 (17.6)
Beta-blockers	38 (13.0)	33 (14.8)	4 (7.8)	1 (5.80)

*Mean ± standard deviation or number (%) of patients; † Based on echocardiography done in 165 patients. ACE, angiotensin-converting enzyme; anticoagulants, warfarin sodium, aspirin; beta-blockers, carvedilol, metoprolol, atenolol; diuretics, furosemide, hydrochlorothiazide, Spironolactone; LVEF, left ventricular ejection fraction by echocardiography; N, number; NYHA, New York Heart Association; SBP, systolic blood pressure.

During a mean hospital stay of 5 ± 4 days (range, 0 to 28 days) 17 (6%) patients died of progressive pump failure. The mortality distribution of patients in 3 baseline temperature groups is presented in Table 2. Temperature at admission had a non-normal distribution (Kolmogorov-Smirnov test; *P*=.051), with a mean of 97.31.1 F in all patients, 97.31.0 F in survivors and 96.61.0 F in non-survivors and the difference between the two was significant (Mann-Whitney test; *P*=.005). Admission temperature was significantly associated with time to in-hospital death on univariate survival analysis, and unadjusted hazard ratio for T_{adm} [95.5 - 96.5°F] was 2.95 ($CI_{95\%}$ 0.93-9.32, *P*=0.065), and for T_{adm} <95.5°F was 5.83 ($CI_{95\%}$: 1.80- 18.79, *P*=0.003). Figure 1 presents the cumulative survival functions, showing decreased survival for patients with temperatures of ≤95.5 °F.

Table 2.
Adjusted Hazard Ratios of the Association of Body Temperature on Admission and Time to In-Hospital Death

Temperature (°F)	Patient Demographic Characteristics*	No. (%) of Events *	Adjusted Hazard Ratio, † $CI_{95\%}$ and *P*-value
≤95.5	N=17; Age (y): 73±9 (SD); M:F 9:8	5 (29.4%)	4.46 [1.38- 14.3] (*P*=0.012)
95.6 to 96.5	N=51; Age (y): 67±10 (SD); M:F 29:22	5 (9.8%)	2.76 [0.86- 8.80] (*P*=0.085)
>96.5	N=223; Age (y): 67±14 (SD); M:F 99:124	7 (3.1%)	1.00
			P for trend = 0.0283
All	N=291; Age (y): 73±13 (SD); M:F 137:154	17 (5.8%)	

* The difference of ages in the 3 groups was nonsignificant (Kruskal-Wallis Test); the difference of gender distribution in the 3 groups was nonsignificant (Cramer's V); † Adjusted for New York Heart Association functional class (III or IV vs. reference group of I and II); F: female; M: male; N: number; yr: years

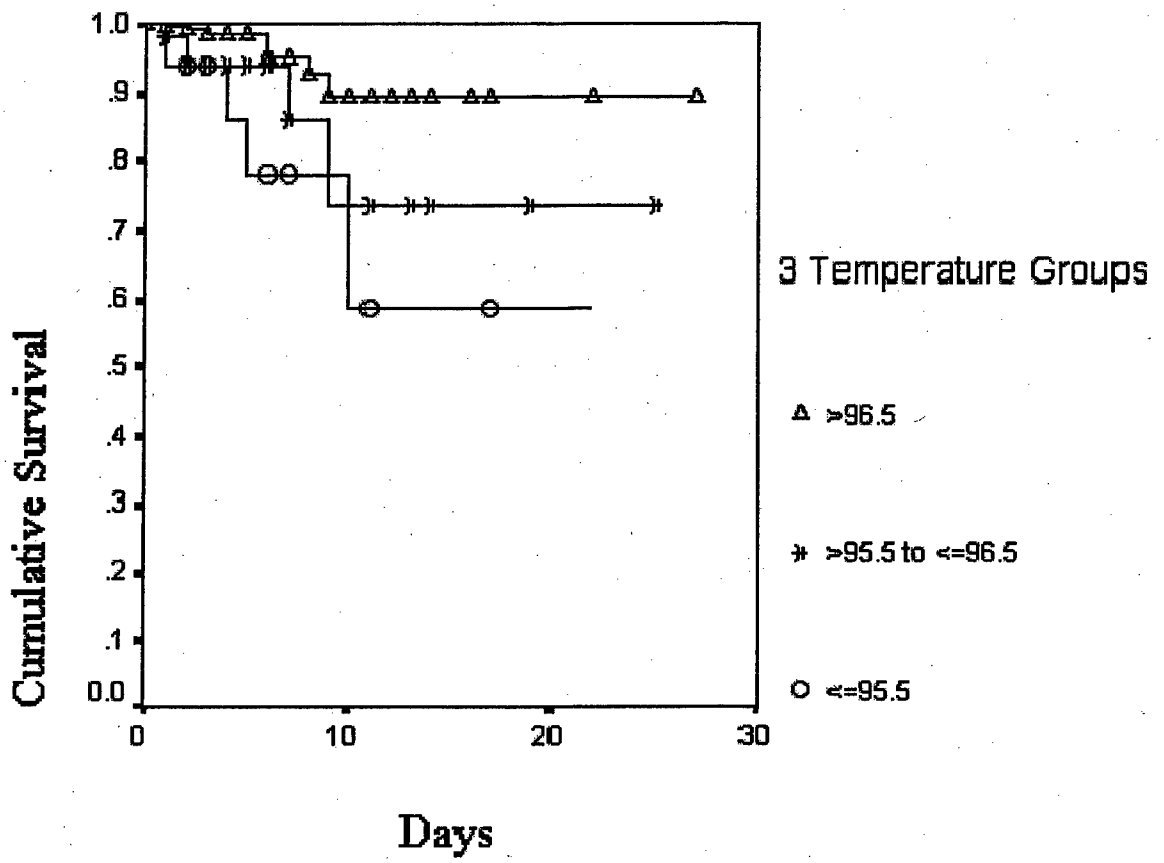

Figure 1.
Cumulative survival functions for patients in the three temperature groups.

In addition to admission body temperature, the following variables were associated with mortality in this cohort of CHF patients: male gender, high NYHA functional class, low systolic blood pressure, ventricular tachycardia, supraventricular tachycardia, and high serum creatinine. Of those, NYHA functional class, high serum creatinine, and low systolic blood pressure were associated with hypothermia, and only NYHA functional class materially affected the hazard ratio of hypothermia.

Admission temperature was significantly associated with time to in-hospital death on univariate survival analysis. Hazard ratios, their confidence intervals and associated *P*-values for T_{adm} [95.5 - 96.5°F] and for T_{adm} <95.5°F, adjusted for NYHA functional class are presented in Table 2. The case-fraction

weighted average of excess hazard associated with hypothermia on admission at these two levels was 41.5%. The trend of the increase of hazard ratio from normothermic (T_{adm} > 96.5°F) to hypothermic was significant as well (C^2 trend = 4.812, P = 0.0283). Admission temperature remained significantly associated with time to in-hospital death in the final multivariate model for time to death for the whole population. Hazard ratios and their corresponding confidence intervals for admission temperature in this model were 3.03 [$CI_{95\%}$ 0.91-10.03, P=0.069] for T_{adm} [95.5 - 96.5°F], 3.48 [$CI_{95\%}$ 1.04-11.69, P=0.0430] for T_{adm} <95.5°F, adjusted for gender, NYHA functional class, hypotension, and presence of ventricular tachycardia.

Discussion

This study of patients with CHF identified a novel predictor of mortality: mild hypothermia. Temperature at the time of admission to hospital was studied together with other known bedside, electrophysiologic and laboratory variables routinely measured in a teaching hospital. Hypothermia emerged as an independent bedside predictor of death caused by progressive pump failure and retained significance after adjustment for potential confounders. NYHA functional class was the only factor found to confound the association of hypothermia and time to in-hospital death among these patients. NYHA functional class, a measure of a patient's level of physical activity, has confounded this association probably because body temperature would be lower in patients with less activity. The finding that hypothermia stayed significant after adjusting for NYHA showed that the association was independent of a patient's level of physical activity. Patients who had admission body temperatures of 95.5 °F or below were 4.46 times more likely to die of progressive pump failure at any time during their hospital stay as compared to patients who had admission body temperatures above 96.5 °F, adjusted for baseline NYHA functional class, and cumulative survival was significantly decreased for hypothermic patients (Figure).

These results confirmed our previous pilot study that used a different design. In that small, preliminary case-control study published in abstract form [8] we found that 50% of CHF nonsurvivors were hypothermic. In the present study, we examined more variables and included a larger number of patients receiving current therapies. The common finding in all these studies was the predictive value of hypothermia. This is the first full publication of this novel finding.

Robustness of findings

As in all chart reviews, missing and non-standard data made it impossible for all published prognostic variables to be included. Nevertheless, the significance of temperature as a predictor of death was strongly suggested by univariate analysis and multivariate comparisons. Moreover, we only used the last admission of patients in the period of a year for inclusion in the study. While this made survival data simpler to interpret for the study of the association of hypothermia and time to in-hospital deaths, it made it impossible to use information pertaining to previous admissions as potential risk factors.

Additionally, because measured temperatures were not recorded in a uniform fashion (i.e. patients might have oral, aural, rectal and bladder temperature measurements on admission), this would presumably lead to bias in the estimation of the prognostic value of hypothermia. Similarly, the study included only temperatures on admission. Continuous temperature monitoring might augment the prognostic value of temperature measurement in CHF patients.

One other issue of note was the identification of pump failure. Reviewers had *a priori* set criteria for defining pump failure death. Nonetheless, there remains the possibility of reviewer bias in the study, which could not be addressed by blinding because of the logistics of the study.

Temperature and Other Recognized Prognostic Factors

Clinically, CHF prognostic predictors can be grouped into 4 sets: bedside (or office), electrophysiologic, hemodynamic, and biochemical variables. [9] Since physicians often monitor CHF patients by telephone, in the office, or on hospital rounds, and manage their conditions by evaluating their symptoms and physical findings, bedside factors may have the most influence on the management of CHF. Electrocardiography, echocardiography, and laboratory tests are not obtained as frequently as vitals signs. Most bedside predictors that have traditionally been considered strong, such as advanced age, male gender, [10] coronary artery disease as the etiology of CHF, [11] an S3 gallop, low systolic arterial pressure, low pulse pressure, or poor NYHA status, apply to a limited number of patients and account for only a portion of the variance. In the present study, hypothermia was found to be a significant predictor of progressive pump failure death, while age, coronary artery disease and several other known risk factors were not. Hemodynamic variables including an abnormal left and

right ventricular ejection fraction [2,4,5,12,13] and maximal oxygen consumption during exercise, [14] predict prognosis but are difficult to monitor on a continuous basis. Predictive biochemical variables, including plasma norepinephrine, [15,16] and plasma atrial and brain natriuretic peptides [4] likewise are not monitored continuously. Frequent ventricular extrasystoles [17] and ventricular tachycardia [10] are better predictors of sudden arrhythmic death than of progressive CHF. Therefore, if confirmed in future studies, hypothermia could be useful for continuous monitoring of CHF patients.

Pathophysiologic implications of findings

The potential mechanisms of hypothermia discussed below are speculative. As tissue oxygen delivery decreases, maximal tissue oxygen extraction capability is exceeded, oxygen consumption declines, and heat production decreases. [18,19] Other factors that might lower body temperature include malnutrition; [20] cell senescence; vasodilator therapy (likely to transfer core heat to the skin so that heat is lost to the environment); norepinephrine and epinephrine; [21] brain stem hypoxia, and venous congestion causing decreased liver and/or gastrointestinal metabolism.

Metabolic factors are probably significant: CHF patients have increased lactate levels that, together with increased resting basal metabolic rates [22] indicate inefficient use of oxygen. Indeed, in some CHF patients, muscle and femoral temperatures decrease at the beginning of exercise. [23] Additionally; pulmonary artery temperature decreases after 5 to 10 minutes of exercise, whereas in the normal population it increases after exercise. [24]

Therapeutic implications

Better identification of prognostic variables in CHF might have significant practical implications for patient selection and success of heart transplantation in these patients. In a recent study that used the presence of coronary artery disease, intraventricular conduction delay, left ventricular ejection fraction, heart rate, serum sodium concentration, mean arterial pressure, and peak oxygen uptake to stratify CHF severity in heart transplant candidates, there were no significant intergroup differences in the outcome of transplantation, [25] and only the sickest patients benefited from transplantation.

Additionally one might ask, if hypothermia is a marker of risk in CHF, does it contribute to mortality? Hypothermia, long recognized as an ominous predictor of death in trauma victims,

[26] has been found to independently contribute to death in those patients. [27] In CHF patients, cold has been reported to exacerbate their condition. [28,29] Besides increasing the heart rate and blood pressure, cold triggers vasoconstriction, which increases the afterload and can cause coronary constriction. [30] Cold increases plasma norepinephrine [28,29] and endothelin-1 levels; [29] and both norepinephrine and endothelin-1 predict CHF outcome. Norepinephrine can increase myocardial oxygen demand (due to increased inotropy and chronotropy) and trigger coronary spasm, arrhythmias, and platelet aggregation. Severe hypothermia is a well-recognized cause of coagulopathy. [26,27] Studies of conditions other than CHF suggest that treatment of hypothermia might lessen complications such as metabolic acidosis and arrhythmias. [31] Alterations in temperature and pH negatively affect the dissociation curve of oxyhemoglobin in human blood. [31] Also, hypothermia can cause shivering, which may further stress the heart because of the increased cardiac output necessary to supply the involved muscles. [24]

In summary, there are several plausible biological mechanisms by which cold may increase the risk of mortality in CHF. Several of these, such as vasoconstriction, are amenable to therapy. Indeed, warming may itself be therapeutic. In two reports by one research group, [32,33] thermal therapy in CHF patients improved symptoms, hemodynamic variables and levels of biochemical markers but mortality was not investigated. These findings, together with the fact that not all hypothermic patients died and those who died did not do so in a matter of minutes, but over several days, argues against the notion that hypothermia is an agonal event or that treatment is futile.

In order to better determine if, which and when additional interventions might be needed for hypothermic CHF patients, prospective studies are needed. One potential design for such a study is a trial, which would allocate hypothermic and normothermic CHF patients to an intensified care protocol. The intensified care protocol might include warming, further laboratory workout, use of continuous physiologic monitoring, and the like. Comparison of the results in the hypothermic patients who did and did not receive the intensified treatment will determine whether these patients can be saved.

Conclusion

Hypothermia appears to be a novel univariate and multivariate predictor of imminent death in hospitalized CHF patients. Prospective studies are needed to determine whether hypothermia can help identify patients who benefit from intensified

therapies. The physiology of exposure to cold suggests several mechanisms by which cold may increase mortality, but further studies are needed to elucidate the molecular basis of CHF's relationship to temperature and to determine whether maintenance of normal temperature can reduce mortality.

References

1. American Heart Association. 2001 Heart and Stroke Statistical Update. Dallas, TX: American Heart Association, 2000.

2. Parameshwar J, Keegan J, Sparrow J, et al. Predictors of prognosis in severe chronic heart failure. Am Heart J 1992;123:421-6.

3. Rector TS, Cohn JN. Prognosis in congestive heart failure. Annu Rev Med 1994;45:341-50.

4. Gradman AH, Deedwania PC. Predictors of mortality in patients with heart failure. Cardiol Clin 1994;12:25-35.

5. Cohn JN, Rector TS. Prognosis of congestive heart failure and predictors of mortality. Am J Cardiol 1988;62:25A-30A.

6. Hallstrom A, Pratt CM, Greene HL, et al. Relations between heart failure, ejection fraction, arrhythmia suppression, and mortality: analysis of the Cardiac Arrhythmia Suppression Trial. J Am Coll Cardiol 1995;25:1250-7.

7. Cohn JN. Prognostic factors in heart failure: poverty amidst a wealth of variables. J Am Coll Cardiol 1989;14:571-2.

8. Siddiqui H, Patel S, Lal BN, et al. Hypothermia: a new indicator of imminent death in congestive heart failure. *J Am Coll Cardiol.* 1999; 33: 212A

9. Givertz M, Colucci W, Braunwald E. Clinical aspects of heart failure: high-output failure; pulmonary edema. In: Braunwald E, editor. Heart Disease: A Textbook of Cardiovascular Medicine, 6th ed. Philadelphia: W B Saunders, 2001:546-9.

10. Adams KF, Dunlap SH, Suteta CA, et al. Relation between gender, etiology and survival in patients with symptomatic heart failure. J Am Coll Cardiol 1996;28:1781-8.

11. Bart BA, Shaw LK, McCants CB, et al. Clinical determinants of mortality in patients with angiographically diagnosed

ischemic or nonischemic cardiomyopathy. J Am Coll Cardiol 1997;30:1002-8.

12. Gradman A, Deedwania P, Cody R, et al. Predictors of total mortality and sudden death in mild to moderate heart failure. Captopril-Digoxin Study Group. J Am Coll Cardiol 1989;14:564-70.

13. de Groote P, Millaire A, Foucher-Hossein C, et al. Right ventricular ejection fraction is an independent predictor of survival in patients with moderate heart failure. J Am Coll Cardiol 1998;32:948-54.

14. Myers J, Gullestad L, Vagelos R, et al. Clinical, hemodynamic, and cardiopulmonary exercise test determinants of survival in patients referred for evaluation of heart failure. Ann Intern Med 1998;15:286-93.

15. Cohn JN, Levine TB, Olivari MT, et al. Plasma norepinephrine as a guide to prognosis in patients with chronic congestive heart failure. N Engl J Med 1984;311:819-23.

16. Francis GS, Cohn JN, Johnson G, et al. Plasma norepinephrine, plasma renin activity, and congestive heart failure: Relations to survival and the effects of therapy in V-HeFT II. The V-HeFT VA Cooperative Studies Group. Circulation 1993;87(Suppl 6):VI40-VI48.

17. Dargie HJ, Cleland JG, Leckie BJ, et al. Relation of arrhythmias and electrolyte abnormalities to survival in patients with severe chronic heart failure. Circulation 1987;75:IV98-IV107.

18. Weg JG. Oxygen transport in adult respiratory distress syndrome and other acute circulatory problems: relationship of oxygen delivery and oxygen consumption. Crit Care Med 1991;19:650-7.

19. Shibutani K, Komatsu T, Kubal K, Sanchala V, Kumar V, Bizzarri DV. Critical level of oxygen delivery in anesthetized man. Crit Care Med 1983;11:640-3.

20. Anker SD, Ponikowski P, Varney S, et al. Wasting as independent risk factor for mortality in chronic heart failure. Lancet 1997;349:1050-3.

21. Zeisberger E. The roles of monoaminergic neurotransmitters in thermoregulation. Can J Physiol Pharmacol 1987;65:1395-1401.

22. Poehlman ET, Scheffers J, Gottlieb SS, et al. Increased resting metabolic rate in patients with congestive heart failure. Ann Intern Med 1994;121:860-2.

23. Shellock FG, Swan HJ, Rubin SA. Muscle and femoral vein temperatures during short-term maximal exercise in heart failure. J Appl Physiol 1985;58:400-8.

24. Brengelmann GL. Body temperature regulation in heart failure. Cardiologia 1996;41:1033-43.

25. Deng MC, De Meester JM, Smits JM, Heinecke J, Scheld HH. Effect of receiving a heart transplant: analysis of a national cohort entered on to a waiting list, stratified by heart failure severity. Comparative Outcome and Clinical Profiles in Transplantation (COCPIT) Study Group. BMJ 2000;321:540-5.

26. Jurkovich GJ, Greiser WB, Luterman A, Curreri PW. Hypothermia in trauma victims: an ominous predictor of survival. J Trauma 1987;27:1019-24.

27. Gentilello LM, Jurkovich GJ, Stark MS, Hassantash SA, O'Keefe GE. Is hypothermia in the victim of major trauma protective or harmful? A randomized, prospective study. Ann Surg 1997;226:439-49.

28. Westheim A, Os I, Thaulow E, et al. Haemodynamic and neurohumoral effects of cold pressor test in severe heart failure. Clin Physiol 1992;12:95-106.

29. Rodriguez-Garcia JL, Paule A, Dominguez J, et al. Effects of the angiotensin II antagonist losartan on endothelin-1 and norepinephrine plasma levels during cold pressor test in patients with chronic heart failure. Int J Cardiol 1999;70:293-301.

30. Lassvik CT, Areskog N. Angina in cold environment. Reactions to exercise. Br Heart J 1979;42:396-401.

31. Astrup P, Engel K, Severinghaus JW, et al. The influence of temperature and pH on the dissociation curve of oxyhemoglobin of human blood. Scand J Clin Lab Invest 1965;17:515-23.

32. Tei C, Horikiri Y, Park JC, et al. Acute hemodynamic improvement by thermal vasodilation in congestive heart failure. Circulation 1995;91:2582-90.

33. Kihara T, Biro S, Imamura M, et al. Repeated sauna treatment improves vascular endothelial and cardiac function in patients with chronic heart failure. J Am Coll Cardiol 2002;39:754-9.

Project I.D.

Up-regulation of P450: A Natural, Broad-Based Defense Against Chemical and Biological Threats

Investigator: Henry W. Strobel, Ph.D.

INTRODUCTION

The cytochrome P450 4F and 2D subfamilies play a major role in modulating the inflammatory cascade initiated by chemical and biological agents as well as by physical insults. Chemical and biological agents tend more often to have multi site systemic effects whereas one would expect a physical blow (i.e. head trauma) to be confined to a single site. At the outset of our studies we proposed a two pronged approach to define the role of CYPs 4F and 2D by using two modules of inflammation based on the proposition that head trauma led to focal injury whereas biological and chemical agents resulted in multi site systemic responses.

Closed head injury patients pose one of the most difficult clinical circumstances to address. Traumatic brain injury (TBI) model in rat closely simulates closed head injury in humans who have been in traffic accidents or experience blunt trauma. TBI initiates complex biochemical cascades including induction of genes whose protein products contribute to production of pro-inflammatory eicosanoids like leukotrienes and prostaglandins. The cytochrome P450 enzymes (CYPs) are involved in a diverse array of physiological and xenobiotic metabolic pathways. CYP4F subfamily in particular metabolizes leukotriene B_4 and prostaglandins A_1 and E_1 to their inactive products thereby limiting immigration of cells, fluids and ions to the site of injury or infection.

The overall hypothesis of this proposal is that leukotriene and prostaglandin ω-hydroxylases i.e. CYP4Fs play an important role in response to TBI by regulating concentrations of their substrates. This hypothesis is illustrated in the following diagram.

The preliminary data suggests that during the pro-inflammatory phase after injury, elevation of leukotriene and prostaglandin mediators occurs due to increase in 5-lipoxygenase (5-LOX) and cyclooxygenase-2 (COX-2) with a concomitant decrease in CYP4F expression. With time these conditions reverse. At 2 weeks after injury, increased CYP4F and decreased 5-LOX and COX-2 expression reduce the concentrations of leukotrienes and prostaglandins leading to recovery and repair.

Increased prostaglandin and leukotriene B_4 levels are associated with the initial response phase in traumatic injury (as shown in the diagram) and these signals prompt the accumulation of ions, fluids and cells into the injured area resulting in the classic dolor, rubror, calor, and turgor associated with inflammation. We have observed that cyclooxygenase II (COX II) levels and lipoxygenase 5 (LOX-5) levels peak at 24 hours after traumatic brain injury and that at the same time two of the cytochromes P4504F subfamily members are suppressed to their lowest levels in brain enabling leukotriene B_4 and prostaglandins to rise to their highest levels.

After 24 hours and increasing to 2 weeks after injury (the recovery period) CYP4F levels rise to above base line levels while COX II and LOX-5 levels fall back to baseline levels allowing the CYP4F enzymes to degrade the elevated levels of leukotriene B_4 and prostaglandin A_1 and E_1 thereby moderating inflammation. We determined these results using Real Time Quantitative PCR and Western blot techniques using a polyclonal antibody to antibodies. These results have led to our hypothesis that the CYP4F subfamily mediates recovery from traumatic injury especially head trauma. This hypothesis when established has military significance in terms of evolving modalities to cope immediately with battlefield injuries as well as medical significance in terms of fostering recovery from inflammatory diseases before surgical intervention is required.

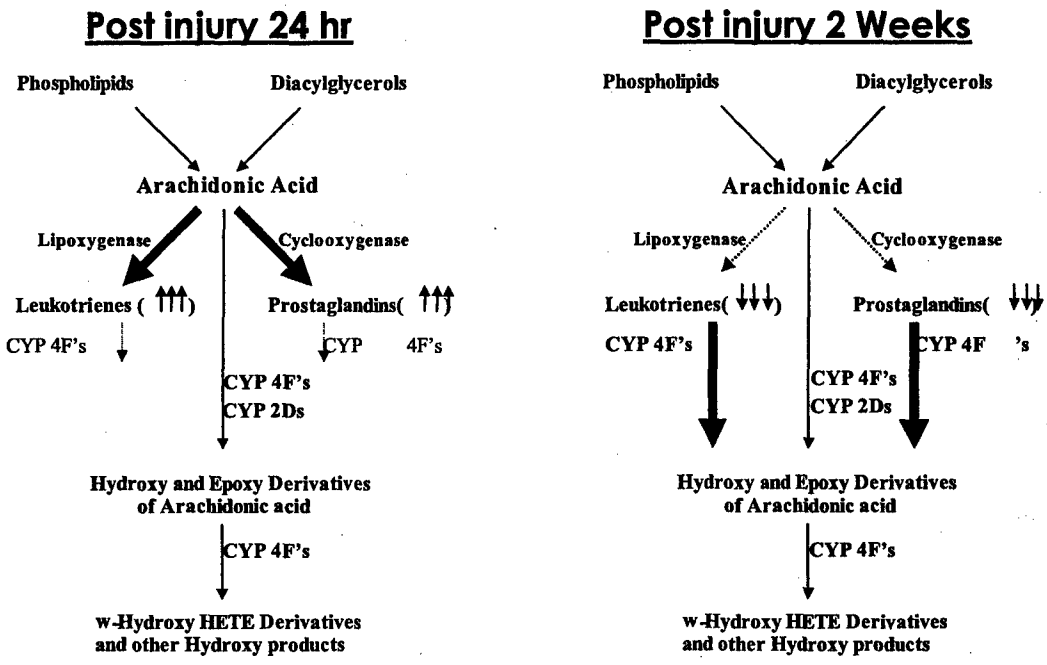

Scheme I. Differences in metabolic flow of leukotriene and prostaglandin mediators in proinflammatory (24 hrs) and anti-inflammatory periods (2 weeks).

Thus we focused on the effects of brain trauma and chemical/biological prompts of the inflammatory cascade on the CYP4F and 2D regulation of inflammation.

BODY

Injury whether physical, chemical or biological initiates changes in the body's natural defense systems including the expression of the Cytochrome P450 4F subfamily. We have shown in a body of work summarized below that injury and insult stimulate the expression of cyctooxygenase II (COX-II) and lipoxygenase-5 (LOX-5) in the same time frame as expression of the CYP 4F subfamily is suppressed. Both the induction of COX-2 and LOX-5 lead to the production of signals (prostaglandins and leukotriene B_4 respectively) which promote inflammatory response while the CYP4Fs metabolize these signals and lead to recovery from inflammation. At 24 hours after onset of injury, LOX-5 and COX-II reach maximum expression increasing production of inflammatory signals while CYP4Fs are reduced to their lowest levels of expression contributing to the rise in inflammatory signals. After 24 hours the recovery period

(reduction of LOX-5 and COX-II expression and increased expression of CYP4Fs) leads to reduction of inflammation by metabolism of the signals to products incapable of prompting inflammation.

Remarkable in this process is the finding that carefully controlled physical injury to the brain of experimental animals leads to an inflammatory response in liver lung heart and kidney in addition to the site of injury, the brain. This is consistent with many clinical studies pointing out that major complications of closed head injury patients stem from management of heart, lung and kidney functions.

How does signaling of injury occur between brain and extra cranial tissues? Our evidence so far implicates the agency of cytokines especially IL-1β IL-6, TNF-α etc. We can replicate changes seen in liver CYP4F expression of animals treated with lipopolysaccharide by treatment of cultured hepatocytes with IL-1β. These discoveries are being pursued.

KEY RESEARCH ACCOMPLISHMENTS

The key research outcomes for this project will be reported in the Reportable Outcomes Publications sections combined together.

- cloning, expression and characterization genome structure of
- demonstration that mice involves the $PPAR_{\alpha}$ receptor
- demonstration that traumatic brain injury results in loss of CYP4F expression concomitant with elevation of cyctooxygenase II and lipoxygenase 5 expression in brain
- demonstration that specific injury in brain leads to dramatic increases in the inflammatory cascade in extra-cranial tissues such as lung, liver, kidney and heart

- demonstration that the CYP4F subfamily isoforms catalyze the metabolism of therapeutic drugs at a brisk rate (CYP4F 11 is about as good as CYP3A4 for metabolism of erythromycin)
- demonstration of CYP4F changes in kidney may lead to alterations in kidney function

REPORTABLE OUTCOMES

Publications

1. Kalsotra, A., Cui, X., Antonovic, L., Robida, A.M., Morgan, E.T. and **Strobel, H.W.**: Inflammatory prompts produce isoform-specific changes in the expression of leukotriene B_4 W-hydroxylases in rat liver and kidney, *FEBS Letters*, **555**: 236-242, 2003.

2. Cui, X., Kalsotra, A., Robida, A.M., Matzilevich, D., Moore, A.N., Boehme, C.L., Morgan, E.T., Dash, P.K., and **Strobel, H.W.**: Expression of cytochrome P450 4F4 and 4F5 in infection and injury models of inflammation. *Biochemica et Biophysica Acta*, **1619**: 325-331, 2003.

3. Cui, X., Kawashima, H., Barclay, T.B., Peters, J.M., Gonzalez, F.J., Morgan, E.T., **Strobel, H.W.**: Molecular Cloning and Regulation of Expression of Two Novel Mouse CYP4F Genes Expression in PPARα Deficient Mice upon LPS and Clofibrate Challenges, *Journal of Pharmacology and Experimental Therapeutics*, **296**: 547-555, 2001.

4. Cui, X, Nelson, D.R., **Strobel, H.W.**: A Novel Human Cytochrome P450 4F Isoform (CYP4F11): cDNA Cloning Expression and Genomic Structure Characterization, *Genomics*, **68**:161-166, 2000.

5. **Strobel, H.W.**, Thompson, C.M. and Antonovic, L. Cytochromes P450 in Brain: Function and Significance. *Current Drug Metabolism*, **2**: 199-214, 2001.

Book Chapters

1. **Strobel, H.W.**, Kalsotra, A., and Dash, P.K. "Cytochrome P450 4Fs: Response and Role Following Brain Trauma" in Cytochromes P450, Biochemistry, Biophysics and Drug Metabolism (P. Anzenbacher and J. Hudecek, eds) Monduzzi Editore S.p.A. MEDIMOND Inc. Roma pgs. 107-111,2003.

CONCLUSIONS

- CYP4F isoforms, differentially distributed in extra cranial tissues, metabolize leukotriene B4 to different products, which may have vastly different functional consequences

- Regulation of CYP4F by cytokines may be an important regulatory mechanism in response to inflammation.

- The pronounced ability of the CYP4Fs to metabolize drugs used clinically to regulate lung function and heart output/rate (eq theophyline or verapamil/may be a source of complexity in management of combat injuries since the very enzymes which increase to resolve inflammation also clear supportive therapeutic agents faster as their expression increases.

Project I.E.

Detection and Quantitation of *Bacillus anthracis* in Macrophages

Investigator: Theresa M. Koehler, Ph.D.

Abstract

The poly-D-glutamic acid capsule of *Bacillus anthracis* is essential for virulence. Control of capsule synthesis occurs at the level of transcription and involves positive regulation of the capsule biosynthetic operon *capBCAD* by a CO_2 signal and three plasmid-borne regulators: *atxA*, *acpA* and *acpB*. Although the molecular mechanism for control of *cap* transcription is unknown, *atxA* affects *cap* expression via positive control of *acpA* and *acpB*, two genes with partial functional similarity. Transcriptional analyses of a genetically complete strain indicate that *capB* expression is several hundred-fold higher during growth in 5% CO_2 compared to growth in air. *atxA* was expressed appreciably during growth in air and induced only 2.5-fold by CO_2. In contrast, expression of *acpA* and *acpB* was induced up to 23-fold and 59-fold respectively by CO_2. 5′-end mapping of gene transcripts revealed *atxA*-regulated and *atxA*-independent apparent transcription start sites for *capB*, *acpA* and *acpB*. Transcripts mapping to all *atxA*-regulated start sites were increased during growth in elevated CO_2. The *acpA* gene has one *atxA*-regulated and one *atxA*-independent start site. *acpB* lies downstream of the *capBCAD* operon. A single *atxA*-independent start site maps immediately upstream of *acpB*. *atxA*-mediated control of *acpB* occurs via transcriptional read-through from *capBCAD* and *atxA*-dependent start sites 5′ of *capB*. Two *atxA*-regulated and one *atxA*-independent start site map upstream of *capB*. Transcription from the *atxA*-regulated start sites was significantly reduced in an *acpA acpB* double mutant but unaffected in mutants deleted for only *acpA* or *acpB*, in agreement with the current model for the epistatic relationships between the regulators.

Introduction

Control of virulence gene expression in *Bacillus anthracis* is highly dependent upon *atxA*, a regulatory gene located on virulence plasmid pXO1 (3). In genetically

complete strains harboring pXO1 and the second virulence plasmid pXO2, *atxA* acts as a global regulator controlling expression of the pXO2-encoded capsule biosynthetic gene operon, *capBCAD* (3, 6, 9, 17), the toxin structural genes, *pagA, lef* and *cya* on pXO1 (4, 11, 16), and a number of other genes located on the plasmids and chromosome (3). The mechanism by which *atxA* exerts its affect on target gene transcription is unknown. A direct affect of *atxA* on transcription has not been demonstrated for any *atxA*-controlled gene.

In our current model for capsule gene regulation, *atxA* controls *cap* gene transcription and capsule synthesis via the positive regulation of two pXO2-encoded regulators *acpA* and *acpB*. The model arose from studies employing a genetically complete ($pXO1^+$ $pXO2^+$) parent strain and isogenic mutants deleted for *atxA, acpA* and/or *acpB* (6). In $pXO1^+$ $pXO2^+$ strains, while deletion of *acpA* or *acpB* alone does not appreciably affect *capB* transcription or capsule synthesis, an *acpA acpB* double mutant exhibits drastically reduced *capB* transcription and is noncapsulated. Thus, *acpA* and *acpB* have some functional similarity. The amino acid sequences of the predicted products of these genes are approximately 62% homologous. Moreover, the proteins also share significant amino acid sequence similarity with the predicted product of *atxA*.

For many *atxA*-controlled genes, including *acpA* and *acpB*, expression is induced during growth in 5% atmospheric CO_2 or in media containing bicarbonate (2, 6, 10, 11, 14, 17, 18). CO_2-induced transcription of all three toxin genes has been demonstrated in experiments employing promoter-reporter gene fusions (2, 11, 14). RNA slot blot analysis of the *capB*, the first gene of the capsule biosynthetic operon, and *acpA* transcripts demonstrated an increase in both transcripts during culture in elevated CO_2 (17, 18). We recently demonstrated elevated *acpB* expression during growth in 5% CO_2 using RT-PCR (6).

CO_2/bicarbonate is likely to be a physiologically significant signal encountered by the bacterium in the host environment. Concentrations of bicarbonate/CO_2 (15-40mM) in the bloodstream of the host (5), are comparable to the concentration of bicarbonate/CO_2 present in the bicarbonate-supplemented growth media during culture *in vitro* (48mM). Although induction of *cap* gene expression *in vivo* has not been assessed quantitatively, our recent experiments employing a mouse model for inhalation anthrax

demonstrate the importance of the capsule biosynthetic operon and its regulators during infection (7). The noncapsulated *acpA acpB* mutant is completely attenuated in the mouse model. The LD_{50} and MTD (mean time to death) for the mutant were comparable to those of a mutant deleted for the entire capsule biosynthetic gene operon, *capBCAD*, suggesting that the regulators function similarly during *in vivo* and *in vitro* growth.

Here we further investigate the expression patterns of *capB* and the *cap* gene regulators, *acpA* and *acpB*, with respect to the CO_2/bicarbonate signal during culture *in vitro*. We also identify *atxA* and CO_2-controlled transcripts of *capB*, *acpA* and *acpB* to further elucidate the relationships between these regulators and this important cue.

Materials & Methods

Strains. Table 1 contains a complete list of strains, including plasmid content and relevant genotypes.

Table 1. Strains used in this study

Strain name	Plasmid content	Genotype	Relevant characteristics[a]	Reference
UT500	pXO1$^+$ pXO2$^+$	--	pXO2 from 6602 transduced into 7702	(3)
UT501	pXO1$^+$ pXO2$^+$	*atxA*	Km^r	(3)
UT502	pXO1$^+$ pXO2$^+$	*acpA*	Sp^r	(3)
UT525	pXO1$^+$ pXO2$^+$	*acpB*	Km^r	(6)
UT526	pXO1$^+$ pXO2$^+$	*acpA acpB*	Sp^r Km^r	(6)
UT538	pXO1$^+$ pXO2$^+$	*atxA acpB*	Sp^r Km^r	(7)

[a] Abbreviations: Km^r, kanamycin resistance; Sp^r, spectinomycin resistance.

Media and growth conditions. For analysis of gene expression during growth in elevated CO_2, strains were grown in conditions known to promote capsule synthesis as described previously (6, 8). $NBYCO_3$ medium was Nutrient Broth Yeast (8) supplemented with 0.8 % sodium bicarbonate (wt/vol). LBgoh was Luria-Bertani (1) broth containing 0.5 % glycerol to suppress sporulation. When indicated, media contained kanamycin (50 g/ml) (Fisher Scientific, Pittsburg, PA) and/or spectinomycin (100 g/ml) (Sigma-Aldrich, St. Louis, MO). Briefly, 30 ml of LBgoh (plus antibiotic[s] when required) in a 250-ml flask was inoculated with vegetative cells from an $NBYCO_3$ plate. Cultures were incubated at 30°C with agitation (200 rpm) for 12-14 h. Cultures were diluted into 50 ml of $NBYCO_3$ broth (without antibiotics) to obtain an initial optical density at 600 nm (OD_{600}) of approximately 0.1. Cultures were grown in 5 % CO_2 at 37°C with stirring (200 rpm) and sampled at early-, mid-exponential, late-exponential, and early-stationary phases. Under these growth conditions the parent and isogenic mutant strains had similar growth rates. For analysis of gene expression during growth in air, duplicate cultures were grown in unsupplemented NBY broth and incubated in air at 37°C with agitation (200 rpm).

Real-Time (Quantitative) Reverse Transcription PCR (Q-RT-PCR). RNA was extracted from cultures using the protocol and reagents of the Ribopure Bacteria kit (Ambion, Austin, TX). Typically, 10-30 g of RNA was obtained from 1 ml of culture. RNA preparations were treated with DNase-Free (Ambion, Austin, TX) according to the protocol of the supplier. The protocol and equipment used for Q-RT-PCR assays were described previously (6). The primer and probe sequences for the assays are shown in Table 2.

Table 2. Primer & probe sequences used in QRT-PCR assays.

Gene	Accession no.	Forward primer (+) Anti-sense primer (-)	Probe (5′FAM)[a]
gyrB	NC003997.3:4584-6506	(+) ACTTGAAGGACTAGAAGCAG (-) TCCTTTTCCACTTGTAGATC	CGAAAACGCCCTGGTATGTATA
atxA	NC001496.1:150042-151469	(+) ATTTTTAGCCCTTGCAC (-) AAGTTAATGTTTTATTGCTGTC	CTTTTATCTCTTGGAAATTCTATTACCACA
acpA	NC002146.1:68909-70360	(+) ATTATCTTTACCTCAGAATCAG (-) AACGTTAATGATTTCTTCAG	CAATTTCTGAAGCCATTTCTAATCTT
acpB	NC002146.1:49418-50866	(+) TTTTTCAATACCTTGGAACT (-)AATGCCTTTTAGAAACCAC	CTTGAAGAATCATTAGGAATCTCATTACA
capB	NC002146.1:56089-57483	(+) TTTGATTACATGGTCTTCC (-) CCAAGAGCCTCTGCTAC	ATAATGCATCGCTTGCTTTAGC

[a] FAM = 6-carboxyfluorescein

Nonquantitative RT-PCR. RNA was isolated and DNase-treated as described above for Q-RT-PCR. Nonquantitative RT-PCR was performed using the protocol and reagents supplied in the RETROscript kit by Ambion. The protocol has been described previously (6). Primers MD62 and MD129 were employed. Primer sequences are shown in Table 3.

Table 3. Primer sequences used in primer extension and non-quantitative PCR assays.[a]

Gene	Primer name	Primer sequence (5′-3′)
acpA	MD28	CTGTTTGTCATGTAAATAATTCTT
	MD33	AGAAATGGCTTCAGAAATTG
	MD34	TCGGCTAATATCTTTTTCCAT
acpB	MD62	TGTAAACCATTTTTCTTCGC
	MD64	TCCCTTGCTTTTAAGAATGT
	MD65	GTCAGAATCCCTGGTTTGTA
	MD108	GATTCAGCAGTGTTTCCAAT
	MD129	AGGCCTTAATTAAAGACGAGA
capB	PE2	CCATTTCTATACTAGATGTTGCATG

[a] DNA oligonucleotides were purchased from Integrated DNA Technologies (Coralsville, Iowa). PCRs were performed using a PE-Applied Biosystems (Norwalk, Conn.) PCR system 9700.

Primer extension. For primer extension analysis, RNA was extracted from cultures using RNAwiz (Ambion, Austin, TX) according to the protocol provided by the supplier. Typically between 20-100 μg of RNA was obtained per ml of culture. The method for primer extension analysis has been described previously (11, 15). Briefly, 30-50 μg of RNA was incubated in the presence of end-labeled primer [γ-32P] ATP (10mCi/ml). Reverse transcription reactions were carried out with Superscript (Invitrogen, Carlsbad, CA). Primer sequences are listed in Table 3. Primers MD28, MD33 and MD34 were used for analysis of *acpA* transcripts. Primers MD62, MD64, MD65 and MD108 were used for analysis of *acpB* transcripts. For analysis of the *capB* gene, the original primer (PE2) developed by Uchida et al (17) was employed.

The 5′ ends of the *acpA*, *acpB* and *capB* genes were sequenced using the *fmol* Sequencing Kit (Promega, Madison WI) according to protocol of the supplier. Primers employed in the sequencing reactions were the same primers used for the corresponding primer extension reactions (listed above).

Results

Quantitative and temporal assessment of CO_2-enhanced *capB*, *acpA*, and *acpB* expression during culture. Although CO_2-enhanced expression of *capB*, *acpA*, and *acpB* has been reported, the expression patterns of the regulators and the capsule biosynthesis gene during culture were not known. We used quantitative real-time RT-PCR (Taqman) to accurately measure *capB* transcript levels during growth in air and in 5% atmospheric CO_2 (Figure 1A). The *capB* gene is the first gene in the capsule biosynthetic gene operon. Throughout growth, *capB* transcript levels were 57- to 448-fold higher when cells were cultured in the presence of 5% CO_2, compared to cells grown in air. *capB* transcription was extremely low during growth in air, but increased 12- to 15-fold as the culture entered late-exponential growth phase (Fig. 1A box insert). The highest *capB* transcript

levels observed during growth in air were still remarkably less than levels observed at any time throughout growth in elevated CO_2.

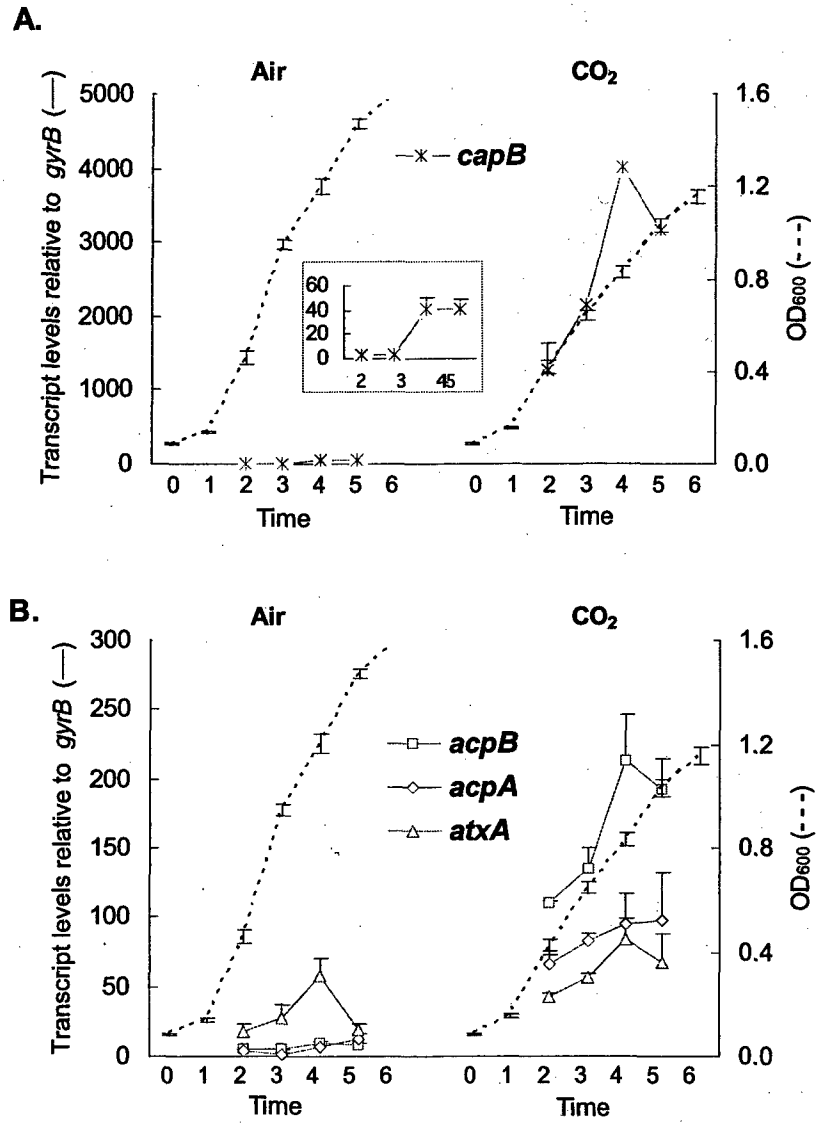

FIG. 1. Real-time transcript levels detected during growth in elevated CO_2 and during growth in air for (A) *capB* (B) *atxA*, *acpA* and *acpB*. Transcript levels shown represent four different data sets that were normalized to *gyrB* transcript levels. A representative growth curve is shown for each experiment. The boxed inset in A shows *capB* transcript levels using a different scale.

We used the same method to assess the relative transcript levels of *atxA*, *acpA* and *acpB* throughout growth in the presence of elevated CO_2 and during growth in air (Figure 1B). Q-RT-PCR results revealed that during growth in air, *acpA* and *acpB* expression was relatively unchanged and very low. *atxA* was expressed at a higher level than either *acpA* or *acpB* (2 to 5-fold) and expression levels were highest at late-exponential phase under this growth condition. The expression of *acpA* and *acpB* was markedly higher in 5% CO_2 than during culture in air. Expression of the *acpA* and *acpB* genes was induced 16- to 23-fold and 7- to 59-fold, respectively, depending on the growth phase. In contrast, the presence of CO_2 only affected *atxA* gene transcription approximately 2.5-fold.

The *capB* gene has *atxA*-regulated and *atxA*-independent transcriptional start sites. A previous report indicated two major transcriptional start sites for *capB*, P1 and P2, located 731bp and 625 bp upstream of the translational start, respectively (Figure 2) (17). These results were obtained from experiments employing strains lacking both virulence plasmids and carrying *capBCA* and *acpA* or *atxA* on multi-copy vectors. The data indicated that P1 and P2 were *atxA*- and *acpA*-regulated, but *acpA* had a much larger effect on transcription than *atxA* (17). We performed *capB* primer extension reactions using the same primer as Uchida et al. (PE2, (17)) and RNA obtained from the $pXO1^+$ $pXO2^+$ strain UT500 and isogenic mutants deleted for specific regulatory genes. All cultures were grown to mid-exponential phase in air or in elevated CO_2.

In contrast to the previous report, we found that transcripts mapping to P1 and P2 was reduced in the *atxA* mutant, but unaffected in the *acpA* mutant (Fig. 3A). Transcription from P1 and P2 was also unaffected in the *acpB* mutant. Nonetheless, steady state levels of transcripts originating at P1 and P2 decreased appreciably in the *acpA acpB* double mutant. These results are in accord with our previously established model for *capB* gene regulation (6) in which one of the two regulators, *acpA* or *acpB*, is required for *atxA*-mediated *trans*-activation of *capB* transcription. Deletion of either *acpA* or *acpB* does not significantly affect *capB* transcripts because the two regulators have some partial functional redundancy.

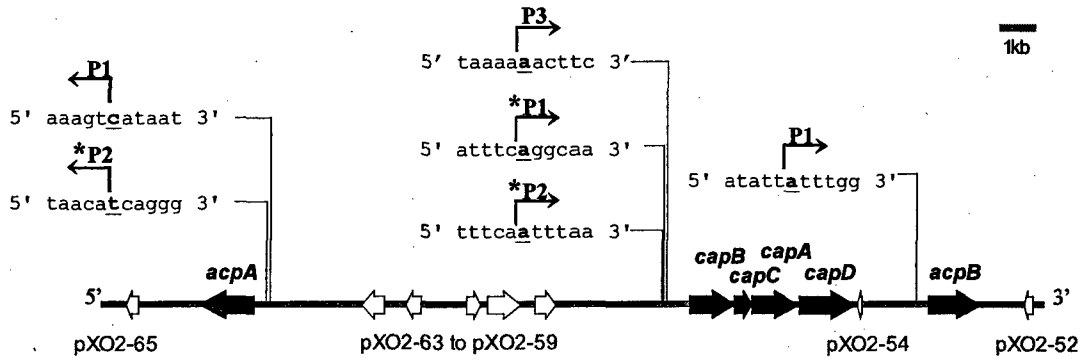

FIG. 2. Model showing transcriptional start sites for the capsule biosynthetic gene operon (*capBCAD*) and the *cap* gene regulators, *acpA* and *acpB*. Nucleotides corresponding to the transcriptional start sites are in bold and underlined. *atxA*/CO_2-regulated start sites are denoted with an asterisk. P1 and P2 upstream of *capB* were reported previously by Uchida and co-workers (17).

Our data also revealed a previously unidentified transcriptional start site, P3 that is located 796 bp upstream from the translational start site of *capB* (Fig. 2). P3 transcription is not affected by *acpA* or *acpB* (Fig. 3). We observed a slight but reproducible increase in P3 transcription in the *atxA*-null mutant suggesting that other factors may be involved in regulation of transcription from this start site. It is unlikely that P1 and P2 transcripts are the result of *atxA*-dependent processing of the P3 transcript since P3 transcription remained unchanged in the *acpA acpB* mutant as P1 and P2 transcripts decreased significantly. Other bands (unlabelled in Figure 3) were visualized consistently but did not appear to be affected by the capsule gene regulators. It is likely that these minor bands correspond to regions of RNA with secondary structure that lead to pausing of reverse transcriptase. The *B. anthracis* genome is A-T rich (65% for the chromosome, 67.5% for pXO1 and 67% for pXO2) (13). Alternatively, the bands may represent processed P3 transcripts.

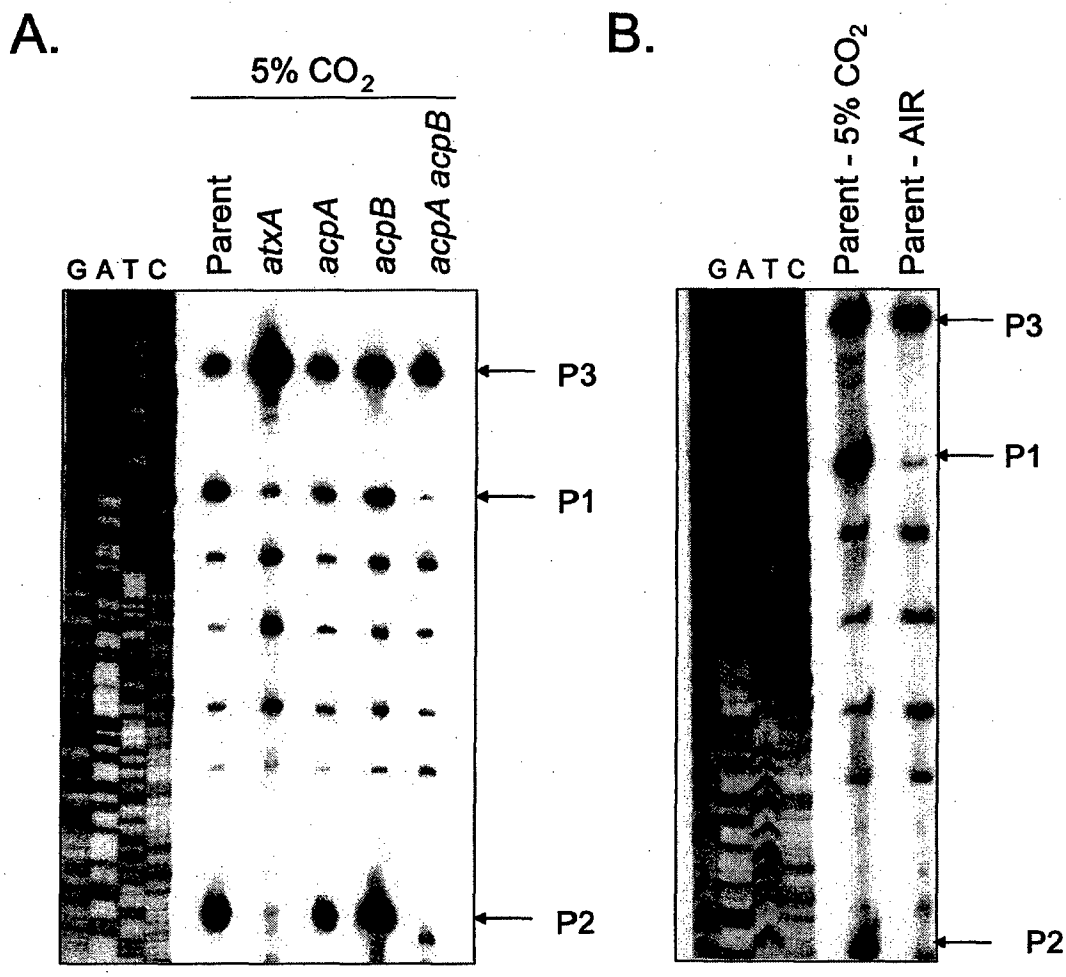

FIG. 3. Primer extension of *capB* transcripts. PE2 primer was employed (17). (A) RNA was extracted from cells grown in 5% CO_2. Lane 1: UT500; lane 2: UT501 (*atxA*); lane 3: UT502 (*acpA*); lane 4: UT525 (*acpB*); lane 5: UT526 (*acpA acpB*). (B) RNA was extracted from cells as shown: Lane 1: UT500 - 5% CO_2; lane 2: UT500 - air; Lane 3; UT501 (*atxA*) - 20% CO_2.

atxA has been linked to CO_2-enhanced gene expression in *B. anthracis* (10, 11). Previous reports of toxin gene expression have indicated *atxA*/CO_2-regulated transcriptional start sites for *lef*, *cya*, and *pagA* (4, 11). The *lef* and *cya* genes each have one apparent start site that is *atxA*-dependent and CO_2-induced (4). The *pagA* gene has two apparent start sites; one is constitutively expressed at a low level, while the other is *atxA*-dependent and CO_2-induced (11). To determine whether the

atxA-regulated transcriptional start sites observed for the *capB* gene were also influenced by CO_2, we compared the primer extension results obtained using RNA from the parent strain cultured in air and RNA isolated from the parent strain grown in elevated CO_2 (Fig. 3B). Levels of transcripts corresponding to both *atxA*-regulated start sites, P1 and P2, were elevated during growth in 5% CO_2. Thus, the low level of *capB* transcript detected during aerobic growth (Fig. 1A) most likely correlates with transcripts initiating at P3.

We searched for consensus sequences upstream of the *capB* transcriptional start sites to reveal putative promoter regions. Conical -10 and -35 sequences typical of *B. subtilis* σ^A promoters were not apparent upstream of the P3 start site, suggesting that additional regulatory mechanisms may be involved in controlling transcription at this start site. We noted a potential -10 but not a -35 consensus sequence upstream of P1. Prototypical -10 and -35 sequences were not readily identifiable for the P2 start site indicating that P2 may be a break down product of P1, as suggested previously by Uchida (17).

acpB is co-transcribed with the _cap_ operon. *acpB* transcript levels decrease significantly (15-fold) in the absence of *atxA* (6). We performed 5'end mapping experiments using RNA isolated from the parent strain and the *atxA*-null mutant to map *atxA*-regulated and *atxA*-independent transcriptional start sites for *acpB* and reveal potential promoter sequences. Using various primers, we identified a single transcriptional start site, P1, located 310 bp upstream from the translational start codon (Fig. 2 and Fig. 4). A weak -10 promoter sequence (GATAAT) was identified upstream of this start site, but a canonical -35 sequence was not readily discernible. Surprisingly, the steady state level of this transcript was unchanged in the *atxA* mutant and no other apparent start sites were noted in the *capD-acpB* intergenic region (data not shown).

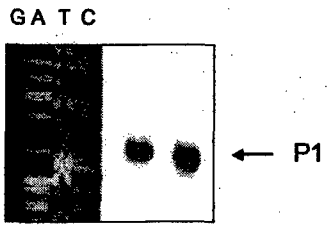

FIG. 4. Primer extension analysis of *acpB* transcripts. MD65 primer was employed (See Methods). RNA was extracted from cells grown in 5% CO_2. Lane 1: UT500; lane 2: UT501 (*atxA*).

The *acpB* gene is located approximately 2 kb downstream and in the same orientation as the *cap* gene operon (Fig. 2). The inability to identify an *atxA*-regulated start site in the region between *capD*, the last gene of the capsule biosynthetic gene operon and *acpB* suggested that *acpB* may be co-transcribed and that *atxA*-regulation of *acpB* was the result of transcription associated with the *cap* operon. We employed RT-PCR to test for transcripts extending from *capD* to *acpB*. Using primers corresponding to sequences of the *capD* and *acpB* genes we obtained the amplicon shown in figure 5. The data indicate that *acpB* is co-transcribed with *capBCAD* and suggest that *atxA*-mediated regulation of *acpB* may occur via the *atxA*-dependent P1 and P2 start sites of *capB*. This finding is somewhat remarkable given the unusually large size of the predicted mRNA molecule (9 kb).

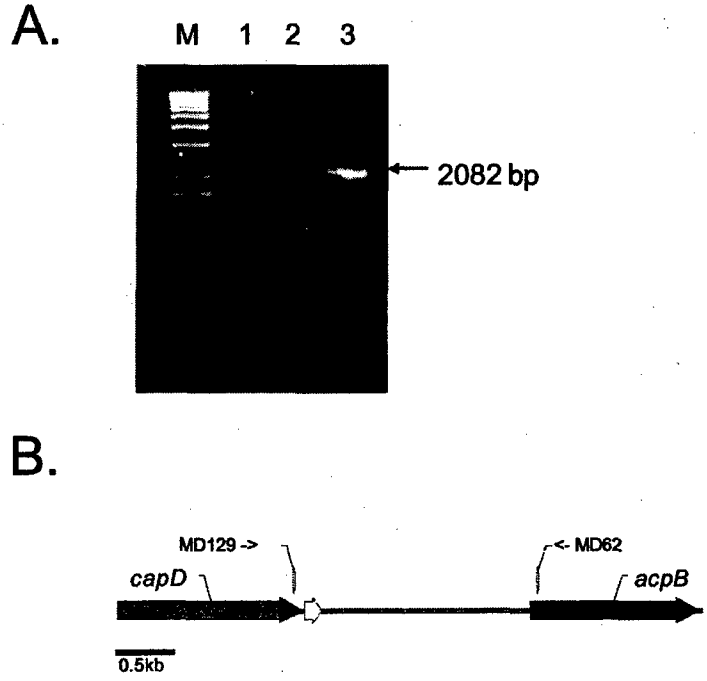

FIG. 5. RT-PCR of the *capD-acpB* region. (A) *capD-acpB* transcript was detected. Lane 1, DNA markers; lane 1, cDNA template, + reverse transcriptase; lane 2, cDNA template, - reverse transcriptase; lane 3, DNA template, PCR control (B) Illustration showing location of primers MD62 and MD129 employed in the PCR reactions used in (A). The open arrow indicates the position of pXO2-54.

The *acpA* gene has *atxA*-regulated and *atxA*-independent transcriptional start sites. We performed a similar analysis of the other *atxA*-controlled *cap* regulator, *acpA*. Primer extension analysis of the *acpA* gene revealed 2 major transcriptional start sites, P1 and P2, located 379 and 353 bp respectively, upstream from the translational start (Fig. 2 and Fig. 6A). P1 expression was unaffected by *atxA* yet P2 expression was *atxA*-regulated since P2 transcripts were undetectable in the *atxA*-null mutant (Fig. 6A). There was no evidence of *acpA* auto-regulation as P1 and P2 transcription did not vary in the *acpA* mutant samples. Similarly, in an *acpB* mutant and an *acpA acpB* double mutant, the *acpA* P1 and P2 transcript levels did not change, indicating that *atxA*-mediated regulation of *acpA* does not appear to require any of these factors. Similar to the results obtained for the *capB* gene, transcripts from the *atxA*-regulated start site of *acpA*, P2, but not the *atxA*-independent start site, P1, were

increased during growth in elevated CO_2 (Fig. 6B). Conical -10 and -35 promoter sequences could not be readily identified upstream of either the P1 or P2 sites indicating that the expression of *acpA* is most likely sigma-A independent.

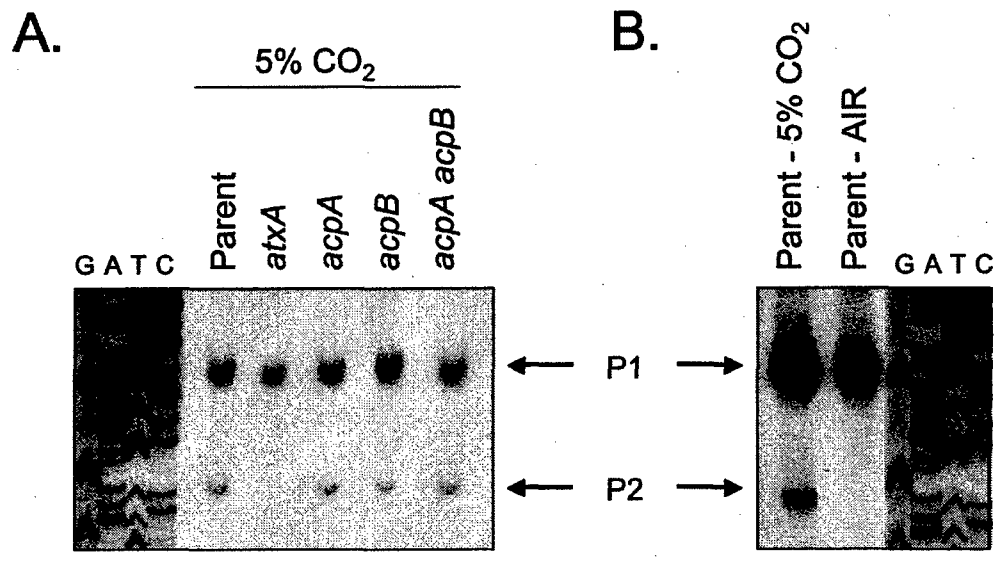

FIG. 6. Primer extension of *acpA* transcripts. MD28 primer was employed. (A) RNA was extracted from cells grown in 5% CO_2. Lane 1: UT500; lane 2: UT501 (*atxA*); lane 3: UT502 (*acpA*); lane 4: UT525 (*acpB*); lane 5: UT526 (*acpA acpB*). (B) RNA was extracted from cells as shown: Lane 1: UT500 - 5% CO_2; lane 2: UT500 - air.

Discussion

In the work described here, we characterized transcription of *capB*, the first gene of the *B. anthracis* capsule biosynthetic operon; *acpA* and *acpB*, functionally similar *cap* regulators; and *atxA*, a master regulator controlling *acpA* and *acpB* expression. In light of the complex regulation of capsule synthesis, we wanted to (1) assess temporal expression of *capB* and the regulators in batch culture, (2) examine expression of the genes in response to elevated CO_2, a signal considered to be important in the host, and (3) establish the apparent

transcriptional start sites for these genes, distinguishing regulated and non-regulated transcripts.

Capsule synthesis and *capB* gene expression correlate directly. When *B. anthracis* is grown in nutrient broth yeast medium (NBY) supplemented with 0.8% bicarbonate in an atmosphere of 5% CO_2, capsule is first observed during mid-exponential phase and cells with the largest capsule diameter are visualized at early stationary phase (6). Quantitiative RT-PCR analyses performed here, indicate that *capB* gene expression was several hundred-fold higher during growth in elevated CO_2 than that observed during growth in air. The highest level of *capB* transcript observed during growth in 5% CO_2 was detected at mid- to late-exponential phase, just before cells become fully capsulated. *capB* transcription is detected throughout growth in air, yet microscopic examination of India Ink preparations of the parent strain do not show capsule on the surface of cells grown in this environment. This suggests that a minimal level of *cap* transcript must be attained before capsule can be readily identified on the bacterial cell surface. Temporal expression patterns of *acpA* and *acpB* indicated that the transcript levels for both regulators in cultures grown in 5% CO_2 were relatively high at early exponential phase and increased further as the culture grew. Taken together, the Q-RT-PCR data suggest that the CO_2 signal is quickly sensed by the bacterium, leading to a rapid increase in expression of both *acpA* and *acpB* that subsequently leads to induction of *capB*.

Two apparent transcriptional start sites for *capB* were identified previously (17). However, the regulation of these start sites did not completely agree with the current model for capsule gene regulation in a genetically complete strain. In the work described here, we have established the apparent transcriptional start sites for *capB*, distinguishing regulated and non-regulated transcripts, in the pXO1$^+$ pXO2$^+$ strain. Results of primer extension of *capB* transcripts confirmed two *atxA*-regulated transcriptional start sites, P1 and P2, as reported previously by Uchida (17). However, in contrast to the previous report, P1 and P2 transcript levels were unaffected in the *acpA* mutant. It is likely that our findings differ from previously published data because the steady state levels of *atxA* and *acpA* are extremely important for regulation of *capB* expression. In the previous study (17), elevated P1 and P2 transcription was

observed in a pXO1$^-$ pXO2$^-$ strain containing the *capBCA* genes and *atxA* or *acpA* cloned on high copy vectors. Taken together, the data suggest that over-expression of *acpA* can lead to an increase in P1 and P2 transcription in the absence of *atxA*. In addition, over-expression of *atxA* may bypass the requirement for *acpA* or *acpB* for *cap* gene activation. We determined that in the pXO1$^+$ pXO2$^+$ *acpA acpB* strain, *cap* gene expression is significantly reduced and the strain is noncapsulated, indicating that the levels of *atxA* normally present in a genetically complete strain are not sufficient for positive regulation of P1 and P2 transcription in the absence of *acpA* and *acpB*. The low levels of P1 and P2 transcripts detected in the *atxA* mutant are likely the result of positive regulation by the low levels of *acpA* and *acpB* transcripts present in an *atxA* mutant. Finally, the non-regulated *capB* transcription start site P3, was not noted previously by Uchida and co-workers (17). The basal level of *capB* transcription observed in the noncapsulated *acpA acpB* mutant and during growth in air most likely results from transcription at this site. A slight increase in P3 transcript was observed in the *atxA* mutant suggesting an additional level of control.

Primer extension of *acpA* transcripts revealed an *atxA*/CO_2-regulated transcript (P2) and an *atxA*-independent transcript (P1). P1 transcription is evident during growth in air and in the absence of *atxA*. *atxA*-regulated P2 transcription is induced in the presence of elevated CO_2. *atxA*-independent expression of *acpB* results from transcription initiating at a start site (P1) immediately upstream of *acpB*, whereas *atxA*-mediated regulation of *acpB* expression occurs via read-through transcription from the P1 and P2 start sites of the *cap* operon. The *cap-acpB* transcript would likely result in a positive feedback loop for *acpB* expression. Curiously, in UT500, expression of *capB* is approximately 50-fold higher than expression of *acpB*. Further work will address the stability of the *capBCAD-acpB* RNA molecule.

The data described here and work published previously suggest that *acpA* and *acpB* levels are limiting for *capB* transcription in the absence of *atxA* and/or elevated CO_2 (6, 17, 18). *B. anthracis* strains cultured in air are normally noncapsulated, but overexpression of *acpA* in a pXO1$^-$ pXO2$^+$ strain leads to capsule production during growth in air (17). Additionally, *capB* primer extension experiments employing RNA from a pXO1$^-$ pXO2$^-$ strain with

the *capBCA* genes and *acpA* cloned on high copy vectors revealed high levels of transcripts mapping to P1 and P2 in the absence of *atxA* (17).

Transcriptional regulation of *atxA* is unlike that observed for *acpA* and *acpB*. We only observed a small increase (2.5-fold) in *atxA* transcript levels during growth in elevated CO_2 compared to that observed during growth in air. *atxA* has a single transcriptional start site and a previous study employing primer extension reactions and Western hybridizations indicated no difference in *atxA* expression during growth in elevated CO_2 versus growth in air (4). Consensus sequences for promoter recognition by sigma A RNA polymerase (-10 and -35 sequences) have been noted upstream of *atxA*. Such sequences have not been found upstream of *acpA*, *acpB*, or *capBCAD*. Finally, some data suggest that, in contrast to *acpA* and *acpB*, *atxA* levels are not limiting for target gene expression. Dai et al (4) demonstrated that over-expression of *atxA* actually leads to a decrease in expression of *pagA* and decreased toxin synthesis and Sirard et al (14) showed that a second copy of the *pagA* promoter cloned on pXO1did not affect expression of the *pagA* gene at the normal pXO1 locus.

The complex regulation of capsule gene expression in *B. anthracis*, which includes the CO_2 signal, a regulatory cascade with functionally similar regulators, multiple regulated and non-regulated transcription start sites, and a positive feedback loop, is made even more intriguing by the amino acid sequence similarity of the three regulatory proteins. The master regulator, AtxA, is approximately 50% similar to the *cap* regulators AcpA and AcpB. AcpA and AcpB are 62% similar to each other. In all cases, the amino acid sequence similarity is throughout the proteins, and not limited to a specific region or predicted domain. Secondary and tertiary protein structure predictions suggest that the proteins are soluble, basic proteins. They do not contain strong motifs indicative of nucleic acid binding; however, blast results indicate some amino acid homology to the transcriptional regulator Mga (40-45% similar) of *Streptococcus pneumonae* and BglG (40-45% similar), an anti-terminator protein in *E. coli*. Mga has been shown to bind directly to the promoter sequences of the genes that it activates (12), while BglG is an anti-terminator protein that binds to the leader sequence of mRNA to allow read-through of its target genes. Neither DNA- nor RNA-binding activities have been ascribed to the

B. anthracis proteins. Further investigations will be directed toward discovery of the molecular functions of these unique regulators and the mechanism by which their expression and/or function is linked to the CO_2/bicarbonate signal.

References

1. **Ausubel, F. M.** 1993. Current protocols in molecular biology. Greene Publishing Associates and Wiley-Interscience, New York, N.Y.
2. **Bartkus, J. M., and S. H. Leppla.** 1989. Transcriptional regulation of the protective antigen gene of *Bacillus anthracis*. Infect Immun **57**:2295-300.
3. **Bourgogne, A., M. Drysdale, S. G. Hilsenbeck, S. N. Peterson, and T. M. Koehler.** 2003. Global effects of virulence gene regulators in a *Bacillus anthracis* strain with both virulence plasmids. Infect. Immun. **71**:2736-43.
4. **Dai, Z., J. C. Sirard, M. Mock, and T. M. Koehler.** 1995. The *atxA* gene product activates transcription of the anthrax toxin genes and is essential for virulence. Mol Microbiol **16**:1171-81.
5. **Davson, H., and M. B. Segal.** 1975. The cell in relation to its environment. The carriage and release of the blood gases, p. 81-112, Introduction to physiology. Academic Press Inc., London.
6. **Drysdale, M., A. Bourgogne, S. G. Hilsenbeck, and T. M. Koehler.** 2004. *atxA* controls *Bacillus anthracis* capsule synthesis via *acpA* and a newly discovered regulator, *acpB*. J Bacteriol **186**:307-15.
7. **Drysdale, M., S. Heninger, J. Hutt, Y. Chen, C. Lyons, and T. M. Koehler.** 2005. Capsule synthesis by *Bacillus anthracis* is required for dissemination in a murine inhalation anthrax. EMBO J. **12**:221-7.
8. **Green, B. D., L. Battisti, T. M. Koehler, C. B. Thorne, and B. E. Ivins.** 1985. Demonstration of a capsule plasmid in *Bacillus anthracis*. Infect. Immun. **49**:291-7.
9. **Guignot, J., M. Mock, and A. Fouet.** 1997. AtxA activates the transcription of genes harbored by both *Bacillus anthracis* virulence plasmids. FEMS Microbiol Lett **147**:203-7.

10. **Hoffmaster, A. R., and T. M. Koehler.** 1997. The anthrax toxin activator gene *atxA* is associated with CO_2-enhanced non-toxin gene expression in *Bacillus anthracis*. Infect Immun **65**:3091-9.

11. **Koehler, T. M., Z. Dai, and M. Kaufman-Yarbray.** 1994. Regulation of the *Bacillus anthracis* protective antigen gene: CO_2 and a *trans*-acting element activate transcription from one of two promoters. J. Bacteriol. **176**:586-95.

12. **Perez-Casal, J., M. G. Caparon, and J. R. Scott.** 1991. Mry, a trans-acting positive regulator of the M protein gene of *Streptococcus pyogenes* with similarity to the receptor proteins of two- component regulatory systems. J Bacteriol **173**:2617-24.

13. **Read, T. D., S. N. Peterson, N. Tourasse, L. W. Baillie, I. T. Paulsen, K. E. Nelson, H. Tettelin, D. E. Fouts, J. A. Eisen, S. R. Gill, E. K. Holtzapple, O. A. Okstad, E. Helgason, J. Rilstone, M. Wu, J. F. Kolonay, M. J. Beanan, R. J. Dodson, L. M. Brinkac, M. Gwinn, R. T. DeBoy, R. Madpu, S. C. Daugherty, A. S. Durkin, D. H. Haft, W. C. Nelson, J. D. Peterson, M. Pop, H. M. Khouri, D. Radune, J. L. Benton, Y. Mahamoud, L. Jiang, I. R. Hance, J. F. Weidman, K. J. Berry, R. D. Plaut, A. M. Wolf, K. L. Watkins, W. C. Nierman, A. Hazen, R. Cline, C. Redmond, J. E. Thwaite, O. White, S. L. Salzberg, B. Thomason, A. M. Friedlander, T. M. Koehler, P. C. Hanna, A. B. Kolsto, and C. M. Fraser.** 2003. The genome sequence of *Bacillus anthracis* Ames and comparison to closely related bacteria. Nature **423**:81-6.

14. **Sirard, J. C., M. Mock, and A. Fouet.** 1994. The three *Bacillus anthracis* toxin genes are coordinately regulated by bicarbonate and temperature. J Bacteriol **176**:5188-92.

15. **Tsui, H. C. T., A. J. Pease, T. M. Koehler, and M. E. Winkler.** 1994. Detection and quantitation of RNA transcribed from bacterial chromosomes and plasmids, p. 179-204. *In* K. W. Adolph (ed.), Molecular Microbiology Techniques, Part A. Academic Press Inc., San Diego, California.

16. **Uchida, I., J. M. Hornung, C. B. Thorne, K. R. Klimpel, and S. H. Leppla.** 1993. Cloning and characterization of a gene whose product is a trans-activator of anthrax toxin synthesis. J Bacteriol **175**:5329-38.

17. **Uchida, I., S. Makino, T. Sekizaki, and N. Terakado.** 1997. Cross-talk to the genes for *Bacillus anthracis* capsule synthesis by *atxA*, the gene encoding the trans-activator of anthrax toxin synthesis. Mol. Microbiol. **23**:1229-40.

18. **Vietri, N. J., R. Marrero, T. A. Hoover, and S. L. Welkos.** 1995. Identification and characterization of a *trans*-activator involved in the regulation of encapsulation by *Bacillus anthracis*. Gene **152**:1-9.

Project II.A.
Pathology Core

Investigators: James T. Willerson, M.D.
L. Maximilian Buja, M.D.
Silvio H. Litovsky, M.D.

In the DREAMS program for 2004, we continued to provide expert pathology assessment of various human and animal tissues that were obtained as part of the various research projects. Methods of analysis for these tissues included routine gross morphology, histology, lipid analysis, electron microscopy, immunohistochemistry, and quantitative morphometry. These techniques have been extremely useful in allowing investigators throughout the DREAMS program to evaluate tissues from experimental animal models to make quantitative determinations that allow them to test their hypotheses, develop their methods more exactly, and promote the development and refinement of new hypotheses.

In 2004, the pathology core continued to interact extensively with the DREAMS investigators in order to get the maximum information from experimental protocols and thus, provide the best possible understanding of the pathology findings. These analyses were available for studies of tissues (i.e., experimental animal & human) that were obtained by investigators throughout the DREAMS project. In this particular part of the DREAMS program, we have again provided financial assistance for the efforts of Dr. Silvio Litovsky, who provide most of the analyses mentioned above, as well as support for the anatomic and laboratory pathology studies.

Project II.D.

Thermal Detection and Treatment of Inflammation and Necrosis

Investigator: S. Ward Casscells, M.D.

Work in the area of intravascular thermography is no longer being performed in our laboratories. The primary investigator on that project, Dr. Morteza Naghavi, left our institution back in 2003 in order to pursue private commercialization of several other medical technologies. Being on the original inventors of the thermography basket catheter and one of the founders of Volcano Therapeutics, Dr. Naghavi was paramount to the success of any future thermographic developments. As a result, we chose to terminate efforts to further develop thermography catheters.

The technology developed in this project throughout the DREAMS program was perhaps the most technologically successful. Of the numerous spin-off companies that came about through DREAMS, Volcano was, and still is, a leader in the development of diagnostic catheters for assessment of cardiovascular disease. The acquisition of Jomed helped build their infrastructure enough to exceed 600 employees. Although the company now seems poised to focus on the utility of intravascular ultrasound (IVUS), Volcano's interest in developing invasive, catheter based approaches for assessing disease was a direct result of our team's thermography research funded through DREAMS.

Project II.E.

Initial Evaluation of a New Axial Flow Pump, Inserted by Minimally Invasive Thoracotomy, to Maintain Cardiac Output in a Porcine Model of Cardiogenic and Hemorrhagic Shock

Investigators: O. Howard Frazier, M.D.
Branislav Radovancevic, M.D.

In 2004, the laboratory of Dr. O.H. Frazier underwent significant personnel changes involving the day-to-day laboratory staff, including Research Assistants, Research Associates, Laboratory Managers, Animal Care Technicians, Veterinary Staff, and Surgical Staff. Because of this, several of the research projects were put on hold in order to better focus on those most appropriate for continuation under minimal staff. The DREAMS project overseen by Dr. Frazier was one such project that we decided to temporarily put on hold until laboratory staffing was more adequate to handle the accompanying tasks required by the project.

As a result, we are not submitting a research report for DREAMS Project II.E for the year of 2004. Furthermore, we did not accrue any expenses that were chargeable to this DREAMS project and thus, the entirety of the project funds is still available. We wish to extend to use of the funds and resume this DREAMS project in year 2005.

Project II.F.

Physiological Magnetic Resonance Imaging

Investigators: James T. Willerson, M.D.
Silvio H. Litovsky, M.D.
Morteza Naghavi, M.D.

Work for this DREAMS project was not continued in 2004, rather we focused our diagnostic imaging endeavors on computed tomography (CT) angiography. We have begun to explore innovative approaches to better assessing cardiovascular disease through the use of CT angiography. Given our strong relationship with GE Healthcare and their commitment to developing CT as the premier platform for cardiac imaging, we chose to terminate our MRI studies.

Throughout the DREAMS program, we were able to make some remarkable advances in the field of magnetic resonance imaging (MRI). Through collaboration with researchers at the University of Houston, departments of Physics and Electrical Engineering, were successfully developed various state-of-the-art hardware items for improving temporal and spatial resolution in MRI. We helped develop an intraluminal MRI probe for performing intravascular MRI in the coronary arteries in order to image lipid-rich plaques. Although early work demonstrated unparalleled resolution in rabbit atherosclerotic arteries ex vivo, obtaining similar resolution in humans would require extensive catheterization. Additional work in this field by our group showed that superconducting quantum interference devices (SQUID's) could be engineered to achieve an order of magnitude better spatial resolution in ex vivo samples. However, the limitation of acquisition time and the dynamic motion of the heart limit the potential commercial potential of SQUID devices for cardiac imaging.

In the extension of DREAMS, our new program, T5: Texas Training & Technology Against Trauma and Terrorism, aims to focus heavily on cardiac CT development in order many of goals originally set forth in the DREAMS project description for this project (II.F).

Project III.A.

Induction of Chemokine Expression in Endothelial Cells by C-Reactive Protein

Investigator: Edward T.H. Yeh, M.D.

Introduction

Inflammation is a major risk factor in the development of atherosclerosis and its subsequent events, such as acute coronary syndrome. C-Reactive Protein (CRP) is probably the best clinical marker of inflammation. It can be used in the prediction of complications in patients with acute coronary syndrome. Most importantly, it can also be used to predict future cardiovascular events in apparently healthy men and women. CRP's predictive power in cardiovascular risk prediction could be indirect due to its ability to measure systemic inflammation. Alternatively, CRP's predictive power could be a result of its direct biological activity in augmenting vascular inflammation.

Research accomplishments

Our laboratory has shown that CRP can directly activate human coronary endothelial cells to express adhesion molecules and secrete chemokines [1,2]. Thus, CRP is not only a marker of inflammation, but also a culprit in setting up a chain of events that eventually leads to heart attack [3-5].

We have also shown that CRP can be produced by vascular smooth muscle cells, but not by endothelial cells[6]. The ability of vascular smooth muscle cells to produce CRP is clinically important because the locally produced CRP could play a direct role in augmenting vascular inflammation leading to cardiovascular complications. More recently, we also demonstrated that adipocytes could be stimulated to produce CRP by inflammatory cytokines and adipokines. This discovery links CRP production to metabolic syndrome, one of the very serious clinical problems afflicting the population of the United States and the developed countries.

Conclusions

Our laboratory pioneered in the discovery of CRP's direct biological effect on vascular inflammation. We have identied two additional sources of CRP production, namely the vascular smooth muscle cells and adipocytes. These findings have significant implications for the pathogenesis of vascular inflammation, metabolic syndrome, and acute coronary syndrome.

Publications

1. Pasceri V, Willerson JT, Yeh ET. Direct proinflammatory effect of C-reactive protein on human endothelial cells. *Circulation*. 2000;102:2165-8.

2. Pasceri V, Cheng JS, Willerson JT, et al. Modulation of C-reactive protein-mediated monocyte chemoattractant protein-1 induction in human endothelial cells by anti-atherosclerosis drugs. *Circulation*. 2001;103:2531-4.

3. Yeh ET, Anderson HV, Pasceri V, et al. C-reactive protein: linking inflammation to cardiovascular complications. *Circulation*. 2001;104:974-5.

4. Yeh ET. CRP as a mediator of disease. *Circulation*. 2004;109:II11-4.

5. Yeh ET. C-reactive protein is an essential aspect of cardiovascular risk factor stratification. *Can J Cardiol*. 2004;20:93B-96B.

6. Calabro P, Willerson JT, Yeh ET. Inflammatory cytokines stimulated C-reactive protein production by human coronary artery smooth muscle cells. *Circulation*. 2003;108:1930-2.

Project III.B.

Nitrotyrosine Formation, Metabolism and Function: Functions of Nitric Oxide and Nitrotyrosine in Shock, Sepsis, and Inflammation

Investigator: Ferid Murad, M.D., Ph.D.

INTRODUCTION

The biological effects of nitric oxide may be due to increased cyclic GMP synthesis by guanylyl cyclase or by cyclic GMP-independent pathways. With regard to the latter, one of the important effects of nitric oxide is the interaction with superoxide anion to form peroxynitrite ($ONOO^-$). $ONOO^-$ is very reactive and can modify proteins, DNA and lipids. One of its effects is to form nitrotyrosine with tyrosine residues in proteins or with free tyrosine. Our laboratory is examining the proteins that may contain nitrotyrosine in order to identify these proteins and determine their function. Our hypothesis is that protein nitration is a common mechanism by which inflammation caused dysfunctional changes in cells. Once formed, nitrated proteins may exacerbate the pathogenic process and play a role in the connection between inflammation and following complications.

RESULTS

Task 1: Development of assays for nitrotyrosine and nitrotyrosine-containing proteins.

Immunoprecipitation and immunodetection of nitrated proteins is a well-accepted approach for initial screening. However, for a high level of confidence in the obtained data, we have developed a mass spectrometry-based method for identification of protein nitration (22). Screening includes analysis of MALDI-TOF mass spectra generated for nitrated proteins. A typical pattern of MALDI-TOF mass peaks for tyrosine nitrated peptide includes $[MH^+]$, $[MH^+ + 13]$, $[MH^+ + 15]$, $[MH^+ + 29]$, and $[MH^+ + 45]$ peaks. $[MH^+]$ and $[MH^+ + 45]$ peaks represent non-nitrated and nitrated peptide, respectively. All of other peaks derive from the photodecomposition of nitrotyrosine.

Fig. 1A shows the pattern generated *in vitro* for a model nitrated peptide, angiotensin II. $[MH^+ + 13]$ and $[MH^+ + 15]$ peaks of the pattern are always low and it is more problematic to find this pattern in proteins nitrated *in vivo*. However, we have observed partial patterns in many *in vitro* and *in vivo* nitrated proteins. Fig. 1B shows a nitrated peptide found in the mitochondrial protein, Rieske protein, under diabetic conditions *in vivo* (19). The pattern is not complete and expected peaks are low in intensity. To prove tyrosine nitration, it was necessary to perform MS/MS scan for $[MH^+ + 45]$ peak. Tandem MALDI/MS spectrum for $[MH^+ + 45]$ *m/z* 1043.4 was generated on QSTAR instrument (Fig. 1C). The y_2 and y_1 ions at *m/z* 383.1 and 175.1, respectively, show the unique mass difference of nitrotyrosine with a residue mass of 208 Da (Fig. 7D). In addition, an immonium ion corresponding to nitrotyrosine is seen at *m/z* 181.1.

A brief summary for the mass spectrometry approach is that the pattern is helpful, however, the identity of nitrated peptides should always be proven by MS/MS spectrum of $[MH^+ + 45]$ ion.

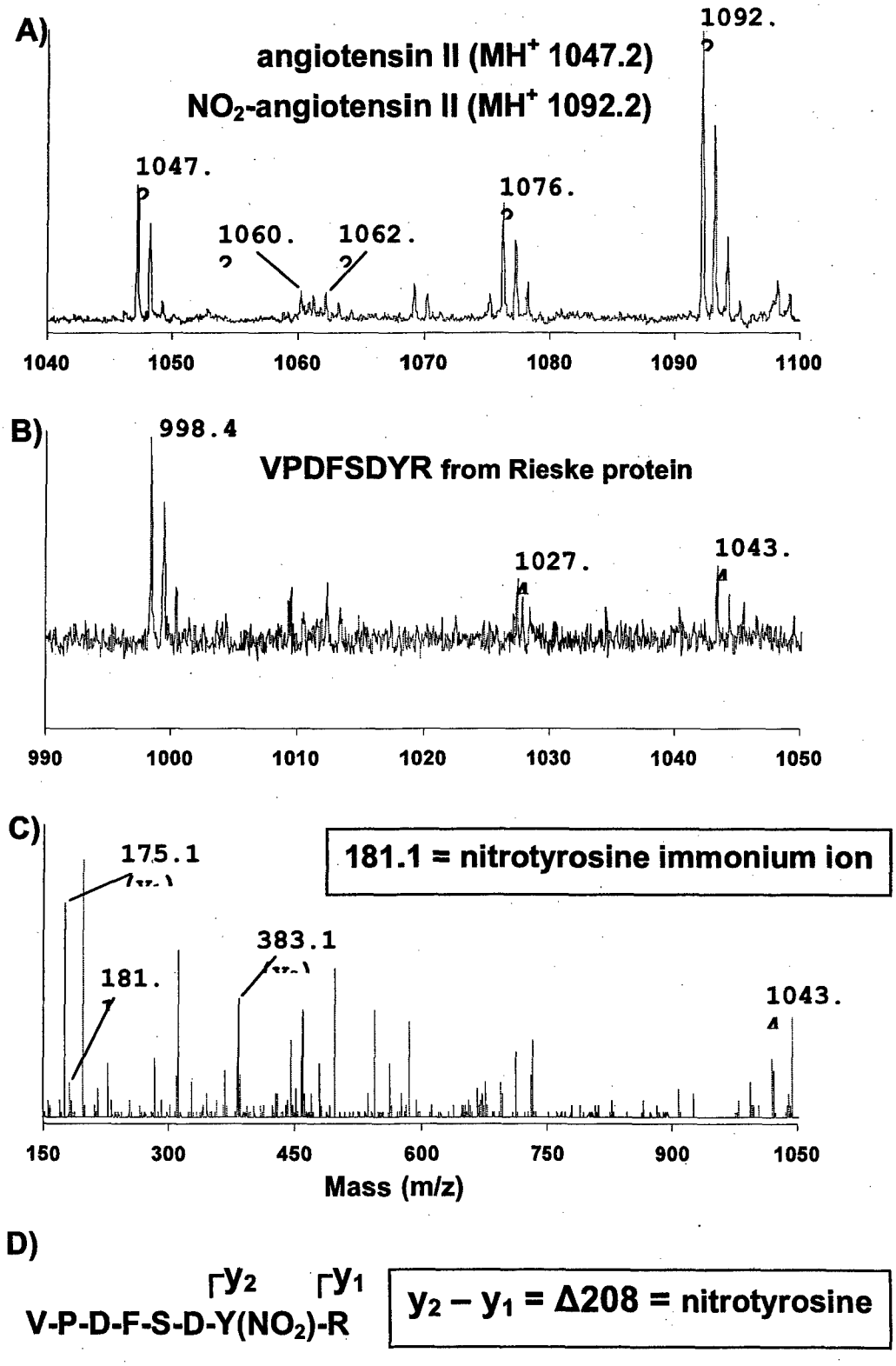

Fig. 1. MS identification of nitration. MALDI (*A* and *B*) and MALDI/MS (*C*) spectra are shown.

Analytical method to measure nitrotyrosine in proteins. To correlate the functional changes of nitrated protein with the degree of protein nitration, we have been able to develop the chemistry that selectively recognizes nitrotyrosine residues in proteins. The procedure includes reduction of nitrotyrosine to aminotyrosine (**1**) followed by diazotation (**2**) to diazotyrosine (Fig. 2). Kinetic analysis revealed that the diazo derivative is stable with a $t_{1/2}$ of approximately 24 hrs at room temperature under conditions suitable for assay. After screening different compounds that can couple with the diazo group, we found a group of compounds, derivatives of naphthylamine, that selectively interact with the diazotyrosine residue and yield the stable colored products. The presence of the R^+-group on naphthylamine creates the option to synthesize the derivative of naphthylamine conjugated with a radioactive marker, a fluorescent probe, or biotin.

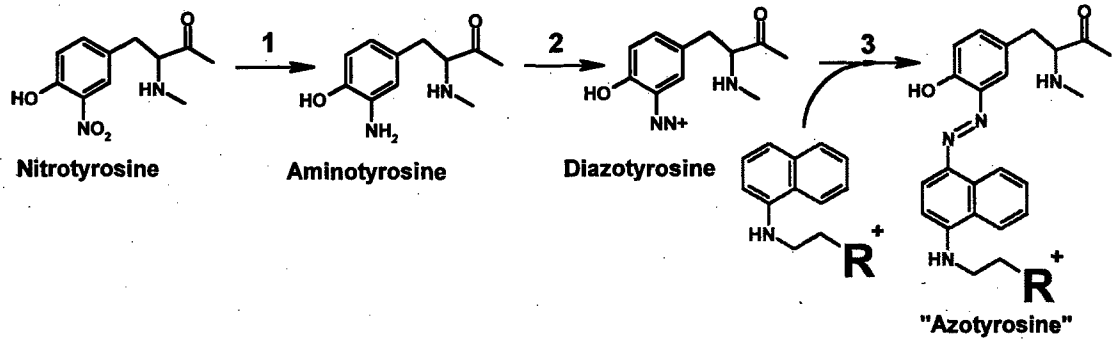

Fig. 2. Chemistry of selective nitrotyrosine detection in proteins.

The important issue was verification of the assay's specificity. Fig. 3 shows HPLC separation of peptides derived from nitrated BSA, which was modified according to the scheme shown in Fig. 2. Detection was performed at 214 nm (lower pattern) and at 580 nm (upper pattern). 580 nm is the maximum of absorbance for the azotyrosine derivative. The azotyrosine derivative of free nitrotyrosine was also synthesized. Its spectral properties were identical to those recorded for two peptides from the upper pattern of Fig. 3. This proves that only nitrotyrosines were derivatized.

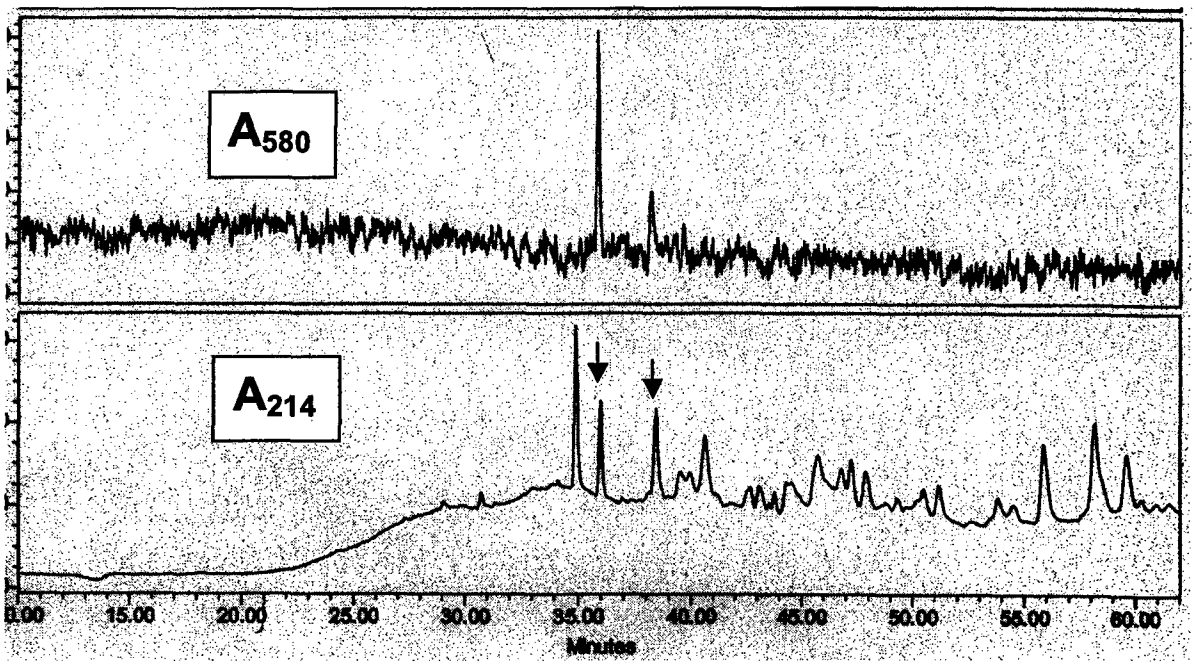

Fig. 3. Reverse-phase HPLC profiles. Arrows indicate the derivatized nitrotyrosine containing peptides.

Using biotin derivative of naphthylamine and a plate-type assay, we have initiated some studies to measure nitrotyrosine proteins in tracheal aspirate, plasma and urine from patients with various inflammatory disorders. These studies are supported with other funds available to the laboratory.

We are very optimistic that this chemical analytical method to assay nitrotyrosine in biological samples can became a simple, specific and sensitive assay method for free and protein associated nitrotyrosine (a patent for this technology is pending). We estimate that the method as currently developed will permit the detection of 100 pM nitrotyrosine or as low as 1 fmol of nitrotyrosine per mg of plasma protein. Using sandwiching techniques, it may be possible to increase the sensitivity of the assay method further, if necessary.

Task 2: Regulation of nitrotyrosine formation.

Possible pathways of protein tyrosine nitration include $ONOO^-$- and heme peroxidase-dependent reactions. However, the contribution of these pathways in *in vivo* nitration was unclear. $ONOO^-$ is more likely to be the predominant

nitrating species in macrophages, while heme peroxidases, such as MPO, may be predominantly responsible for producing nitrating species in neutrophils. Our initial plan was to use macrophages or neutrophils to nitrate model peptide(s) and protein(s) under conditions that favor either of the nitrating pathways. We analyzed nitration of proteins in the extracellular media by Western immunoblots with anti-nitrotyrosine antibody and found that this assay cannot be used to generate reliable data. Properties of the macrophages and neutrophils most likely varied substantially in different preparations and the resulting patterns of nitrated proteins were variable. It was necessary to switch to another biological model of protein nitration. At the same time, we have found that mitochondrial proteins readily undergo tyrosine nitration *in vivo*. Mitochondria have manageable proteomic complexity in comparison to the whole cell and could be highly purified. After examining protein nitration in mitochondrial soluble and membrane fractions of many tissues with various inflammatory models, we choose to switch to protein nitration in mitochondria.

Our *in vitro* approach was a treatment of purified heart mitochondria from mice with ether $ONOO^-$ or $NO_2^-/H_2O_2/MPO$. Our *in vivo* approach to initiate nitration of mitochondrial proteins was a treatment of mice with alloxan (AL) that caused type I diabetes. Diabetes is a proven state of oxidative stress, dysfunctional mitochondria, and, presumably, nitration of mitochondrial proteins. Whole mitochondria in control and treated groups were sonicated and separated into two fractions, which represent soluble mitochondrial proteins and membrane-associated mitochondrial proteins. They were then separately resolved by 2-D PAGE. Following the matching of nitrotyrosine immunopositive spots on Western and Coomassie-stained spots on the gel, the gel pieces were excised for trypsin digestion and protein identification by MALDI-TOF MS. Nine nitrated proteins were found in the soluble and membrane fractions from $ONOO^-$ - and MPO-treated mitochondria (Table I). This includes aconitase 2, Grp75, albumin, succinyl-CoA:3-oxoacid CoA transferase (SCOT), creatine kinase, peroxiredoxin 3, superoxide dismutase 2 (SOD2), β-subunit of trifunctional protein, and 24-kDa subunit of NADH-ubiquinone oxidoreductase. Four of the proteins, SCOT, creatine kinase, peroxiredoxin 3, and β-subunit of trifunctional protein were also found nitrated in the diabetic mitochondria (Table I). Another nitrated protein in

diabetic mitochondria was identified as a voltage-dependent anion channel 1, VDAC1, (Table I).

Table I. *Mitochondrial proteins in nitrotyrosine immunoreactive gel spots.* Heart mitochondria from mice were treated with $ONOO^-$, or with $NO_2^-/H_2O_2/MPO$, or were purified from AL-treated diabetic mice.

Nitrated protein diabetes	$ONOO^-$	$NO_2^-/H_2O_2/MPO$	
1. Aconitase 2	+	+	-
2. Grp75	+	+	-
3. Albumin	+	+	-
4. Succinyl-CoA:3-oxoacid CoA transferase (SCOT)	+	+	+
5. Creatine kinase, sarcomeric mitochondrial	+	+	+
6. Peroxiredoxin 3	+	+	+
7. Superoxide dismutase 2 (SOD2)	+	+	-
8. Trifunctional protein, β-subunit	+	+	+
9. NADH-ubiquinone oxidoreductase, 24-kDa subunit	+	+	-
10. Voltage-dependent anion channel 1 (VDAC1)	-	-	+

Detailed conditions of *in vitro* and *in vivo* nitration of mitochondrial proteins, their identification, verification of their nitration, and the functional properties of nitrated proteins are published in two papers (11, 19).

Incomplete similarity in the pattern of nitrated proteins between *in vitro* and *in vivo* experiments (Table I) suggests alternative pathways of tyrosine nitration in addition to $ONOO^-$- and MPO-dependent pathways. In searching for alternative nitrating pathways, the pro-oxidant effects of free and chelated iron have attracted our attention. We found that heme and free metals may mediate protein nitration in the presence of H_2O_2 and NO_2^- (18).

Task 3: Characterization and purification of nitrotyrosine-containing proteins.

To identify nitrated proteins three animal models of inflammation were used to initiate tyrosine nitration *in vivo*: **a)** Lipopolysaccharide (LPS)-treated rats. This is a model of the systemic inflammatorymresponse. **b)** Streptozotocin (STZ)-treated rats or AL-treated mice. This is a model of type I diabetes. **c)** Mice treated with *Lactobacillus casei* cell wall. This is an inflammatory model of vasculitis, which is associated with coronary aneurysm development.

We have screened different organs for nitrated proteins. Many nitrated proteins were identified; some of them were functionally characterized. Data are presented in several publications (3, 8, 11, 13, 15, 17, and 19). Major findings are summarized in the Key Research Accomplishments.

Task 4: Characterisation and purification of a "denitrase" for nitrotyrosine-containing proteins.

The ultimate goal was to identify the protein that possesses "denitrase" activity. A critical issue for identification of this protein is a rapid and reliable method for measuring "denitrase" activity. A major problem is that a product of this reaction is unknown and any method would be based on utilization of substrate only, a less specific assay method. As a source of "denitrase" activity, we have chosen macrophages because of their apparent resistance to oxidative and nitrative stress. To measure "denitrase" activity in lysates from macrophage-like cells, RAW 264.7 cells, we employed three different approaches.

Our first approach was based on the quenching property of nitrotyrosine towards some fluorescent compounds, like aminobenzoic acid (Abz). Peptides that have nitrotyrosine in close vicinity of the Abz group have their fluorescence internally quenched. Any modification of the nitrotyrosine group (including the "denitrase" reaction) should cause a strong increase in fluorescence of the Abz group. A pitfall of this approach is that any proteolytic cleavage of the internally quenched peptide will also cause release of fluorescence. Keeping this problem in mind, we designed 12 different internally quenched peptides which were very poor substrates to known proteases/peptidases. In addition, the reaction mixtures were supplemented with a set of common protease inhibitors. Nevertheless, our expectation to use these

peptides for measuring a specific nitrotyrosine modifying activity was not realized. HPLC analysis in combination with mass spectrometry identification demonstrated that all 12 peptides are cleaved during incubation with RAW cell lysates, presumably by a novel peptidase(s).

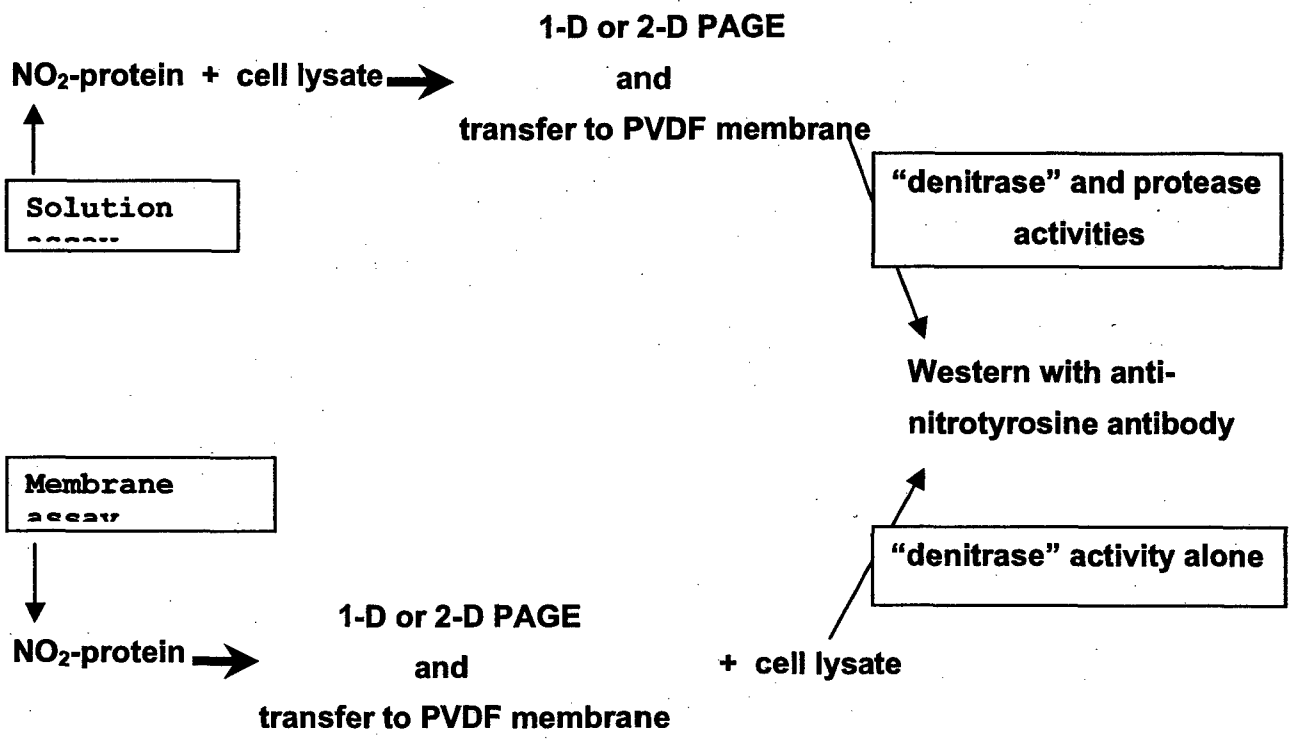

Fig. 4. A scheme that demonstrate the difference between solution and membrane

Second approach was based on the detection of nitrotyrosine clearance using Western immunoblots with anti-nitrotyrosine antibody. A model nitrated protein (BSA or streptavidin) was treated with RAW cell lysates. Proteins separated by SDS PAGE were transferred to PVDF membranes and analyzed by Western immunoblots with anti-nitrotyrosine antibodies. Nitrotyrosine clearance observed was normalized to the amount of nitrated protein added to the assays (Fig. 4, solution assay). This assay, however, demonstrates poor reproducibility. We think that this assay also did not overcome the major problem of assaying "denitrase" activity, namely separation of "denitrase" and protease activities.

Third approach (Fig. 4, membrane assay) represents a modification of the second one. Model nitrated proteins were first separated by SDS PAGE and transferred to PVDF membranes. Membranes were then treated with RAW cell lysate. Immobilization of nitrated proteins resolved a problem of interfering protease activity. We found this approach reliable and were able to measure "denitrase" activity in crude RAW cell lysates (17). We are currently in a process of purification the enzyme.

KEY RESEARCH ACCOMPLISHMENTS

1. The new methods i) to detect and quantify nitrated ptoteins and ii) to measure "denitrase" activity were developed.

2. The patterns of nitrated proteins generated with $ONOO^-$ or $NO_2^-/H_2O_2/MPO$ *in vitro* are remarkably similar and resemble those obtained using the animal models of *in vivo* nitration. This suggests a common nitrating species derived from different nitrating pathways that is responsible for the majority of nitrotyrosine formed. In addition, our study suggests that nitration from free heme or metal ions is also a highly likely event in biological systems.

3. Protein tyrosine nitration is a protein and tissue selective process. Certain proteins can be preferential targets for nitration. The nitration of some proteins is a dynamic process over time with increases and decreases in their nitrotyrosine immunostaining on Western blots.

Studies on functional consequences of nitration provide evidence that nitration adversely affects properties of proteins.

Specific proteins nitrated *in vivo* in the different models of inflammation are involved in major cell functions, such as signal transduction (L-type Ca^{2+} channel, cGMP-dependent protein kinase I), energy production (many mitochondrial proteins), antioxidant defense (Se-binding protein, peroxiredoxin-3), and apoptosis (VDAC-1).

REPORTABLE OUTCOMES

a) 5 review articles
b) 17 research articles
c) 1 provisional patent application

CONCLUSIONS

It is evident that inflammatory diseases are associated with progressive changes in the production of reactive oxygen and nitrogen species and with increased formation of tyrosine nitrated proteins. The nitration of protein tyrosine residues has been Cutting used as a marker of oxidative stress in inflammation. Understanding how protein nitration occurs and what are the functional consequences of nitration will offer new options for design of antioxidant therapy in the treatment of inflammatory diseases.

The current study represents a systematic effort to investigate the biological role of protein tyrosine nitration.

PUBLICATIONS DURING THE DREAMS SUPPORT

(1) Martin, E., Davis, K., Bian, K., Lee, Y.C., and Murad, F. Cellular signaling with NO and cyclic GMP. Seminars in Perinatology 24, 2-6, 2000.

(2) Kildsgaard, J., Hollmann, T., Matthews, K., Bian, K., Murad, F. and Wetsel, R. Cutting edge: targeted disruption of the C3 gene demonstrates a novel protective anti-inflammatory role for C3a in endotoxin shock. Journal of Immunology. 165, 5406-5409, 2000.

(3) Ishii, N., Patel, K.P., Lane, P.H., Taylor, T., Bian, K., Murad, F., Pollock, J.S., and Carmines, P.K. Nitric oxide synthesis and oxidative stress in the renal cortex of rats with diabetes mellitus. J. Amer. Soc. Nephrology 12, 1630-1639, 2001.

(4) Mendes, R.V., Martins, A.R., de Nucci, G., Murad, F., and Soares, F.A. Expression of nitric oxide synthase isoforms and nitrotyrosine immunoreactivity by B-cell non-Hodgkin's lymphomas and multiple myeloma. Histopathology 39, 172-178, 2001.

(5) Bian, K., Harari, Y., Zhong, M., Lai, M., Castro, G., Weisbrodt, N., and Murad, F. Down regulation of inducible nitric oxide synthase during parasite-induced gut inflammation. A path to identify a selective NOS-2 inhibitor. Molecular Pharmacology 59, 939-947, 2001.

(6) Mailman, D., Guntuku, S., Bhuiyan, B. and Murad, F. Sites of LPS-induced nitric oxide production in the anesthetized rat. Nitric Oxide: Biology and Chemistry 5, 243-251, 2001.

(7) Davis, K., Martin, E., Turko, I. and Murad, F. Novel effects of nitric oxide, Annual Review of Pharmacology and Toxicology. 41, pp. 203-236, 2001.

(8) Marcondes, S., Turko, I., and Murad, F. Nitration of succinyl Co-A-axoacid transferase decreases enzyme activity with endotoxin administration. Proc. Nat. Acad. Sci. 98, 7146-7151, 2001.

(9) Seminara, A.R., Krumenacker, J.S., and Murad, F. Signal transduction with nitric oxide, guanylyl cyclase and cyclic GMP. In Proc. of the NATO meeting on Nitric Oxide, Sicily, NATO Science Series 317, 5-22, 2001.

(10) Hanafy, K., Krumenacker, J. and Murad, F. Nitric oxide and cyclic GMP cellular signaling. Proceedings of the Vascular Biology Conference, Cracow, Poland, Medical Science Monitor 7 (4), 801-819, 2001.

(11) Turko, I., Marcondes, S., and Murad, F. Diabetes-associated nitration of tyrosine and inactivation of succinyl-CoA:3-oxoacid CoA transferase. Physiol. Amer. J. Physiol., Heart Circ 281, H2289-H2294, 2001.

(12) Bian, K., Harari, Y., Zhong, M., Lai, M., Castro, G., Weisbrodt, N., and Murad, F. Down regulation of inducible nitric oxide synthase (NOS-2) during parasite-induced gut inflammation: A path to identify a selective NOS-2 inhibitor. Mol Pharmacol. 59(4):939-47, 2001.

(13) Bian, K., and Murad, F. Diversity of endotoxin-induced nitrotyrosine formation in macrophage - endothelium rich tissue. Free Radical Biology and Medicine 31(4):421-429, 2001.

(14) Turko, I., and Murad, F. Protein nitration in cardiovascular diseases. Pharmacological Reviews 54, 619-634, 2002.

(15) Adewuya, O., Irie, Y., Bian, K., Onigu-Otite, E., and Murad, F. Mechanism of vasculitis and aneurysms in a mouse model of Kawasaki Diseased: Role of nitric oxide. Nitric Oxide: Biology and Chemistry. 8, 15-25, 2003.

(16) Murad, F. The excitement and rewards of research with our discovery of some of the biological effects of nitric oxide. Circulation Research 92:339-41, 2003.

(17) Irie, Y., Saeki, M., Kamisaki, Y., Martin, E., and Murad, F. Histone H1.2 is a substrate for denitrase, an activity that reduces nitrotyrosine immunoreactivity in protein. Proc. Nat. Acad. Sci. 100, 5634-5639, 2003.

(18) Bian, K., Gao, Z., Weisbrodt, N., and Murad, F. The nature of heme/iron-induced protein tyrosine nitration. Proc. Nat. Acad. Sci. 100, 5712-5717, 2003.

(19) Turko, I., Li, L., Aulak, K., Stuehr, D., Chang, R., and Murad, F. Protein tyrosine nitration in the mitochondria from diabetic mouse heart. J. Biol. Chem. 278, 33972-33977, 2003.

(20) Bian, F., and Murad, F. Nitric oxide (NO) - biogeneration, regulation, and relevance to human diseases. Frontiers in Bioscience 8, 264-278, 2003.

(21) Turko, I., and Murad, F. Quantitative protein profiling in heart mitochondria from diabetic rats. J. Biol. Chem. 278, 35844-35849, 2003.

(22) Turko, I., and Murad, F. Mapping sites of tyrosine nitration by matrix-assisted laser desorption/ionization mass spectrometry. Methods in Enzymology, in press, 2005.

PATENTS DURING THE DREAMS SUPPORT

"Methods of detecting nitrotyrosine and aminotyrosine residues of peptides and proteins." A provisional patent application was filed with the United States Patent and Trademark Office on June 11, 2004 (UTHSC-Houston file # 2004-0013)

Project III.C.

Genes Regulating Wound Healing and Susceptibility to Oxidative Injury

Investigators: Yong-Jian Geng, M.D., Ph.D.

In 2004, we continued our work of screening genes that are responsible for regulating DNA repair and wound healing as a result of oxidative injury. Much of what our laboratory did in 2004 was a more thorough examination of what was first explored in the preceding year. In particular, we focused on the role of RNA in perturbing gene expression during transcriptional and translational processed.

Of particular interest to us in this study was to understand the expression of PW29 and rps11 mRNAs during apoptosis as well as their coordinated regulation during the process. The 5′-UTR of PW29 was shown to be hyper-expressed via a CMV promoter controlled by tetracycline in both T-Rex293 cells and mVSMCs to study its effects on cell proliferation and apoptosis. The results indicated that PW29 mRNA expression was enhanced in the aortas, specifically within atherosclerotic lesions, of Apo-E deficient mice. The 5′-UTR of this particular mRNA showed marked complementation to the ribosomal protein s11 mRNA. Further studies confirmed that both PW29 and RPS 11 mRNAs are co-suppressed in cultured smooth muscle cells (i.e., vascular mouse) during 7-ketocholosterol induced apoptosis. Lastly, our results indicated that stable transfection of T-Rex 293 cells with cDNA of the 5′-UTR (PW29) did not affect cell proliferation when compared to un-transfected cells.

Our understanding of gene expression in wound healing, oxidative injury, and apoptosis has benefited heavily from this work funded through the DREAMS program. As a result, we have built upon these studies and developed intensive projects that will look more closely at the apoptotic pathway in atherosclerosis. Furthermore, we are

initiating several stem cell therapy projects that rely heavily upon what we learned about gene expression thought this work. The two major endeavors, that is unraveling the apoptotic pathway in atherosclerosis and studying the benefits of stem cell therapy in wound repair and heart disease, are currently underway within the T5 program and look to add more promise to our knowledge of disease and repair at the cellular level.